INVESTIGATION ON THE PHYSICAL, CHEMICAL, OPTICAL AND ANTIMICROBIAL PROPERTIES OF ZNO AND ZNO-TA NANOSTRUCTURES

AQILAH BINTI KAMARUZAMAN

Master of Science

UNIVERSITI MALAYSIA PAHANG

Universiti Malaysia PAHANG
Engineering • Technology • Creativity

SUPERVISOR'S DECLARATION

I hereby declare that I have checked this thesis and in my opinion, this thesis is adequate in terms of scope and quality for the award of the degree of Master of Science.

(Supervisor's Signature)

Full Name : DR. NURUL AKMAL BINTI CHE LAH

Position : SENIOR LECTURER

Date : 9 FEBRUARY 2021

STUDENT'S DECLARATION

I hereby declare that the work in this thesis is based on my original work except for quotations and citations which have been duly acknowledged. I also declare that it has not been previously or concurrently submitted for any other degree at Universiti Malaysia Pahang or any other institutions.

____

(Student's Signature)

Full Name : AQILAH BINTI KAMARUZAMAN

ID Number : MFA19004

Date : 9 FEBRUARY 2021

STUDENT'S DECLARATION

I hereby declare that the work in this thesis is based on my original work except for quotations and citations which have been duly acknowledged. I also declare that it has not been previously or concurrently submitted for any other degree at Universiti Malaysia Pahang or any other institutions.

____

(Student's Signature)

Full Name : AQILAH BINTI KAMARUZAMAN

ID Number : MFA19004

Date : 9 FEBRUARY 2021

INVESTIGATION ON THE PHYSICAL, CHEMICAL, OPTICAL AND ANTIMICROBIAL PROPERTIES OF ZNO AND ZNO-TA NANOSTRUCTURES.

AQILAH BINTI KAMARUZAMAN

Thesis submitted in fulfillment of the requirements
for the award of the degree of
Master of Science

Faculty of Manufacturing and Mechatronics Engineering Technology

UNIVERSITI MALAYSIA PAHANG

FEBRUARY 2021

ACKNOWLEDGEMENTS

First and foremost, my utmost thankfulness to the Almighty for granting me such a lifetime opportunity. I am heartily thankful to my supervisor, Dr Nurul Akmal Binti Che Lah for her continuous encouragement, guidance and support which enabled me to be able to develop deep understanding of this research work. This thesis would not have been possible without her review and correction of my many mistakes, accompanied by the countless valuable suggestions. I could not have imagined having a better advisor for my research. I also sincerely appreciate and acknowledge for her time spent on proofreading and correcting many of my mistakes.

Special thanks to Encik Mohd Nazarul Zaman from Faculty of Engineering Universiti Malaya, Dr Leo Bey Fern from Faculty of Medicine Universiti Malaya, Mr. Lim from MERIUEX Lab and staffs of UMP Central Lab for assisting and guiding me to conduct the experiment. Also, to my Post gradauates colleagues and friends for spending the time helping and motivating me through this master study.

I also would like to acknowledge the staff of Faculty of Manufacturing & Mechatronics Engineering Technology of University Malaysia Pahang for providing the physical necessities for my project as well as their generous access for unlimited support, either internal or external resources. It is deeply an honour for me to thank the educators and professors for all the theoretical and life lessons learnt for this whole time.

I owe my deepest gratitude to my parents for their undeniable love, understanding and sacrifice throughout my life. It is a pleasure to thank my beloved family for their continuing encouragement and moral support whenever needed. I am sincerely grateful to my fellow colleagues for the willingness of going through all the ups and down together. Lastly, I offer my regards and blessings to all of those who supported me in any respect during the completion of the project.

ABSTRAK

Nanotruktur telah menerima banyak perhatian pada masa kini kerana prestasinya berdasarkan keunikan cirinya yang dapat diaplikasi di dalam kebanyakan sektor dan industri. Prestasi nanopartikel bergantung pada sifat morfologi, fizikal dan optik. Tindak balas kimia, suhu dan kaedah yang digunakan dalam menghasilkan nanopartikel yang juga akan memberi kesan terhadap sifat-sifat nanopartikel. Objektif kajian ini adalah untuk memantau tindak balas di antara reaksi Asid Tanik (TA) melalui pH ZnO dan ZnO-TA nanostruktur. Zink Oksida (ZnO) telah dipilih dalam tesis ini kerana sifatnya yang luar biasa sebagai agen antimikrobial dan penyerapan UV. Ketumpatan TA terhadap ZnO telah dikaji melalui perbezaan pH (pH3 hingga pH 7) telah dikaji dalam tesis ini. TA telah diaplikasi ke atas ZnO untuk mengubah nilai pH. TA dipilih kerana sifatnya sebagai asid yang lemah dan tidak berbahaya atau mengubah struktur ZnO nanopartikel. Penyelidikan ini, melaporkan kaedah sintesis ringkas dari julat saiz kecil struktur nano ZnO (diameter min, d_m < 30 nm) di hadapan Natrium Sitrat (TC) menggunakan serbuk pukal ZnO (d_m > 5 µm) dari kaedah hidroterma, yang terkenal dengan prosedur kos rendah dan mesra alam. Keputusan yang diperoleh menunjukkan bahawa struktur nano ZnO-TA menunjukkan hasil struktur morfologi agregat. Hubungan antara perubahan pH dan agregasi struktur nano ZnO dan dibandingkan dengan sampel ZnO tulen dalam larutan berair dibincangkan dalam ruang lingkup sifat fizikal, struktur kimia, sifat optik dan kecekapan antimikroba. Nostruktur ZnO-TA terbukti mempunyai d_m sedikit lebih besar dan mempunyai panjang gelombang LSPR yang lebih pendek berbanding dengan struktur nano ZnO tulen E_g yang dikira bagi kebanyakan struktur nano ZnO –TA adalah lebih luas (3.41 eV –3.81 eV) berbanding dengan struktur nano ZnO tulen (3.51 eV-3.69 eV). Kecekapan antimikroba struktur nano ZnO-TA terbukti mempunyai prestasi yang baik dengan peratusan membunuh hingga 99.69% “strain” *S. aureus* dalam masa 24 jam daripada struktur nano ZnO tulen (99.39%). Oleh itu, hasil keseluruhan menunjukkan bahawa TA memang mempengaruhi sifat struktur nano ZnO selain dari nisbah permukaan hingga isipadu struktur nano ZnO itu sendiri adalah parameter penting. Dapatan dari kajian ini boleh menjadi salah satu keputusan awal untuk membuat struktur nano ZnO dengan konsep tekstil pintar kita sendiri dengan kawalan antibakteria.

ABSTRACT

To date, nanostructures had received an abundance of attention due to the outstanding intrinsic performances, which mainly depends upon their unique intrinsic properties that have been widely used in revolutionised sectors and industries. Their excellent properties (physical, chemical, optical and biological) are reported to be dependent upon the nanostructure morphology and topology. Hence, producing the nanosize metal oxide, in this case, the ZnO nanostructures, mainly known for its antibacterial properties, is one of the relevant areas of their practical applications. Thus, the work reported the facile synthesis method of a small size range of ZnO nanostructures (mean diameter, d_m < 30 nm) in the presence of sodium citrate (SC) using bulk powder ZnO (d_m > 5 µm) from hydrothermal method, known for the low cost and environmentally friendly procedure. In this reaction, only SC is used and acts as a surfactant to promote the nanosize ZnO formation. Modifying the surface of the synthesised ZnO nanostructures using the tannic acid (TA) is believed could alter the antibacterial performance of the nanostructures. The function of pH variation (7< pH >3) upon the introduction of TA to the surface of ZnO nanostructure showed the increased of particles aggregation as the pH is lowered due to the increased in the acidic medium. The relationship between the pH change and aggregation of ZnO nanostructures and compared with pure ZnO samples in aqueous solution is discussed in a scope of physical properties, chemical structure, optical property and antimicrobial efficiency. ZnO-TA nanostructures shown to have a slight larger d_m (23nm) and possesses shorter LSPR wavelengths as compared to pure ZnO nanostructures. The calculated E_g of most of the prepared ZnO –TA nanostructures are wider (3.41 eV –3.8 eV) compared to the pure ZnO nanostructures (3.51 eV-3.69 eV). The antimicrobial efficiency of ZnO-TA nanostructures shown to have remarkable performance with the killing percentage of up to 99.69% of *S. aureus* strain within 24 hours than that of pure ZnO nanostructures (99.39%). Thus, the overall results indicated that TA does influenced the properties of ZnO nanostructures apart from the surface to volume ratio of ZnO nanostructures itself is the important key parameters. The present work could be one of the baseline decision in order to make ZnO nanostructures to our own concept of smart textiles with antibacterial control.

TABLE OF CONTENT

LIST OF TABLES

LIST OF FIGURES

LIST OF SYMBOLS

λ	Wavelength
Eg	Band Gap Energy
Ef	Fermi Energy
Ev	Valence Energy
dm	Mean Diameter
h	Plank Constant
c	Speed of light
a	Crystalline Edge Length
c	Crystalline Basal Length
ν	Crystalline Volume
u	Crystalline Internal Parameter
L	Lattice length
Xe	Xenon
ZnO	Zinc Oxide

LIST OF ABBREVIATIONS

DL	Deep Level Emission
E	Proton Energy
FESEM	Field Scanning Electron Microscope
FTIR	Fourier-Transform Infra-Red
LSPR	Localised Surface Plasmon Resonance
MW	Molecular Weight
NBE	Near Band-edge Emission
SPR	Surface Plasmon Resonance
TA	Tannic Acid
TC	Trisodium Citrate
TEM	Transmission Electron Microscope
UV	Ultraviolet

LIST OF APPENDICES

CHAPTER 1

INTRODUCTION

1.1 Project Background

Nanotechnology had shown tremendous achievements in almost all field of science and engineering especially the one related to the development of advanced materials at the nano-scale dimension which employed the used of high surface area to volume ratio technique that promised elevated outstanding improved specific properties as compared to the materials counterparts. Particularly, nanostructures is the driving force for nanotechnology achievement. Nanostructures have known for their impressive effects due to the contribution of intrinsic physical and chemical properties of small particle size ranging from 1 nm up to 100 nm (Kondawar, Acharya, & Dhakate, 2011; Lah, 2016). As the size of the structure shifted to nanoscale regime, the remarkable properties which bring enumerate particular signals which totally differes from their bulk counterpart although there are from similar material. The 'magic' continues which also revolutionise towards tailoring and expanding possible range of uses including the nano-bioengineering materials such as zinc oxide (ZnO) that have been used for years in sunscreen to provide protection from the sun while appearing invisible on the skin. (Rai, Yadav, & Gade, 2009).

Zinc is an essential trace element for human system which will not effecting and causing enzymes presence such as carbonic anhydrase, carboxypeptidase, and alcohol dehydrogenase become inactive (K. S. Siddiqi, A. Ur Rahman, Tajuddin, & A. Husen, 2018). Pure Zinc is used as one of the important element in modulating many physiological functions inn biomedical field (Maremanda, Khan, & Jena, 2014; Wijesekara et al., 2010). In its oxide form, zinc oxide (ZnO), a group of II–VI semiconductor demonstrates distinctive intrinsic properties including as a wide-band gap semiconductor (3.37 eV at room temperature) in the near UV spectrum and a natural n-type electrical conductivity depending on their dimension and morphologycal structures, (Surabhi Siva Kumar, 2013). The wide band gap of ZnO has significant effect on its properties, such as the optical absorption. By controlling different reaction parameters of any particular chemical process such as solution concentration, pH, solvent, and temperature, an assortments ZnO nanostructures with different growth morphologyes such as nanoflakes, nanosphere, and nanotubes, can be successfully synthesised. A combination with green chemical elements could enhanced the possibility of functional ZnO in controlling associated bacterial infections. ZnO is known as nearly insoluble in water, it agglomerates immediately with water during synthesis due to the high polarity of water leading to deposition. Issues of aggregation, re-precipitation, settling, or non-dissolution impede the synthesis processes. In this regards, the addition of TA apart from PVA or polyvinylpyrrolidone (PVP) as stabilizers enhanced ZnO morphology and size for the antibacterial activity as well as be able to promote the formation of smaller size of nanostructures. Additionally,TA could also enhance the bioactivity and improved the dispersion of the ZnO (Orlowski et al., 2018)

Herein, the work focused on the synthesis and characterisation of both pure ZnO and ZnO-tannic acid (TA) nanostructures with different size distribution and morphologyes with the TA as a green stabiliser in water emulsion. This work is motivated to achieve small average size distribution of ZnO nanostructures in the presence of trisodium citrate (TC) through control synthesis parameters and monitoring the effect of TA as stabiliser on different sizes and morphologyes of ZnO-TA system. Accordingly, the pH is highly considered upon the exposure of TA in the system. .

Both the pure ZnO and ZnO-TA nanostructures have specific physiochemical, structural and optical properties that permitting remarkable applications. The physiochemical properties highlighted in the present study is divided into morphologycal and biological properties. Each morphology accounts for a certain mechanism of action. The analysis was carried out using Transmission Electron Microscope (TEM) and Field Scanning Emission Electron Microscope (FESEM). Selective morphologycal nanostructured for both pure ZnO and ZnO-TA for the antibacterial tests yielded structures of hexagonal pyramid like structures, with some spherical and ellipsoid shapes with average diameter size < 20 nm displayed pronounced antibacterial effect. Controlling the size of pure ZnO and ZnO-TA nanostructures are crucial to achieve best bactericidal responds. The determination on the purity and the presence of TA element on ZnO nanostructures are observed from EDX result. From here, the domination of element either the ZnO nanostructures or the capping agent TA. To observed the assessment and investigation of antibacterial activity in vitro, broth dilution method, followed by colony count, through plating serial culture broths dilutions which contained pure ZnO and ZnO-TA nanostructures with the targeted bacteria (that mainly presented in human sweat) in appropriate agar medium and incubated were carried out.

To correlate the antibacterial response with ZnO properties, the domination of element ZnO and TA are discovered by monitoring the bonding properties and diffraction peak within the two element. Both element of ZnO nanostructure or TA having different structure of either crystalline or amorphous. By monitoring the peak diffraction of ZnO-TA, the domination of capping agent TA can be investigated as the structure showing majorly in crystal form or amorphous form. Besides, XRD, FTIR are also another technique in determining the type of bonding relation within the two element of ZnO nanostructures and capping agent TA. From FTIR the domination of the capping agent TA could be monioted by referring to stretching of FTIR peak. Domination of capping agent TA would referring to aggregation that occur and the nano-size different between Pure ZnO nanostructure and ZnO-TA nanostructure

As ZnO is well-known for the ability to absorb UV light, thus, a detailed reaction mechanism which explains this phenomenon via optical analysis is carried out. The focus is mainly on the UV-Visible (UV-Vis) and photoluminescence (PL) spectroscopies. The determination whether TA would improve the UV absorbance and PL emission of ZnO nanostructures were successfully analysed. Determine the band gap or energy gap of the ZnO nanoparticle. Band gap change in the near-UV spectral region in both pure ZnO and ZnO-TA nanostructures are presented and discussed further.

The anti-micro bacterial properties of ZnO nanoparticles and its ability of the nanoparticles as a UV-blocking agent are realised and proved. In the subsequent studies, the different pH level of the nanoparticle are said to be affecting the ZnO nanostructure properties. In regards, the pH parameter is one of the primary consideration in this study. The relation of pH value with the morphologycal, physical and performance of ZnO nanoparticle were observed and investigated. As mention in some previous research, pH value of the green chemical would influence the peak absorbance of the nanomaterials (Iravani & Zolfaghari, 2013). Finding of previous reseach found out that low ZnO nanoparticle are believed to have better performance as the nucleation as it is synthesised in pH reaching neutral (Sangeetha Nagarajan and Kumaraguru Arumugam Kuppusamy, 2013). From the finding of the research, a total reduction of captivation of UV occurred at pH 8 and no captivation of UV peak was observed at higher peak up from pH 9 as ZnO nanostructure are cape with alkali medium of agent.

1.2 Problem Statement

Zn and O are classified into groups two and six in the periodic table, respectively which hold ZnO as II-IV semiconductor. ZnO posseses a unique optical, chemical sensing, semiconducting, electric conductivity, and piezoelectric properties made them as the most explored semiconductor as an antibacterial agent in both microscale and nanoscale formulations. Subsequently, the ZnO nanostructures is propose to be infused into fabric material as it could contribute in controlling the lousy odour ignited by fungi and micro bacteria and able in protecting users from UV ray.

The smaller size of nanostructure material are well known for its better performance of properties due to wide surface area of the material compared to bulk material. Unfortunately, only few finding in research able to synthesis ZnO nanoparticle small size of particle (< 30 nm). Thus, the major problem statement of this research is the size reduction on ZnO nanostructure synthesised. In previous research, as ZnO nanostructure are capped with other chemicals and plant extract in green synthesised method, the average size of the ZnO nanostructure synthesised are large (>30nm) (He, Liu, Mustapha, & Lin, 2011; Sangeetha Nagarajan and Kumaraguru Arumugam Kuppusamy, 2013; Ogunyemi et al., 2019; Prasanta Sutradgar, 2015).

Besides, usually, chemicals such as methanol and sodium hydroxide are used in synthesising ZnO nanostructures. But those chemicals are hazardous and not human and environmental friendly. Thus, green synthesised method are presented by using green chemical or plant extract. As for this research, the capping agent are focus on TA. TA as the capping agent in synthesising ZnO nanostructurea re the main interest which also the novelty of this research. Therefor, the other problem statement of this research are the reliability of the capping agent TA as stabiliser and size reducing reagent as they are only few research literate on using TA as capping agent. Furthermore, ZnO nanostructure are tends to exposed to aggregation and agglomeration after synthesised process. Thus, the third problem statement are from this research, the attraction are towards monitoring on how far TA would affect the properties of ZnO nanostructure synthesised and how far it could cause aggregation of the nanostructure. Besides, by capping ZnO with TA, it would enhanced the antibacterial effect of the nanostructure which enhanced the physiochemical properties of the nanostruture.

1.3 Objective

The aim of the present work is to demonstrate the remarkable performance of the as-synthesised pure ZnO and ZnO-TA nanostructures in the in-vitro antibacterial activity. The objectives of the work are as follows:

1. To tailor the size and morphology of both the pure ZnO and ZnO-TA nanostructures via hydrothermal synthesis below 30nm.
2. To investigate the effect of TA addition as stabiliser on ZnO nanostructures via pH reading.
3. To analyse the influenced of TA in the physical, chemical and optical properties of the ZnO nanostructure.
4. To determine the antibacterial effect upon addition of TA in synthesising ZnO nanostructures.

1.4 Scope

Synthesised ZnO nanostructure with narrow average size (< 30nm) by capping with TA. Besides, the scope of this research are by study the reliability of TA as capping agent,through the physiochemical and optical properties of ZnO and ZnO-TA nanostructure from results of TEM, FESEM, XRD, FTIR, U**V-Vis, PL and** Antibacterial growth test.

1.5 Thesis Arrangement

For the thesis arrangement, on **Chapter 1 – Introduction**, the writing presents the background, thesis objective, problem statement that occurs in this research and scopes or limitation of the study. The chapter concludes with a summary of the thesis organization.

Next, in **Chapter 2 - Literature review**, the chapter gives a comprehensive critical literature review summarizing the previously published work in the core area relevant to this thesis. The first part of this chapter includes theory, material and performance of ZnO and TA. Then, an overview results of the previous research in synthesising ZnO nanoparticle capping with other chemicals and extract are presented.

Meanwhile for **Chapter 3 – Methodology**, the chapter presents the method and procedure in synthesising the sample materials. It is then followed with details and method procedure of characterisation chosen together with equation of calculation related with the characterisation.

Furthermore on **Chapter 4 – Results and Discussion**, the chapter discusses the results of morphologycal by reviewing the image in TEM and FESEM. From TEM, graph of distribution are plotted to view the range of size for ZnO NPs while from FESEM, EDX graph are discussed on monitoring the element presented from the sample. Besides, the Optical characterisation are also monitor form the UV Vis and PL plot. Next, type of structure for sample of either crystalline or amorphous are discovered from results of XRD and FTIR. Lastly, the antimicrobial activities are discovered form antibacterial test of media culture.

Lastly, in **Chapter 5 – Conclusion and Recommendation**, the results of this thesis are summarised and concluded. Proposal for future research is also presented.

CHAPTER 2

LITERATURE REVIEW

2.1 Introduction

This chapter presents the review of previous research related to ZnO nanostructures synthesis capped with tannic acid (TA), experimental, and characterisation. The first review describes the theory, sources, and nanostructure of ZnO. Then, it is followed by the brief background of capping agent TA, method of synthesising, antimicrobial properties of ZnO and ZnO-TA nanostructures. Finally this chapter are concluded with summary table of previous research finding on synthesing of ZnO nanostructures.

2.2 Nanostructure Synthesis

As the nanotechnology increasingly gain attention, scientist focus are more diverted towards the discovery of these fascinating small size structures. As the structure size become smaller, the direct effect for example, the surface area are increase relative to its volume. The changed in the surface properties gives distinctive physiochemical properties from their bulk size including the increase in the reactivity process, surface features or topology and inter-particle connection (P. Wang, Lombi, Zhao, & Kopittke, 2016). This raised a situation known as a quantum effect that dominantly occurred as the behaviour of the material changed due to the enhanced in the properties performance. The invention of nanostructure thus leased the benefits in terms of environment and end consumer as the nanostructures already proved to have huge potential in vast industries including pharmacological and biomedical industries specifically for their ability to be loaded with bioactive substances for delivery in targeted sites of a living organism (Laura Soriano, Zougagh, Valcarcel, & Rios, 2018).

In synthesising nanostructures, many approaches are available. The synthesis methods are known to be divided into few characteristics; that are, wet-chemical, sol-gel, hydrothermal and green synthesis techniques (Krol, Pomastowski, Rafinska, Railean-Plugaru, & Buszewski, 2017; Selvarajan & Mohanasrinivasan, 2013). Wet chemical is one of the common synthesis method as this method provides better advantages mainly due to its environmental friendly element. Besides, biological method is also used by employing green chemicals or plant extract as the source of the reductant agent which results in a reaction that is purely eco-friendly and the obtained nanostructure size is controllable. For example, as reported in previous literature, the flowered structure of ZnO nanoparticle was synthesied via low-temperature method in the acetate solution (Wahab et al., 2007). The key parameters that affects the synthesis product are includes the pH medium, concentration of reactants and type of solvent used that result in different morphologies of nanostructures (Sirelkhatim et al., 2015).

Generally, the nanostructures synthesis method are divided into two approaches which are bottom up and top down approaches. For bottom up approach, the nanostructures are synthesised directly from small entities such as molecules and cluster. While, for top down approach, it starts from bulk which then narrowed down to the nanosize powder of nanostructures with the aid of several machines. **Figure 2.1** indicated the different in the synthesis approaches of the nanostructures.

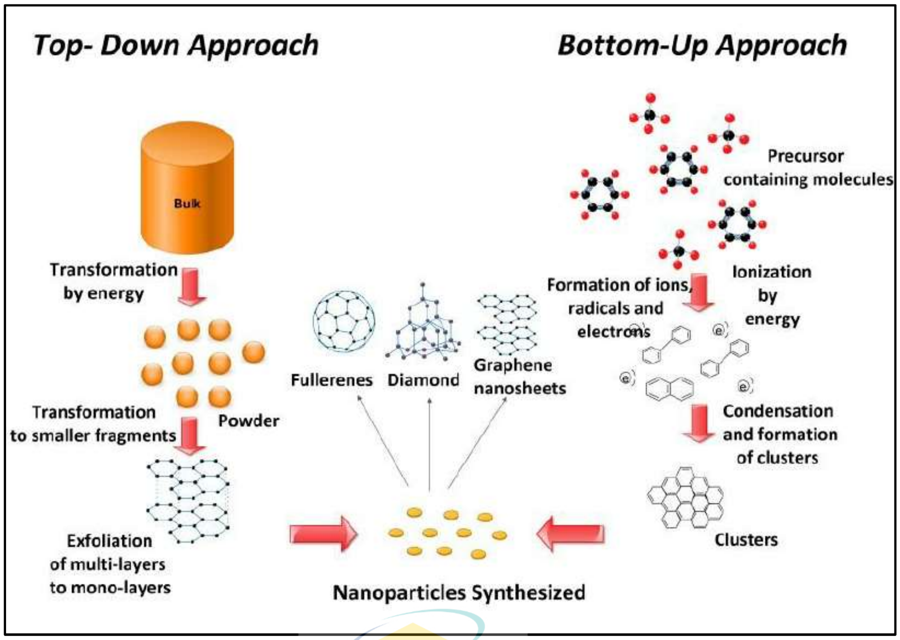

Figure 2. 1: Approach methods for nanostructure syntheses
Source: Picraux (2018)

The current research work proposed the green synthesis approach by hydrothermal method. Hydrothermal method is widely used in synthesising nanostructures as it is straight forward, consumed low energy and cost effective compared to other methods (Ahmad, 2014). The green synthesis method is referring to the ability to manipulates reagents from natural resources such as glucose, plant extract, biodegradable polymer and fruit acid as the capping agents in synthesising nanoparticle (Kharissova, Dias, Kharisov, Perez, & Perez, 2013). Few reported research using green synthesis approach have shown high potential properties of the as-synthesised nanostructures. For ZnO nanostructures that caped with natural glucose of stevia could be used as an antimicrobial agent (Khatami, Alijani, Heli, & Sharifi, 2018). These due to the different properties caused by a broad range of nanostructure size. For example, ZnO nanoparticle capped with seaweed produced nanostructures with the size range of 75 to 185 nm (Sangeetha Nagarajan and Kumaraguru Arumugam Kuppusamy, 2013). Different size range of nanostructure could be synthesised which yield different performance of properties. By defining the sizes and morphologies of nanostructures (nanorod, nanobelt, nanoparticle, nanoplate and etc) their outstanding properties can be tailored (Sadeghi et al., 2012). (Khatami, Varma, et al., 2018).

2.3 ZnO Nanostructures

Zinc Oxide (ZnO) nanostructures is an inorganic nanomaterial which is hydrophobic. Although ZnO nanostructures is insoluble in water, it is aso known as amphoteric oxide which able to react in both acid and base surroundings. ZnO nanostructures is allocated in semiconductor group that indicates few outstanding properties such as high electron mobility, wide band gap and good transparency. As in early history path of human life back in year 500 BC, bulk Zinc compound are widely applied in processed and unprocessed forms such as for paint and also in medical sector which can be found from medical text of Charaka and Greek Physician. Bulk ZnO compound is applied as ointment to treating ulceration and skin cancer (Baldwin et al., 2001; Godfrey, Godfrey Nj Fau - Godfrey, Godfrey Jc Fau - Riley, & Riley, 2001 ; Schechter, Wilkinson, & Carpio, 1984; Welsh, 2008). As time passed by, bulk ZnO is no longer use in cancer treatment but implemented in baby powder and creams to prevent rashes. In the modern technologies, ZnO nanostructures is widely use in calamine lotion, and anti dandruff shampoo which mainly to treated skin and prevent rashes (Baldwin et al., 2001; Zamboni et al., 2003).

As the technology growth, ZnO nanostructures gained a lot of attention for its ability in other enormous sectors. As the size of reduces to nano range (1 to 100nm), the properties of the ZnO nanostructures are enhanced. This are due to the increase in the surface area of the ZnO nanostructures as the size reduces to nano range. Thus, give effect to the whole properties (physical, chemical, electrical, optical and *etc*). The well-known optical properties of ZnO nanostructures raised its name as an efficient ultraviolet (UV) ray preventer which absorb the UV ray (Stassi et al., 2015; Tao et al., 2012). Thus, ZnO nanostructures exhibits reliable optical functional based materials for sunscreen ingredient (Nohynek & Dufour, 2012; Smijs & Pavel, 2011) . It is stated in previous research that ZnO nanostructures have huge potential as photo degradation resistance due to its ability in minimise the UV intensity by retaining and absorbing the UV radiation (M. Li et al., 2015) which then advancing a considerable potential in photo-degradation resistance (M. Li et al., 2015).

In addition, ZnO nanostructures possesses huge catalytic and photochemical reactions (Sirelkhatim et al., 2015). ZnO nanostructures seizes the high optical ability in absorbing UVA within the range of 315 to 400 nm and UVB in range of 280 to 315 nm which are valuable as UV protector material. ZnO nanostructures are predominantly reflect the light along the UV-A and visible ray where the wavelength are above the semiconductor band gap (Cole, Shyr, & Ou-Yang, 2016). They also have large exciton energy (60 meV) and wide direct band gap (3.37 eV) which makes them able to be use in various technological applications especially as a photonic and electronic based-material (Chey, 2015; Kondawar et al., 2011; C.-T. Lee, 2010).

Hexagonal wurtrize and cubic zinc blend are the two main forms of ZnO nanostructures. This structures are commonly known as the most stable nanostructure. The hexagonal crystalline growth at three primary direction of {1010}, {1120} and {0001} (Z. L. Wang, 2004) . Thus, ZnO nanoparticle can perform different morphology-based application with the help of capping agent. The capping agent of plant extract used in synthesising ZnO nanostructures influence the intrinsic properties of the nanostructure. Numerous morphological types of ZnO nanostructures includes nanocomb, nanorod, nanohelix, nanowire and nanorings (Wilson, Tang, & Barnard, 2016; Yi, Wang, & Park, 2005). Basically the morphologies of ZnO nanostructure are depend on the solvent and the types of plant extract capped at the outer layer surface (J.-M. Li, Zeng, Huang, & Xu, 2012; No, Lee, Kim, Cho, & Shin, 2013).

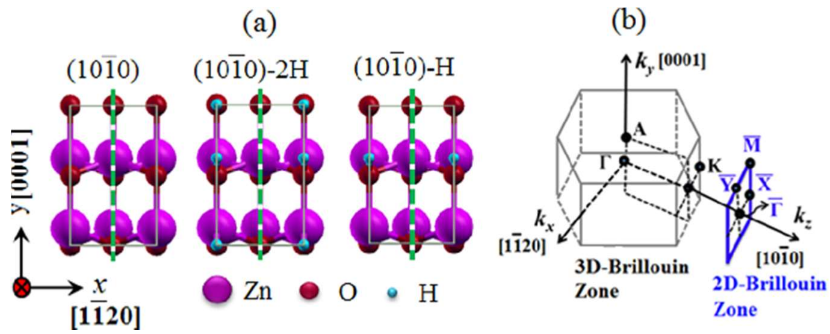

Figure 2. 2: Hexagonal Wurtize Structure of ZnO nanostructure
Source : Absor (2016)

On top of others, pH parameter is also one of the primary consideration which could also effect the output properties and morphology factor of the as-synthesised ZnO nanostructures. The relation of pH value with the morphology, sizes and other properties of ZnO nanostructures are deeply investigated by many researchers. The pH value of the green chemical would influence the UV absorbance ability of the nanostructures (Iravani & Zolfaghari, 2013). As indicated by Kuppusamy, the low pH value caused the increased in the overall performance properties of the ZnO nanostructures as the nucleation stage is vitalised (Sangeetha Nagarajan* and Kumaraguru Arumugam Kuppusamy, 2013). A total reduction of UV captivation occurred at pH 8 and no captivation of UV peak observed at higher peak up from pH 9. Hence, the pH parameter is vital and effects the performance and morphologycal structure of the ZnO nanostructures either will be crystalline or amorphous structures (Ashraf, Riaz, Hussain, & Naseem, 2015). The higher the pH value of ZnO nanostructures, the smaller the gap of the crystallite structure. Also, their UV-Vis shows higher performance, as more acidic or basic pH are implemented during the synthesis reaction.

Due to the unique semiconductor, optical, and piezoelectric properties, ZnO nanostructures is used as the nano-electronic and nano-optical devices, energy storage or nanosensors (Abdelmohsen, Rouby, Ismail, & Farghali, 2017; Gholizadeh, Reyhani, Parvin, Mortazavi, & Mehrabi, 2018; J. Huang, Yin, & Zheng, 2011). ZnO nanostructures is also widely applied in food packaging and medical health industries. ZnO nanostructures is usually doped with other element or capping material to increased the performance with their unique combined properties which benefis a lot in many essential industries. The outstanding antimicrobial properties and anti-cancer properties makes ZnO nanostructures widely used in drug delivery application. Also, the used of ZnO nanoparticle inside the bandage cloth raised the antibacterial effect with the nanostructures produced from green synthesis method. The size range between 5nm to 40nm of ZnO nanostrcutures yield better performance in anti-microbial bandages (Khatami, Varma, et al., 2018). Apart from this, several applications of ZnO nanostructures embedded in other fabric materials including cotton fabrics are also significant. For example, in clothing and footwear that focused in the combined required purposes such as antimicrobial agent, self-cleaning ability and UV-blocker with additional mechanical frictional properties (P. Singh et al., 2011). ZnO nanostructures exhibits better durability of the impregnated fabric and textile due to its ability in possessing high surface energy (Espitia et al., 2012).

2.4 Tannic Acid

In recent years, the correlation of green chemistry with nanotechnology has afforded impressive revolution in synthetic chemical processes (Albrecht, Evans, & Raston, 2006; Murphy, 2018). Tannic acid (TA) is the capping agent that is the central focused of this research. TA is known as a mild acid polyphenol from specific form natural and organic chemicals which known as tannin that were mainly extracted from plants. TA (penta-m-digalloyl glucose) is the simplest structure that used principal hydrolysable tannin to exert anti-oxidative, anti-mutagenic and antimicrobial properties (Buzzini et al., 2008; Coppo & Marchese, 2014; L. C. S. Lopes et al., 2018). TA also well known as the best reducing and stabilising method as it able to help in synthesising nanoparticles with narrow size distribution (Orlowski et al., 2018). The various amount of hydroxyl and phenolic group present in the dendritic structure of the TA help to perform as a stabiliser and a reducing agent as well (Ahmad, 2014; Iravani & Zolfaghari, 2013). These phenol and hydroxyl groups in charge in redox reaction where electron are donated and oxidised the ZnO in forming the metal nanoparticle (Ahmad, 2014). The summary of TA properties is indicated in **Table 2.1**.

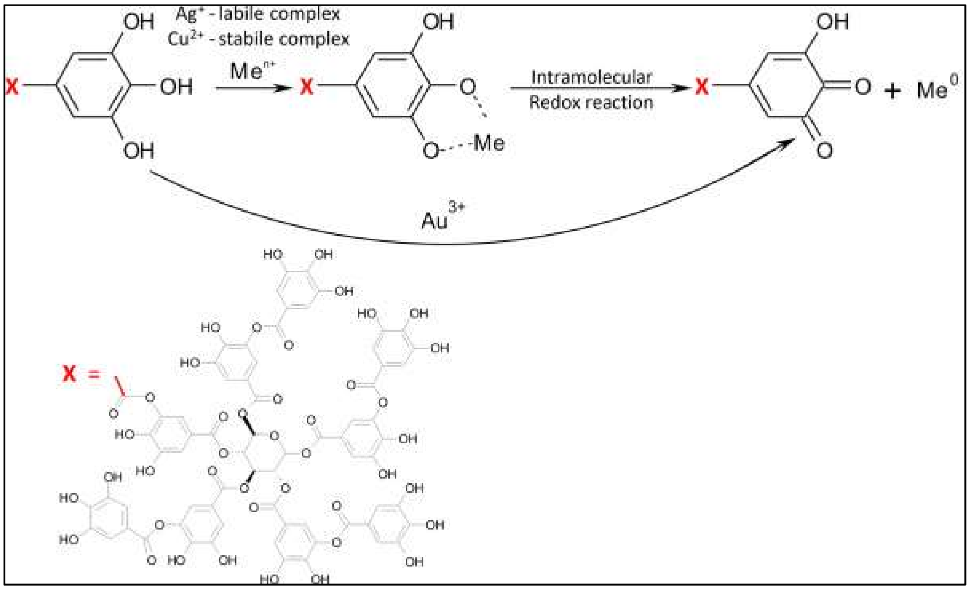

Figure 2. 3: Redox reaction of metal with TA

Source : Ahmad (2014)

The antibacterial activity of TA has also been highlighted extensively till today (Akiyama, Fujii, Yamasaki, Oono, & Iwatsuki, 2001; Cipriano-Salazar et al., 2018; Dong et al., 2018) . Few type of hydrosable tannin in TA complexes have been shown to impede the growth of both methicillin-resistant (MRSA) and methicillin-sensitive (MSSA) strains of *staphylococcus aureus* bacteria which is the common type of bacteria that cause skin infection (Buzzini et al., 2008). Purified forms of these tannins help in minimising the inhibitory concentration (MIC) of 62.5 μg/mL(Machado et al., 2003) of the bacteria based on the screening surveys towards large sets of target bacterial species. TA inhibited the growth of *bacillus anthracis, pseudomonas aeruginosa, salmonella spp., shigella dysenteriae, s. aureus, streptococcus pneumoniae* and other salivary bacteria in a dose-dependent manner (Asres, Mazumder A Fau - Bucar, & Bucar, 2006; Lim, Darah, & Jain, 2006).

TA also promoted the formation of smaller size of nanostructures. Tannic acid 's reducing properties owe its structure to the various phenolic groups. These phenols form quinones and donate electrons to engage in redox reactions (Ahmad, 2014). The donated electrons in metal salts dissolve the oxidised metal ions to form corresponding metal nanoparticles. TA helps in reducing and stabilising Ag nanoparticles which enhanced it ability in wound healing and gives the antimicrobial effect (Orlowski et al., 2018). The size of the nanostructures is reduced as TA is used in the reaction of Ag nanoparticles with better performance in wound healing and anti-bacterial effect. Also, TA helps in stabilising and improved the dispersion of nanoparticles (L. C. S. Lopes et al., 2018).

Table 2. 1: Properties of Tannic Acid (Books, 2017)

Attributes	**Results**
Appearance	Yellow to brown
pH	3.5
Molecular formula	$C_{76}H_{52}O_{46}$
Molecular Weight	1701.19 g/mol
Density	2.12 g/cm^3
Crystallite	Amorphous
Melting Point	200 °C
Flash Point	390 °F

2.5 Antimicrobial analysis of ZnO Nanostructures

As noted beforehand, apart from UV blocking and semiconductor properties, ZnO nanostructures is also well-known for its antimicrobial properties that efficiently inhibit the growth of microorganism, pathogens and germs which causing fungal activity and diseases. Few studies claimed the effectivity of ZnO nanostructures as an inorganic anti-microbial agent which are preferable for its stability and long-life time (Sawai, 2003). Similar to other semiconductors and metal nanostructures, the reduced size of ZnO nanostructures yields excellent performance of anti-microbial agent (Blum, Edwards, Prozialeck, Xiong, & Zelikoff, 2015; Shi et al., 2014). The unique morphologies of ZnO nanostructures contributed in inhibiting the growth of bacteria and microorganism (Jones, Ray, Ranjit, & Manna, 2008; Padmavathy & Vijayaraghavan, 2008).

The inhibition of microbes done by ZnO nanostructures have been reported in many literatures (Baek & An, 2011; Banoee et al., 2010; Dutta, Sharma, Bhargava, Kumar, & Pandey, 2010; Siddiqi & Husen, 2017; Khwaja Salahuddin Siddiqi, Aziz Ur Rahman, Tajuddin, & Azamal Husen, 2018; Tuomela et al., 2013). Smaller size of ZnO nanostructures exhibits greater antibacterial activity than the microscale particles (Yamamoto, 2001). Although contradictory results have been reported, many reported works showed positive effect of ZnO nanostructures on bacterial cells. For example, ZnO nanostructures with the size range between 10 to 14 nm could internalised (when exposed to microbes) and damaged the bacterial cell membrane (Brayner et al., 2006; Khwaja Salahuddin Siddiqi et al., 2018). Additionally, as the size of ZnO nanostructures is smaller than 12 nm, it is proved to inhibits the growth of *S. aureus*, but when the size exceeds 100 nm, the inhibitory effect is minimal (Yamamoto, 2001). A research reported by Ragupathi also indicated that the viable cell determination during the exposure of bacterial cells to ZnO nanostructures decreased significantly in the number of cells recovered with decrease in size of ZnO nanostructures (Raghupathi, Koodali, & Manna, 2011).

The acidic pH of ZnO-TA are one of the constitutive properties that help to prevent the colonization and infection by *S. aureus* (Grice et al., 2009; Grice & Segre, 2011; Ryu, Song, Seo, Cheong, & Park, 2014). The bacteria protein are noticed to be effected at low pH due to mild acid stimulation. Many observation noticed the huge impact of mild acid towards microbes are decreased expression of some secreted protein in which result into down regulation of locus for *S.aureus* (Tintino et al., 2016; Weinrick et al., 2004). ZnO nanostructure remain intact at around neutral or biological pH but rapidly dissolve under acidic conditions (average of pH 5) in the lysosome of the microbes leading to their death. ZnO dissolves in acidic condition produces Zn^{2+} ions, which bind to the biomolecules inside the bacterial cell inhibiting their growth. (Cho et al., 2011; Sharma, Anderson, & Dhawan, 2012; Tuomela et al., 2013)

Furthermore, TA are found to degrade the cell wall of bacteria *S.aureus* (Dong et al., 2018; Miajlovic, Fallon, Irvine, & Foster, 2010; Weinrick et al., 2004). TA may bind directly to the cell wall peptidoglycan of the microbes and interfere with their integrity. This are prove by a finding where TA enhance the effect of lyososome destroying bacteria by hydrolysing peptidoglycan in their cell wall (Reed et al., 2015). Additionally, it is also verified the bacterial mechanism of TA where TA inhibited beta-ketoacyl-ACP reductase (FabG), which is a key enzyme in bacterial fatty acid synthesis in which causing the bacteria to degrades. (Dong et al., 2018; J.-H. Lee et al., 2013). The polyphenolic compound of tannic acid also one of the factor in inhibiting *S.aureus* colonisation. The phenolic compound of TA interrupt the protein of microbes *S.aureus* in which inhibited the biofilm formation and reduce the colonization of the microbes (Payne et al., 2013). Phenolic agents also inhibit bacterial growth and protease activity by damaging its cell wall and cytoplasm (Andrade et al., 2006; Mentes Colak, Yapici, & Yapici, 2010). Besides the phenolic compound, as discussed before, caping TA with ZnO nanostructure also result into aggregation and this aggregation of nanoparticles influences cytotoxicity of macrophages. As the nanostructures aggregations, it was found to secrete more cytotoxin in which degrades the cytoplasm of microbe and inhibit their growth (Chiang et al., 2012; Khwaja Salahuddin Siddiqi et al., 2018).

The present work agrees that textiles and polymer impregnated with ZnO nanostructures are having a significant anti-microbial ability which focuses on preventing Gram-negative bacteria (Fiedot-Tobola et al., 2018). Here, it can be founded that ZnO nanostructures are widely accepted into many applications due to its ability and performance properties. ZnO nanostructures are used in medical industries for its general ability in anti-microbial properties. Besides, it is also impregnated into textiles, fabric, food packaging and polymers.

2.6 Summary

This chapter has presented a comprehensive current critical literature review of ZnO nanostructures and TA ligand that benefist the modern technology and application. The number of studies has proved that few methods in the synthesis of ZnO nanostructures is possible through hydrothermal method which widely used in a straight forward, less energy consuming and cost effective approach compared to other methods. The detail process of the synthesis procedure of pure ZnO and ZnO-TA nanostructures are explained in the next chapter. Number of reported research emphasised the benefits of ZnO nanostructures and TA ligand especially in the UV protection application and inhibiting the growth of bacteria. The measured performance of the ZnO nanostructures are mainly depends upon the size and morphologies of the nanostructures. **Table 2.2** sumarised the literature reviews obtained in this chapter and tabulated based on the synthesis method and properties of the ZnO nanostructures.

Table 2. 2: previous research related with synthesising and properties of ZnO

Nano-material	**Solvent**	**Range diameter**	**Crystalline size range**	**UV-Vis absorbance peak range**	**PL peak range**	**Antibacterial ability**	**Reference**
ZnO- *A. Betulina*	*d*H_2O	12- 26nm	19.4 nm	-	-	-	(Thema, Manikandan, Dhlamini, & Maaza, 2015)
ZnO- Moringa *Oleifera*	*d*H_2O	32-61nm	-	350 -380 nm	-	-	(Matinise, Fuku, Kaviyarasu, Mayedwa, & Maaza, 2017)
ZnO- *Solanum nigrum*	*d*H_2O	29.79 nm	-	-	402 - 483 nm	• S. paratyphi (17 mm) • *S. aureus* (18mm) • V. cholerae (11mm) • E. coli (7 mm)	(Ramesh, Anbuvannan, & Viruthagiri, 2015)
ZnO- CTAB	NaOH	-	3-50nm	315–340 nm	-	• *B. subtilis* (23 mm) • *E.coli* (17mm) • *C. Albicans* (20mm)	(Khan et al., 2016)

Table 2.2 continued

Nano-material	Solvent	Range diameter	Crystalline size range	UV-Vis absorbance peak range	PL peak range	Antibacterial ability	Reference
ZnO- *P. niruri*	*d*H_2O	25- 30 nm	-	-	664 nm	-	(Anbuvannan, Ramesh, Viruthagiri, Shanmugam, & Kannadasan, 2015)
ZnO-*L.Nobilis*	*NaOH*	21-26nm	-	350nm	-	-	(Fakhari, Jamzad, & Kabiri Fard, 2019)
ZnO –potato dictrose	*d*H_2O	70±15nm in length	-	-	-	• *P.expansum*.	(He et al., 2011)
ZnO- A. hydrophila	*d*H_2O	-	42–64 nm	peak focused at 374 nm	-	• Pseudomonas aeruginosa (22±1.8 mm) • Aspergillus flavus (19±1.0 mm).	(Jayaseelan et al., 2012)
ZnO-Starch	*d*H_2O	30 to 50 nm.	21 ± 2, 36 ± 2, and 42 ± 2 nm,	-	-	-	(Khorsand Zak, Abd. Majid, Mahmoudian, Darroudi, & Yousefi, 2013)

Table 2.2 continued

Nano-material	**Solvent**	**Range diameter**	**Crystalline size range**	**UV-Vis absorbance peak range**	**PL peak range**	• **Antibacterial ability**	**Reference**
ZnO- *Prunus yedoensis Matsumura*	*d*H_2O	26.12 nm, 41.14	-	378 nm	-	• *B. linen a* (14mm) • *S. epidermidis* (12mm)	(Velmurugan et al., 2016)
ZnO-Cassia fistula	*d*H_2O	-	5-15 nm	370nm	-	• Klebsiella Aerogenes (12.67±0.33) • Escherichia coli (14.67±0.33) • Staphyloccus aureus (10.07±0.33) • Pseudomonas desmolyticum (12.67±0.33)	(Suresh et al., 2015)

Table 2.2 Continued

Nano-material	Solvent	Range diameter	Crystalline size range	UV-Vis absorbance peak range	PL peak range	• Antibacterial ability	Reference
ZnO-Seaweeds	*d*H_2O	90 -186 nm	36 nm	365-380nm	-	• S. mutans • M. luteus • V. cholera	(Sangeetha Nagarajan and Kumaraguru Arumugam Kuppusamy, 2013)
ZnO- olive leaves (Olea europaea)	*d*H_2O	41.0 ± 2.0 nm,	48.2	380	-	• Xanthomonas oryzae pv. Oryzae (bacterial reduction of 59.4%)	(Ogunyemi et al., 2019)
ZnO-chamomile flower (Matricaria chamomilla L.)	*d*H_2O	51.2 ± 3.2nm	65.4	384	-	• Xanthomonas oryzae pv. oryzae (bacterial reduction of 50.2%)	(Ogunyemi et al., 2019)

Table 2.2 continued

Nano-material	Solvent	Range diameter	Crystalline size range	UV-Vis absorbance peak range	PL peak range	• Antibacterial ability	Reference
ZnO- red tomato fruit (Lycopersicon esculentum M.)	*d*H_2O	51.6 ± 3.6nm	61.6nm	386	-	• Xanthomonas oryzae pv. Oryzae (bacterial reduction of 46.3%)	(Ogunyemi et al., 2019)
ZnO- Azadirachta indica (L.)	*d*H_2O	-	18 nm.	370nm	430 - 408 nm	• S. aureus, (14.4 ± 0.76) • B. subtilis,(13.0 ± 0.50) • P. aeruginosa, (10.1 ± 0.28) • P. mirabilis (13.3 ± 0.56) • E. coli (12.6 ± 0.76)	(Elumalai & Velmurugan, 2015)
ZnO- CH_3OH (methanol)	C_2H_5OH (ethanol)	28 nm	-	-	-	• E. coli	(Chakrabarti & Banerjee, 2014)

Table 2.2 continued

Nano-material	Solvent	Range diameter	Crystalline size range	UV-Vis absorbance peak range	PL peak range	Antibacterial ability	Reference
ZnO- Tea leaf	*d*H_2O	50 nm	-	368nm	438 nm	-	(Prasanta Sutradgar, 2015)
p-ZnONP	*d*H_2O	-	25-35 nm	362nm	-	• Bacillus subtilis Staphylococcus aureus,	(Arakha, Saleem, Mallick, & Jha, 2015)
n-ZnONP	*d*H_2O	-	35-45 nm	369nm	-	• S. flexneri	(Arakha et al., 2015)

CHAPTER 3

METHODOLOGY

This chapter explains the details of synthesis, characterisation and preparation of analysis methods applied to the present work. All of the steps and process begin from the data collection to information process methods are gathered together for further analysis to proof the concept which will be presented in later chapter (**Chapter 4**).

3.1 Background of Research Flow

Chapter 3 demonstrated an overview of the process flow of the synthesised ZnO nanostructures starting with the introduction of the chosen chemical reactants, the selection of chemical reaction process which then further proceeds to the selection of characterisation techniques as well as the specific preparation of each chosen characterisation techniques All the preparation and synthesis procedures of ZnO nanostructures were executed in Materials Laboratory, Faculty of Manufacturing and Mechatronics Engineering Technology, Universiti Malaysia Pahang (UMP), Pekan. Whilst, the characterisation methods have been divided into several parts, in which the PL, UV-Vis, XRD and FTIR were done at UMP, meanwhile, the SEM and TEM were carried out at University of Malaya (UM). The overall process of the present work is indicated in the flowchart in .

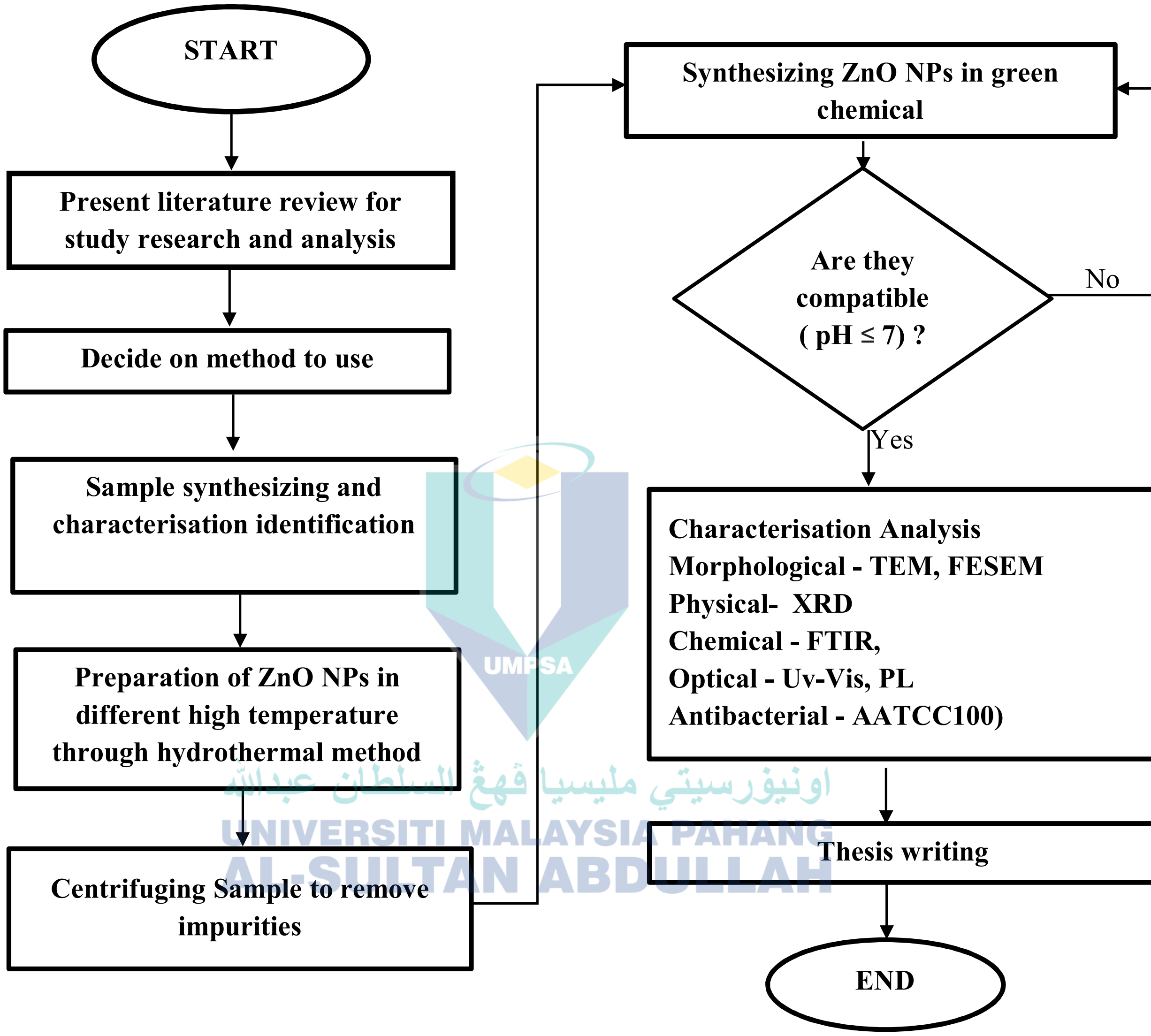

Scheme 3. 1**:** The overall flowchart of the present work.

3.2 Synthesis Of ZnO Nanostructures

3.2.1 Chemicals and Materials

In the present work, all chemicals used were of analytical grade (≥95% pure) and were used as received without any further purification. All the chemicals were purchased from Sigma Aldrich Company (Malaysia) and R&M Chemical (Evergreen Engineering & Resources, Malaysia). The bulk ZnO powder in uncoated and non-nano was used as a source of ZnO (Sigma Aldrich, ACS reagent, ≥ 99%). The trisodium citrate (TC) ($Na_3C_6H_5O_7.2H_2O$, Sigma Aldrich) acts as the buffering or emulsifying agent while tannic acid (TA) ($C_{76}H_{52}O_{46}$, R&M Chemical, ACS reagent) acts simultaneously as reducing agent and stabilizer All solutions were prepared with purified water available at Materials Laboratory, Faculty of Manufacturing and Mechatronics Engineering Technology, Universiti Malaysia Pahang (UMP), Pekan

3.2.2 Synthesis of ZnO Nanostructures

Preparation of ZnO Nanostructures

The method opted for the synthesis of ZnO nanostructures is an hydrothermal method which involves the direct mixture of the respective chemical powders with certain solvent under heat, in this case, water is used as the solvent. Few samples were prepared based on the reactant parameters shown in Table 3.1. The preparation involves the use of 0.4g of ZnO powder which was diluted in 100 ml of distilled water in the first step (**Figure 3.1A**) After the ZnO powder are completely dissolved, 0.2g of TC and TA were added and continuously stirred without any heat using magnetic stirrer (**Figure 3.1B**) . As the mixture completely dissolved, the mixture is then placed on a hot plate under continuous magnetic stirring at 50˚C for approximately 90 minutes. Similar process continued for other samples but at different reactant temperatures (60, 70, 80 and 90℃). The focus of hydrothermal method is to synthesis the nanostructure in high solvent temperature (Gan, Jayatissa, Yu, Chen, & Li, 2020). The chosen temperature are the maximum five temperature with interval of 10 ℃ for nanostructure synthesising before the solvent reach it boiling point at 100℃ .

(a)  (b) 

Figure 3. 1**:** (a) ZnO powder diluted with distilled water and (b) mixture of diluted ZnO powder with TC and TA.

Table 3. 1: The reactant paramaeters involves in the preparation of ZnO nanostructures. Noted that the variation in temperature is the key for the formation of ZnO nanostructures at difeerent sizes.

Sample	**TC (g)**	**ZnO (g)**	**Distilled Water (ml)**	**Concentration of ZnO nanostructures (M)**	**Temperature (˚C)**
Sample 1	0.2	0.4	100	0.05	50
Sample 2	0.2	0.4	100	0.05	60
Sample 3	0.2	0.4	100	0.05	70
Sample 4	0.2	0.4	100	0.05	80
Sample 5	0.2	0.4	100	0.05	90

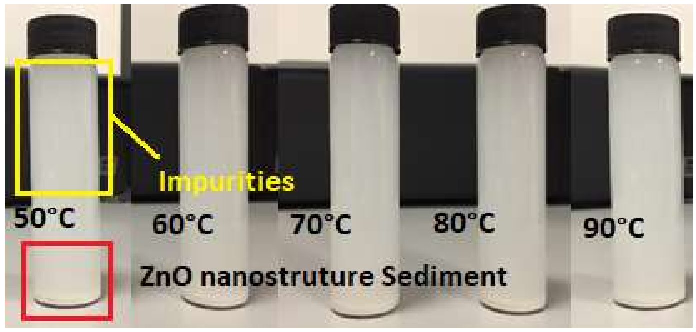

Figure 3. 2: The as-synthesised ZnO nanostructures prior to the centrifuge process. Noted that the sediment of the ZnO nanostructures can be found at the bottom of the bottle for each samples due to hydrophobic reaction of ZnO.

Centrifugation of the ZnO Nanostructures

The as-synthesised ZnO nanostructures samples were s then centrifuged (**Figure 3.3A**) in order to purified the samples in which all the impurities were drained out from the samples (**Figure 3.3B**). Upon centrifugation, a clean sediment appeared with clear colour of water at the top part of the samples (**Figure 3.3C**).

Figure 3. 3: (a) Centrifuging sample of ZnO nanoparticles. (b) sample of ZnO nanoparticles after centrifuged and (c) sample of ZnO nanoparticles after centrifuged and excess liquid are removed.

(c)

Figure 3.3 continued

3.2.3 Preparation of ZnO Nanostructures with Tannic Acid (TA)

The formation of ZnO-TA is the crucial step in the present work. The use of TA is important in order to elucidate the role of TA in the size distribution which also effect the morphologycal structures of ZnO nanostructures. At this stage, the samples were divided into few subsample based on their pH values. The subsample were prepared by direct mixing of TA through drop wise method for the aggregation procedure. Prior to this, each concentrated as-synthesised ZnO samples was diluted in 100 ml distilled water and further divided into five subsamples. Later, these five samples were then added with different volume of TA for the manipulation of pH value. For the first subsample for all as-synthesised ZnO nanostructure samples (denoted as 1A, 2A and 3A), no TA was added and acts as the control sample in order to monitor the change of the pH reading.. As for the second subsample (1B, 2B and 3B), approximately 10 µl of TA are dropped wisely and shaked well. The volume of TA were increased to 10 µl , 50 µl, 100 µl and 200 µl for C, D and E, respectively,. The concentration of TA is calculated based on ***Equation 3.1***. **Table 3.2** summarised the reaction parameters involved in the preparation of ZnO-TA nanostructures.

$$c = \frac{m}{v} \, x \, \frac{1}{MW} \qquad 3.1$$

where c is referring the molar concentration (mol.L^{-1}), m is referring to the solute mass (g), V is the solution volume (L) and MW is referring to the molecular weight based on periodic table (g.mol^{-1}).

Table 3. 2: Summary of the parameters used in the preparation of ZnO-TA.

ZnO Sample	**Sample Volume (µl)**	**Subsample**	**TA (µl)**	**Concentration of Tannic Acid (M)**	**pH**	**Remarks**
Sample 1	300	1A	0	0	7	Sample is shake in room temperature until it fully dissolves
		1B	10	0.042	6	
		1C	50	0.207	5	
		1D	150	0.623	4	
		1E	300	1.24	3	
Sample 2	300	2A	0	0	7	Sample is shake in room temperature until it fully dissolves
		2B	10	0.042	6	
		2C	50	0.207	5	
		2D	150	0.623	4	
		2E	300	1.24	3	
Sample 3	300	3A	0	0	7	Sample is shake in room temperature until it fully dissolves
		3B	10	0.042	6	
		3C	50	0.207	5	
		3D	100	0.623	4	
		3E	300	1.24	3	
Sample 4	300	4A	0	0	7	Sample is shake in room temperature until it fully dissolves
		4B	10	0.042	6	
		4C	50	0.207	5	
		4D	150	0.623	4	
		4E	300	1.24	3	
Sample 5	300	5A	0	0	7	The sample is shaken in room temperature until it fully dissolves
		5B	10	0.042	6	
		5C	50	0.207	5	
		5D	100	0.623	4	
		5E	300	1.24	3	

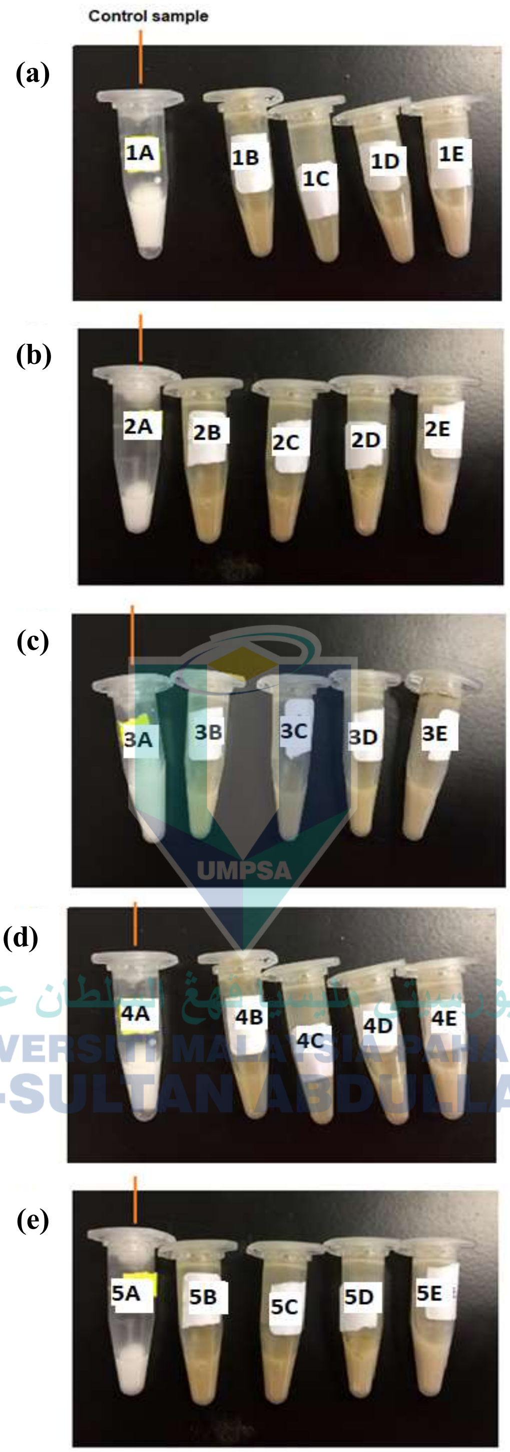

Figure 3. 4**:** ZnO-TA nanostructures of (a) sample 1, (b) sample 2, (c) sample 3, (d) sample 4 and (e) sample 5.

3.3 Characterisation Techniques

3.3.1 Optical properties

3.3.1.1 UV-Visible (UV-Vis) Spectrometer

UV visible spectrometer is the measurement for reflection and absorption of light or photon in the function of frequency and wavelength of a sample. Generally, the spectrometer measures the relative light intensity in visible range by monitoring it along with the wavelength of the electromagnetic spectrum. During characterisation testing, as the light passes through the Nanostructuresample, part of the light would be absorbed, and some other portion would be reflected, transmitted or dispersed. The Ultraviolet or bright region is ranging from190nm to 400nm and visible region of 400nm to 800nm. The graph of absorbation ability versus wavelength (in nm unit) are plotted which referring to the absorption for nanoparticles based on the controlled variable (size and shape) properties. From the analysis, the absorbance wavelength and ability relation can be confirmed by referring to Beer's Law as stated in **Equation 3.2.**

$$A = a(\lambda) * b * c \qquad 3.2$$

where A is referring the measured absorbance (a.u), $a(\lambda)$ is referring Wavelength-dependent absorptivity coefficient (M^{-1} .cm^{-1}), b is the Path length (m) and c is referring to the Analyte concentration ($Mol.L^{-1}$).

Excitation of electrons during analysing lead to absorption of UV. When atoms or particle absorb energy, it will excite which allowed it to vibrate and rotates vigorously. Thus these movements excrete energy which considered it to have more electronic energy. Most organic material, the absorbance spectroscopy increase and peak the spectrum region of 200nm to 700nm due to the bond energy. As the particle is reduced into molar sizing, it can lead to shorter wavelength due to strong polarity attraction between molecule or particle.

During analysing as shown in **figure 3.5**, the light source of either UV or visible light transmit coloured light which is then diffracted by a prism which acts as the diffraction grating. The diffracted light is then filtered before reflected into two different coloureds of light which is magenta and blue. Blue light will passes through the cuvette with a reference sample while a magenta beam of light will passes through a cuvette containing the liquid sample. The intensities of light absorb for both reference (I_0) and sample (I) are detected by the electronic detector. The wavelengths are then generated by the spectrometers. Different value of absorbance will results in a different wavelength. While if there are the absence of absorbance, thus the intensity of sample beam I will be equal to intensity of reference I_0

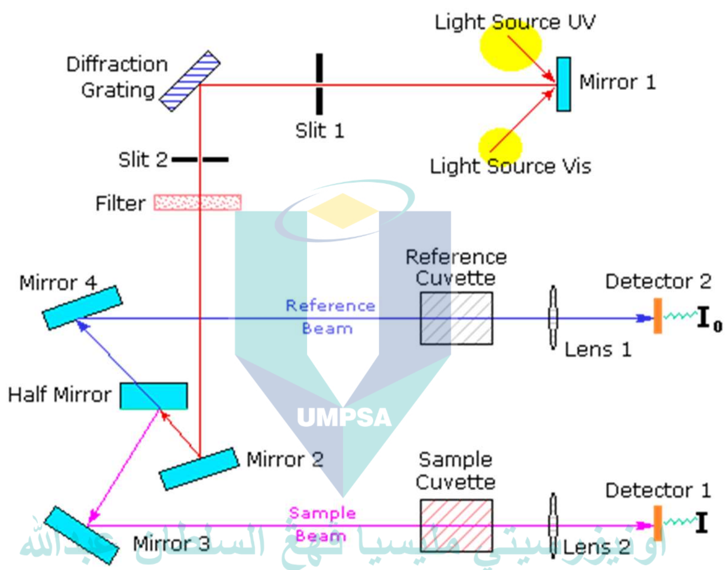

Figure 3. 5: Mechanism or UV-Vis Spectroscopy

Source : MSU (2017)

3.3.1.1.1 Energy Band Gap

From UV absorbance value, the band gap can be determined by Tauc Plot. As band gap are divided into direct and indirect band gap in which determine the composition of the materials. As for this research, the focus are on direct band gap as ZnO are semiconductor materials which exposed the properties of direct band gap The value for direct band gap of pure ZnO and ZnO-TA nanostructures is obtained from the plot of hv versus (αhν)2 using the value of absorption coefficient, α as based on the **Equation 3.3**

$$(\alpha h\nu)2 = (A\frac{1}{Log\, e\,(L)}h\nu)^2 \qquad 3.3$$

where A is the absorbance value obtain from the absorbance plot of UV-Vis . L is the thickness of cuvette used (1mm). hν is the incident light energy and Log e is the constant value which result to 2.303. The extrapolation of the linear part of the graph with the x-axis inflicts the value of the band gap (H. Zhang et al., 2011). Hence, the *Eg* is found to be d_m dependent that cause the decreased in the *Eg* of the ZnO nanostructure with a decrease in d_m (Debanath & Karmakar, 2013).

Based on the band gap, energy level can be calculated based on the concept of HOMO LUMO energy level. The optical band gap, *Eg* of ZnO and ZnO-TA are calculated based on **Equation 3.4**

$$Eg = E_{LUMO} - E_{HOMO} \qquad 3.4$$

where E_{LUMO} and E_{HOMO} are the energies of the lowest unoccupied molecular orbital (LUMO) and that of the highest occupied molecular orbital (HOMO), respectively. From the calculated energy band gap, the valence band edge, E_v are calculated based on the Fermi level as stated in **Equation 3.5**

$$\text{Valence band edge } (E_V) = E_F - Eg \qquad 3.5$$

where *Eg* of direct band gap, E_F is the Fermi energy and, E_V is valence band edge. In addition, E_V is defined as the separation band between the *Eg* and E_F

UV-Vis Sample preparation

Distilled water is filled into cuvette to perform as the reference sample. As for the testing sample, 2 ml ZnO Nanostructure sample are added to 5ml distilled water and mixed well. The solution is then poured into a rectangular cuvette and ready for testing. Sub-sample with different pH are prepared with the same steps.

Figure 3. 6: Shimadzu UV-Vis Spectrometer in Faculty of Manufacturing & Mechatronic Engineering Technology, UMP Pekan.

3.3.1.2 Photoluminescence (PL) Spectrometer

Photoluminescence spectroscopy is a non-destructive method in examining the light emission after absorption of a photon. Photoexcitation happens to the particle of the sample as it absorbs energy when light is emitted onto the sample — the photoexcitation or also known as photoluminescence cause vigorous movement of the electron of the particle. As the electrons return to its equilibrium state, emission of light may cause the excess of energy. This emission is due to energy level different or electron movement during the transition of equilibrium and excitation state. The amount of light emitted is related to the radiative techniques. With this character, PL able to determine the tendency of sample segregation. Besides, PL also able to determine the quality of the crystalline structure of a material. PL is also able in determining the presence of impurities and defects of a sample.

The intensity of light emitted through radiation due to the excitation phase are measured during PL analysis. The excitation spectrum or also known as absorbance spectrum is collected by varying the excitation wavelength and compared with monitored emission at a fixed wavelength. While in the emission spectrum, the intensity of the emitted radiation is monitored where fixed wavelength are used to excite the sample. From a molecule of sample, we can get one excitation spectrum and two emission spectrum which are known as fluorescence and phosphorescence. The photoluminescence peak of the spectrum would determine the band gap energy of the nanoparticle. Photon equation of energy can be used in determining the band gap energy as in **Equation 3.6.**

$$E = hc/\lambda \tag{3. 6}$$

where E is referring the Photon Energy (eV), h is referring to Plank constant to (J.s), c is the speed of light ($m.s^{-1}$) and λ is referring peak wavelength of PL spectroscopy (n.m)

As in **figure 3.7** the monochromator will select the excitation wavelength and the second monochromator will observe the luminescence. The incident light is placed at 90° from the second monochromator to reduce the scattered of incident light before reaching the detector. Emission spectrum is produced as the excitation wavelength are fixed, and emitted radiation is scanned.

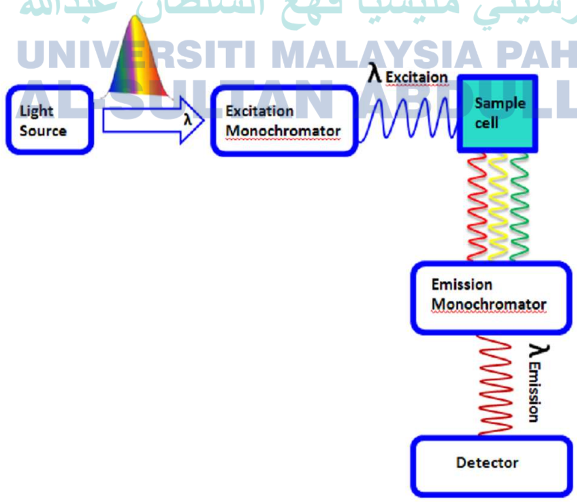

Figure 3. 7: Mechanism of Photoluminescence Spectroscopy

Source : Arif (2017)

PL Sample Preparation

Distilled water are filled into cuvette to perform as the reference sample. as only one cuvette are used during PL, therefore, after reference sample is tested, it is removed and replace with a testing sample where 2ml ZnO Nanostructure sample are added to 5ml distilled water and mixed well. The solution is then poured into a rectangular cuvette and ready for testing. Sub-sample with different pH are prepared with the same steps. As during the characterisation, filter lense are adjusted based on peak of UV absorption for each sample.

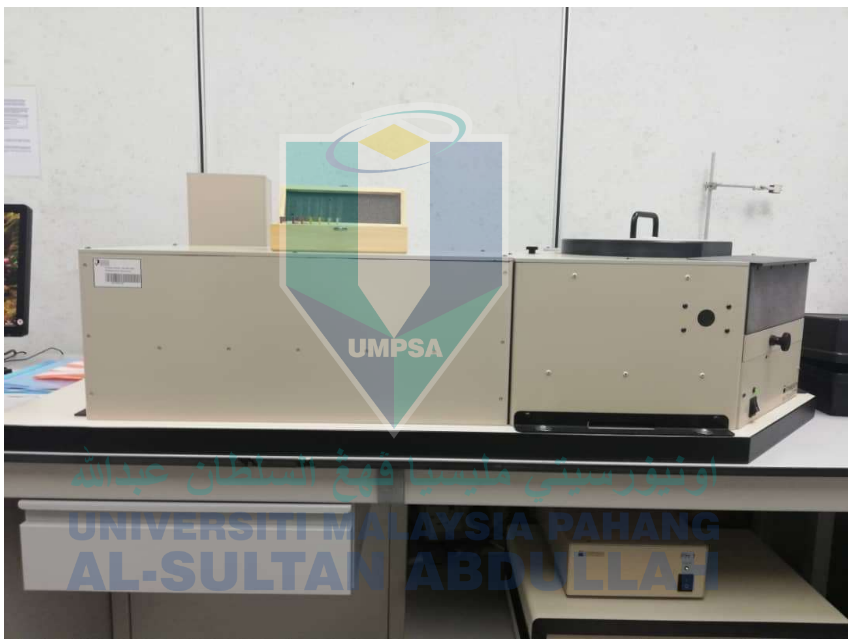

Figure 3. 8: Photoluminescence Spectroscopy taken at Research Centre UMP Gambang, 2019

3.3.2 Morphological Properties

3.3.2.1 Transmission Electron Microscopy (TEM)

TEM is microscopic equipment that has high resolution due to the used of the electron as its light source. The wavelength is much smaller which cause it to generates more exceptional resolution and better magnitude optical structure of a sample. A very high beam of electron is shot into a very thin sample which is then react and able to interpret very details the inert structure of a sample.

The electron beam is shoot into the condenser layer which allows it to produce a thinner and coherent beam. The focused beam is then passes through the condenser aperture which results into a restricted beam without any high angle electron. The electron beam is then focused and strikes onto the sample. Some part of the beam will be transmitted depending on the thickness of the sample. The transmitted beam is focused by the objective lens. Objective aperture is then blocked electron diffraction which will enhance the contrast of the image. Finally, the image will be enlarged as the transmitted electron passes through the projector lens. Phosphor screen is used in displaying the image. As if less electron is transmitted through the sample, the darker image will be displayed, and lighter image is displayed when more electron is transmitted through the sample.

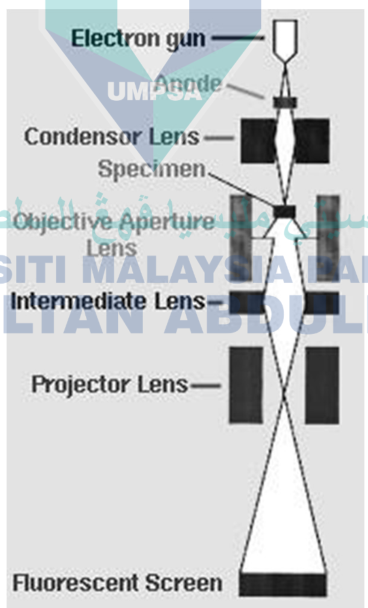

Figure 3. 9: Schematic illustration of TEM mechanism

Source: Mbule (2019)

3.3.2.1.1 TEM Sample preparation

8 to 10 ml of concentrated ZnO Nanostructure are diluted with distilled water. The solution is vigorously shaken and poured into the sample vial. The sample vial is then undergo sonication in the sonicated bath. After about 20 minutes of sonication, the sample is ready for TEM analysis. A drop of sample is drop onto blank microscope slide. The sample are ready to be observe under TEM.

Figure 3. 10: Transmission Electron Microscopy Machine in UM advance research centre

3.3.2.2 Field Emission Scanning Electron Microscope (FESEM)

A FESEM is used to visualize very small topographic details on the surface or entire or fractioned objects. Researchers in biology, chemistry and physics apply this technique to observe structures that may be as small as 1 nanometre. Electrons are liberated from a field emission source and accelerated in a high electrical field gradient. Within the high vacuum column these so-called primary electrons are focussed and deflected by electronic lenses to produce a narrow scan beam that bombards the object. As a result secondary electrons are emitted from each spot on the object. The angle and velocity of these secondary electrons relates to the surface structure of the object. A detector catches the secondary electrons and produces an electronic signal. This signal is amplified and transformed to a video scan-image that can be seen on a monitor or to a digital image that can be saved and processed further.

The generation of the X-rays in a SEM is a two-step process. In the first step, the electron beam hits the sample and transfers part of its energy to the atoms of the sample. This energy can be used by the electrons of the atoms to "jump" to an energy shell with higher energy or be knocked-off from the atom. If such a transition occurs, the electron leaves behind a hole. Holes have a positive charge and, in the second step of the process, attract the negatively-charged electrons from higher-energy shells. When an electron from such a higher-energy shell fills the hole of the lower-energy shell, the energy difference of this transition can be released in the form of an X-ray.

To detect them, the latest systems use the so-called silicon-drift detectors (SDDs). These are superior to the conventional Si(Li) detectors due to higher count rates, better resolution, and faster analytical capabilities. These detectors are placed under an angle, very close to the sample, and have the ability to measure the energy of the incoming photons that belong to the X-rays. The higher the solid angle between the detector and the sample, the higher the X-rays' detection probability, and therefore the likelihood of acquiring the best results. The data that is generated by EDX analysis consists of *spectra* with peaks corresponding to all the different elements that are present in the sample.

FESEM Sample preparation

2-3ml of ZnO Nanostructure sample are drop onto aluminium foil. The sample is then heated up on top of glass layer at the heating plate to avoid direct heating. The sample are heated up until it is dry into powder. The process are repeated for all sample. The samples are then placed on to pin mount specimen and placed into the FESEM machine.

3.3.3 Crystalline Structure Properties

3.3.3.1 X-ray powder diffraction (XRD)

X-Ray Diffraction, frequently abbreviated as XRD, is a non-destructive test method used to analyse the structure of crystalline materials. XRD analysis, by way of the study of the crystal structure, is used to identify the crystalline phases present in a material and thereby reveal chemical composition information.

X-ray diffraction is based on constructive interference of monochromatic X-rays and a crystalline sample. These X-rays are generated by a cathode ray tube, filtered to produce monochromatic radiation, collimated to concentrate, and directed toward the sample. The interaction of the incident rays with the sample produces constructive interference (and a diffracted ray) when conditions satisfy Bragg's Law. This law relates the wavelength of electromagnetic radiation to the diffraction angle and the lattice spacing in a crystalline sample. These diffracted X-rays are then detected, processed and counted. By scanning the sample through a range of 2θangles, all possible diffraction directions of the lattice should be attained due to the random orientation of the powdered material. Conversion of the diffraction peaks to d-spacing allows identification of the mineral because each mineral has a set of unique d-spacing. Typically, this is achieved by comparison of d-spacing with standard reference patterns.

To monitor on the crystalline size of particle, Scherer equation **(Equation 3.7)** are used to determine the crystalline structure based on the plot of diffraction and relation to Bragg’s Law.

$$D = \frac{K\lambda}{\beta\ Cos\ \theta} \qquad 3.7$$

where D reffering to mean size of the ordered (crystalline) domains (n.m), K is referring Dimensionless shape factor, with a value close to unity (0.9), λ is the X-ray wavelength (n.m), while β is referring to The line broadening at half the maximum intensity -FWHM (n.m) and θ is referring to the Bragg angle (°)

From the crystalline size of XRD results, the parameters of lattice in nanostructures can be determined from **Equation 3.8**, 3.9, 3.10 and 3.11 in order to determine a,c value, volume .

$$\frac{1}{d^2} = \frac{4}{3}\frac{(h^2+k^2+hk)}{a^2} + \frac{l^2}{c^2} \qquad 3.8$$

with d is referring to the spacing of inter-planar system where the h, k and l are known as the miller indices. Therefore, the volume, V of the unit cell of ZnO hexagonal wurtzite structure is calculated from **Equation 3.10.**

$$V = \frac{\sqrt{3}}{2}a^2c \qquad 3.10$$

Hence, U is t be determine where u referring to the position parameter which is a crucial variable for the calculation of ZnO bond length, L and is calculated based on **Equation 3.11.**

$$u = \frac{a^2}{3c^2} \qquad 3.11$$

Lastly, the Length, L of the crystalline structure are to be determine from **Equation 3.12.**

$$L=[\frac{a^3}{3}+(\frac{1}{2} - u)^2c^2]^{\frac{1}{2}} \qquad 3.12$$

XRD Sample preparation

The sample are heated on the heating plate to remains it powder form. Few tenths of a gram (or more) of the material, are place into a sample holder or onto the sample surface. Packing of fine powder into a sample holder. Smear uniformly onto a glass slide, assuring a flat upper surface pack into a sample container sprinkle on double sticky tape. Typically the substrate is amorphous to avoid interference. Care must be taken to create a flat upper surface and to achieve a random distribution of lattice orientations unless creating an oriented smear.

3.3.3.2 Fourier-transform infrared spectroscopy (FTIR)

A Fourier Transform InfraRed (FT-IR) Spectrometer is an instrument which acquires broadband Near InfraRed (NIR) to Far InfraRed (FIR) spectra. FTIR spectrometers collect all wavelengths simultaneously. This feature is called the Multiplex or Felgett Advantage. FT-IR is a method of obtaining infrared spectra by first collecting an interferogram of a sample signal using an interferometer, and then performing a Fourier Transform (FT) on the interferogram to obtain the spectrum. An FT-IR spectrometer collects and digitizes the interferogram, performs the FT function, and displays the spectrum.The basic components of a dispersive IR spectrometer include a radiation source, monochromator, and detector. The common IR radiation sources are inert solids that are heated electrically to promote thermal emission of radiation in the infrared region of the electromagnetic spectrum. The monochromator is a device used to disperse or separate a broad spectrum of IR radiation into individual narrow IR frequencies.

FTIR dispersive spectrometers have a double-beam design with two equivalent beams from the same source passing through the sample and reference chambers as independent beams. These reference and sample beams are alternately focused on the detector by making use of an optical chopper, such as, a sector mirror. One beam will proceed, traveling through the sample, while the other beam will pass through a reference species for analytical comparison of transmitted photon wave front information. After the incident radiation travels through the sample species, the emitted wave front of radiation is dispersed by a monochromator (gratings and slits) into its component frequencies. A combination of prisms or gratings with variable-slit mechanisms, mirrors, and filters comprise the dispersive system. Narrower slits gives better resolution by distinguishing more closely spaced frequencies of radiation and wider slits allow more light to reach the detector and provide better system sensitivity. The emitted wave front beam (analog spectral output) hits the detector and generates an electrical signal as a response.

The absorption of IR radiation by the sample, producing a change of IR radiation intensity, which gets detected as an off-null signal. Each frequency that passes through the sample is measured individually by the detector which consequently slows the process of scanning the entire IR region.

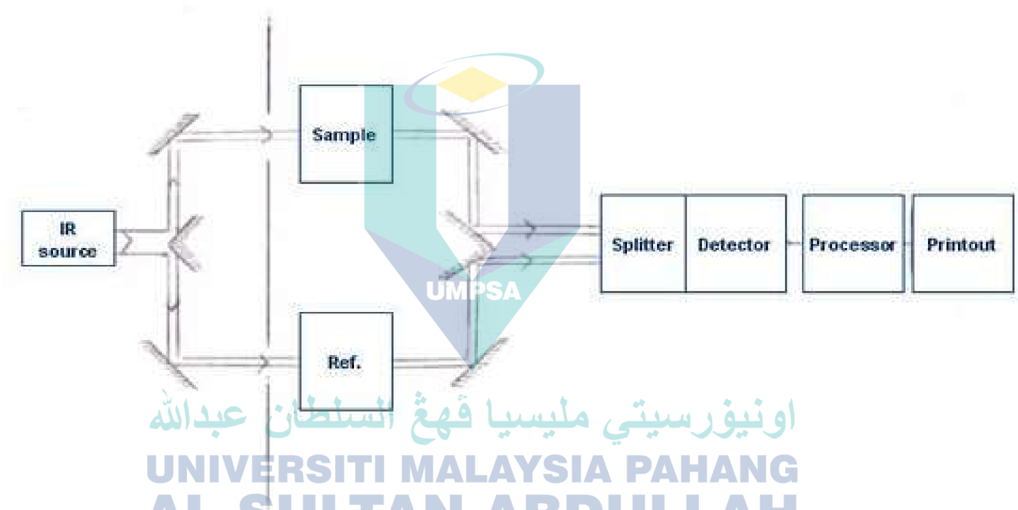

Figure 3. 11: FTIR schematic illustration

Source : Nancy Birkner (2019)

FTIR Sample preparation

Obtain a few gram of the material, as pure as possible. Place into a sample holder or onto the sample surface. Packing of fine powder into a sample holder. Smear uniformly onto a glass slide. The slides are then placed in to the FTIR spectroscopy and characterisation are begin.

3.3.4 Biological Properties

3.3.4.1 AATCC-100

AATCC-100 is an assay in determining the minimum inhibitory concentration (MIC) which is the lowest concentration of an antimicrobial (like an antifungal, antibiotic or bacteriostatic) drug that will inhibit the visible growth of a microorganism after overnight incubation. MICs can be determined on plates of solid growth medium (called agar) or broth dilution methods (in liquid growth media) after a pure culture is isolated. For example, to identify the MIC via broth dilution, identical doses of bacteria are cultured in wells of liquid media containing progressively lower concentrations of the drug. The minimum inhibitory concentration of the antibiotic is between the concentrations of the last well in which no bacteria grew and the next lower dose, which allowed bacterial growth. The percent bacterial reduction are calculate based on the efficacy calculation as in **Equation 3.13** :

$$\textit{Bacterial reduction efficacy from challenge inoculums (\%)} = \left(\frac{(A-B)}{A}\right) x\ 100 \qquad 3.13$$

where, *A* is the number of bacteria recovered from the inoculated treated test specimen immediately after inoculation (CFU/sample) and *B* is the number of bacteria recovered from the inoculated treated test specimen over the contact period (CFU/sample)

In this research, the bacterial focussed is on Staphylococcus aureus because the presence of bacterial in the agar are significant with the bacterial that presence in human sweat. Thus it will indicates the inhibition growth as ZnO-TA are tested onto it.

AATCC 100 Sample preparation

Bacteria Staphylococcus aureus (ATCC 6538) had been cultured on suitable agar till it ripe and fruiting (18-24 hours) at 35.0 ºC. By scraping the fruity culture, the spore collected had been transferred to 9 mL sterilized nutrient broth in a test tube to obtain a microbial count of about 108 CFU/mL. Then, the inoculums stock was diluted to a microbial count of about 105 CFU/mL. The test tube then was vortexed to bring the spores into suspension. This suspension was used as the spiking inoculum for the test. Sample was immersed into 4.8 ± 0.1 cm dimension fabric and placed in a sterile container. 1.0 ± 0.1mL of 105 CFU/mL spiking inoculum of the test organism was placed onto the top of sample in the container and allowed to wick through the sample. The inoculated sample was incubated for 24 hours at 35.0 ºC.

3.4 Summary

In order to recap, two syntheses methods are applied in the present work which are hydrothermal and green synthesised methods. The hydrothermal is employed for the ZnO nanostructures synthesis by using different reactant temperatures with similar concentration of sodium citrate (SC). Meanwhile, a green synthesis method is used for the formation of ZnO-TA nanostructures which yield different pH values upon the introduction of TA during the process. The as-prepared samples of pure ZnO and ZnO-TA nanostructures undergo properties measurements to confirm the structure, size, morphology, optical and antimicrobial performances. Different test equipments are used to determine different properties of samples. As for optical properties, the samples used UV-Visible and Photoluminescence spectroscopies to determine the UV absorbance and emission abilities which related to their band energy. For morphological properties determination, the samples are run using TEM and FESEM for physical structure, shape and size of the nanostructure. FTIR test is used to determine the chemical bonding properties of the ZnO nanostructures where the elements of the nanostructure are probed. Lastly, the biological test using AATCC 100 method to determine the microbacterial inhibitory ability of the nanostructure is used. The results of the experiment obtained are discussed in details in the next chapter.

CHAPTER 4

RESULTS AND DISCUSSION

4.1 Physical Properties

4.1.1 Surface Morphology and Mean Sizes of Nanostructures

The morphological structures for both ZnO and ZnO-TA nanostructures are examined using transmission electron microscope (TEM) and field-emission scanning electron microscopy (FESEM)-EDX with 125000X and 20000X magnification respectively. Ex-situ high magnification images of nanostructures are clearly seen from the TEM micrograph and shown in **Figure 4.1**. The interconnected aggregations of polyhedron ZnO nanostructures with smooth surface that extend along the [001] direction shown to have an average diameter, d_m of 10 ± 5 nm with narrow size range which synthesised at highest reaction temperature, 90℃ as shown in **Figure 4.1(a)**. As the temperature is decreases to 70 (**Figure 4.1 (b))** and 50℃ (**Figure 4.1 (c)),** the particle size is reduced to similar d_m at 8 ± 2 nm as well as the particle size distribution is confined in the range of 4 to 30 nm. The size distribution is described by a Gaussian function (noted as red line). These indicates that these three samples have only slight different dominated size range with virtually uniform and spherical in shape. It shall be noted that the structures studied in this thesis does highlighted the linear changes in the d_m with the changes in temperatures for the pure ZnO nanostructures. The images also show that the aggregations are crystalline which was further consolidated by the XRD data (**Subsection 4.1.2**). As we can noticed the cumulative distribution of the pure ZnO nanostructure showing steeper gradient which indicate presence of narrower size distribution of nanostructure. Thus, we can observe, the range size for pure ZnO nanostructure are smaller compared to ZnO-TA nanostructure.

For ZnO-TA nanostructures, the TEM micrographs show the morphologies of the samples made using the previous pure ZnO nanostructures (pH 7) synthesised at 70℃ added with TA are shown in **Figures 4.1 (d)** and **(e)** with the measured pH of 5 and 3, respectively. The 70℃ is chosen as the representative sample to indicate the morphological and the pH changes as the ZnO is introduced to TA. It could be seen that the size distributions of the nanostructures are drastically changed in which the histograms show the d_m of 18$\pm$ 3 nm and 22$\pm$ 4 nm, for pH 5 and 3, respectively, as compared to the pure one (8$\pm$2 nm) shown in **Figure 4.1(b)**). These conditions proved that the aggregation and agglomeration are occurred as the acidic environment is created by the TA. As the TA amount is increases (decreases the pH value), the aggregation is induced in which results from the coalescence of small particles from the attachment growth that depends fully on the volume of the projected particles of the samples (Ahmad, 2014). The merging of the particles is helps by the minor fluctuations caused by the acidic surrounding which caused a jump to contact. This condition is also known as oriented attachment (OA) or oriented aggregations which is an important crystal growth mechanism.

This can be considered as a direct evidence of OA which reveals the basic changes on the structure, surface chemistry of the nanocrystals, the solvent between the crystal and the resulting particles responds to the surrounding. In acidic condition, the presence of proton attack at the surface of ZnO is high. Generally, at lower pH (<pH 6), the tendency to produce a soluble ion of Zn2+ and Zn(OH)+ are higher. Therefore, the aggregation occurred as the protonation of the phenolic group take place in which reduced the accessibility of the functional group to squeeze between the ZnO nanocrystals (jump contact) and created larger attached particle. Upon the contact, the connecting neck between the particles are vanished. Particularly, for mild acidity of TA is considered between pH 7 and pH 3 (Bian, Mudunkotuwa, Rupasinghe, & Grassian, 2011). Apart from this, the drying process for TEM sample preparation, also promotes non-homogeneous deposition, thus, the aggregation of ZnO nanostructures is inevitable as the solvent evaporates (Lourdes C. S. Lopes et al., 2018; Michen et al., 2015).

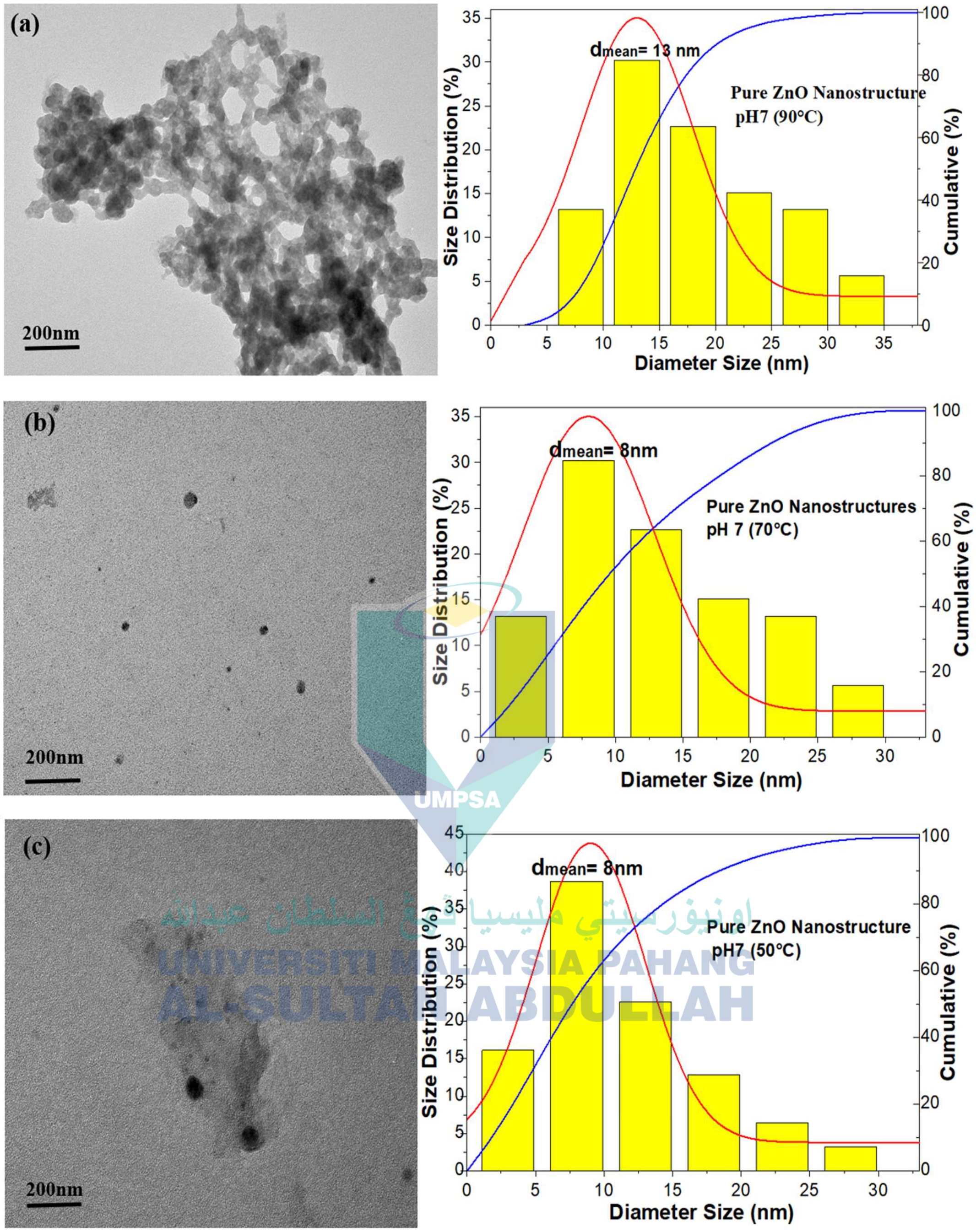

Figure 4. 1: TEM micrographs with size distribution of pure ZnO nanostructure synthesised at (a) 90, (b) 70 and (c) 50˚C. The TEM micrographs of ZnO-TA nanostructure made from the pure ZnO synthesised at 70 ˚C are shown in (d) for pH5 and (e) for pH 3. Noted that the size distribution of the particles is calculated based on the Gaussian distribution (red line)

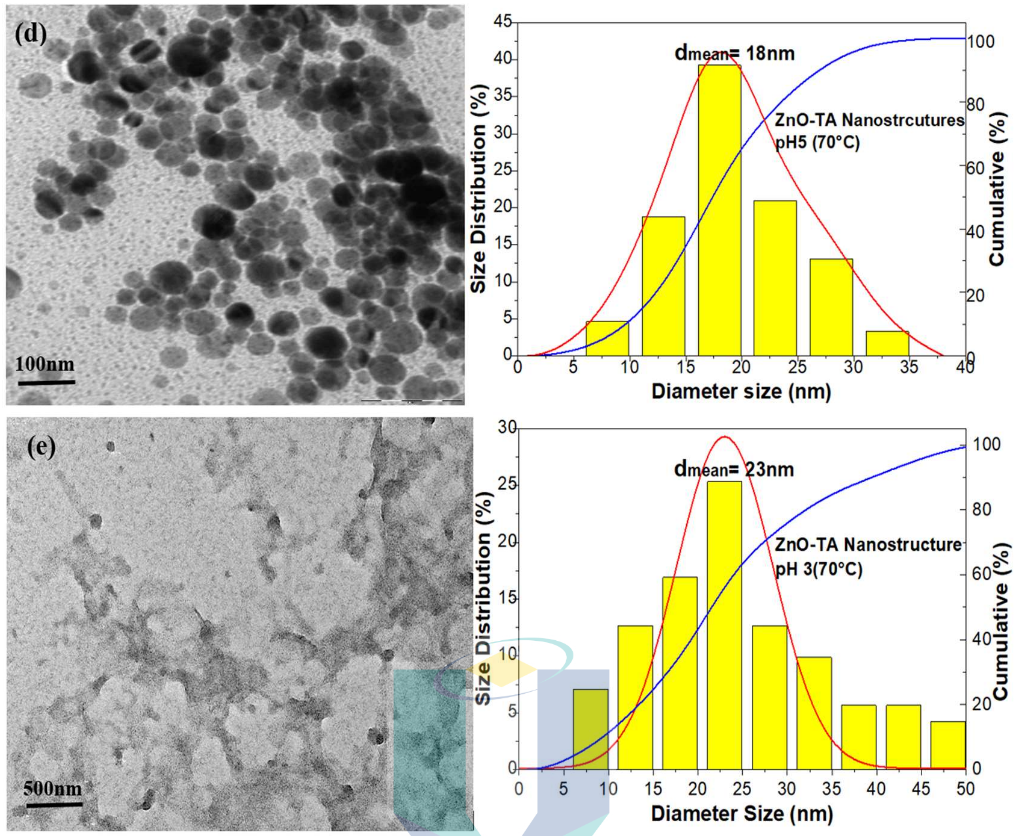

Figure 4.1 continued.

Table 4.1: Summary of the $\boldsymbol{d_m}$ for both ZnO and ZnO-TA nanostructures.

Nanostructure	**pH**	**Temperature (℃)**	d_m **(nm)**
ZnO	7	90	13
		70	8
		50	8
ZnO-TA	5	70	18
	3	70	23

For FESEM, the micrographs reveal the morphologies of ZnO and ZnO-TA nanostructures at magnifications ranging from 1000X to 20000X. It is observed that the morphological characteristics of pure ZnO nanostructures shown to have nanoplate-like structures which associated with different angle of orientation and sizes as indicated in **Figure 4.2(a)** to **4.2(c)** that synthesised at temperatures of 90, 70 and 50˚C, respectively. The measured smooth surface nanoplate-like structures show to have the d_m of 70 ± 20, 65 ± 15 and 80 ± 20 nm for 90, 70 and 50˚C, respectively. Clearly, the different measured d_m using TEM and FESEM is due to the different optimal spatial resolution whereas FESEM resolution is limited to ~0.5 nm, while TEMs, images with spatial resolution of even less than 50 pm. It is noted that the aggregation of nanostructures is clearly visible for all samples and mainly formed during the drying process of the FESEM samples. Similar morphology and aggregationd condition was observed from few reported works on ZnO nanostructures (Abdelmohsen et al., 2017). The associated energy dispersive x-ray (EDX) of FESEM for those three samples show the presence of Zn and O as the major elements with the mass percent of 79.94% and 17.85%, respectively. Hence, the results proved that the synthesised pure ZnO nanostructures are of high purity, which represents high Zn and O element compositions. Noted that the presence of small mass percent of Al element (2.21%) is due to the aluminium foil that used as a substrate for FESEM viewing. Interestingly, there are no trace of $Na_3C_6H_5O_7$ from the mass percent which proved that the emulsifying agent is fully removed during centrifugation process.

The attained morphologies and size variations of ZnO-TA nanostructures are shown in **Figures 4.2 (d)** to **(g)**. The measured pH 5 of samples upon the addition of TA are noted for **Figures 4.2 (d)** to **(f)** using the synthesised pure ZnO nanostructures at 90, 70 and 50˚C, respectively, whilst for **Figure 4.2 (g)** shows the measured pH 3 sample prepared using pure ZnO nanostructure sample synthesised at 90˚C. It is shows that the aggregation of nanoplate structures is significant which influenced by the pH due to the addition of TA. The structures are visibly connected to each other and believed is due to the TA present at the surface **(Scheme 4.1)** and have been discussed under the TEM section. The formation of interlink between the nanostructures without any space in between the particles are observed in which shows that the pure ZnO nanoplates are changed into the continuous connected coated ZnO nanoplate during ZnO-TA formation, which believed is due to the introduction of TA. The structures appeared to be bound together into continuous aggregation of various sizes with decrease in pH attributed to the increase of ionisation of TA. At low pH conditions, ionisation of TA is weak as described follows:

$$C_{76}H_{52}O_{46} = C_{76}H_{51}O_{46}^{-} \; + \; H^{+} \leftrightarrow \qquad pH < 6 \tag{4.1}$$

The surface dissolution of smooth polygonal nanoplate network at low pH conditions results in the formation of connected ZnO nanostructures (Abdelmohsen et al., 2017) revealed that the addition of TA controls the pH based on the breakable level of carbon and oxygen molecules bonding which proved by the increased in mass percent of carbon of 34.96, 42.76, 39.89 and 33.67% for pH 5(90°C), pH 5(70°C), pH 5(50°C) and pH 3(90°C), respectively from the EDX. Noted that TA compound ($C_{76}H_{52}O_{46}$) consists of long chain of carbon and oxygen atoms. The small percentage of composition of Al and Mg are due to usage of aluminium foil as a substrate during viewing.

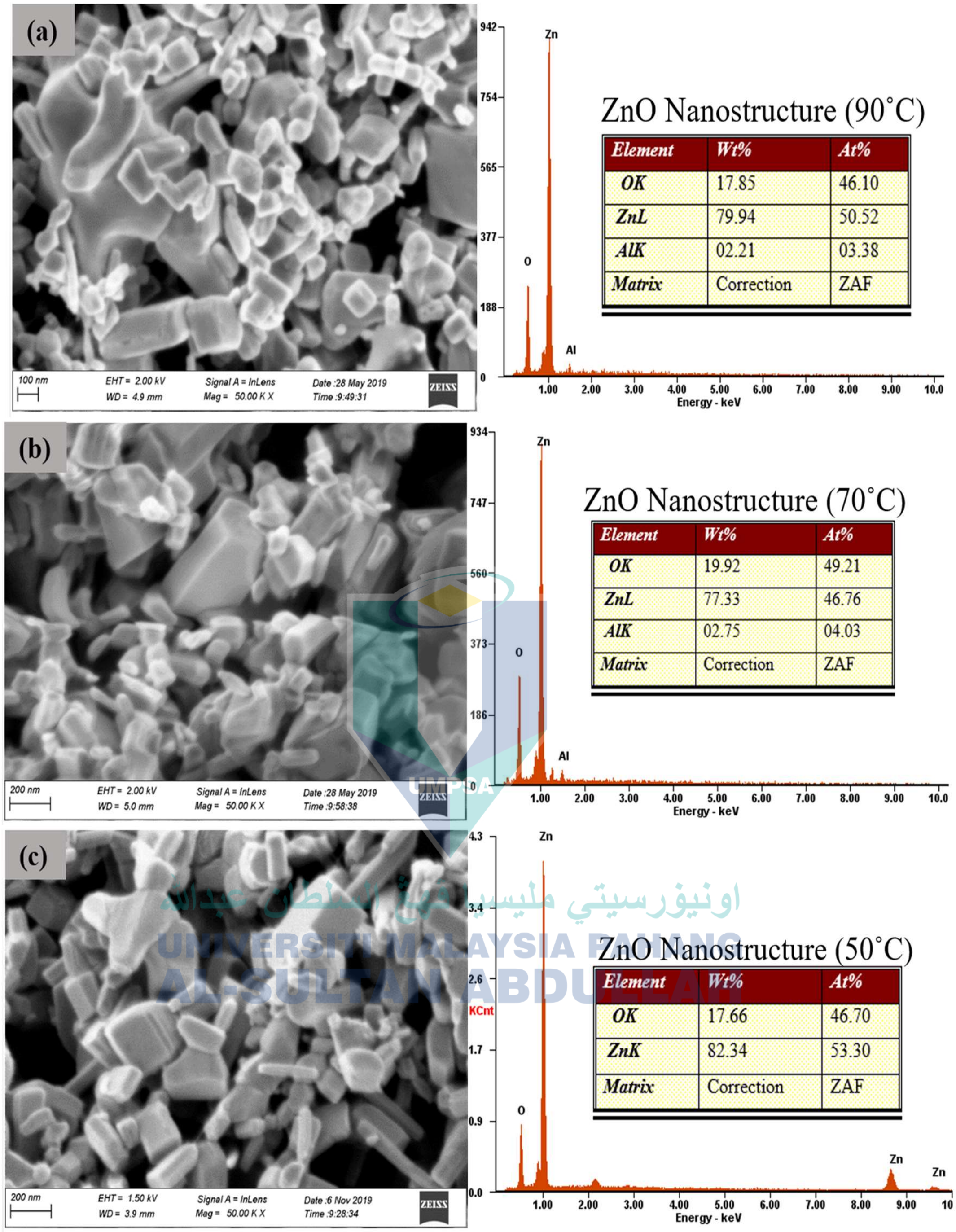

Figure 4. 2: FESEM images of the prepared pure ZnO nanostructures synthesised at (a) 90 ˚C, (b) 70 ˚C, (c) 50 ˚C and ZnO-TA nanostructure prepared using (d) 90 ˚C, (e) 70 ˚C, (f) 50 ˚C pure ZnO nanostructures for pH 5 and (g) 90 ˚C pure ZnO nanostructures for pH 3. The corresponding EDX graphs are also included for each samples.

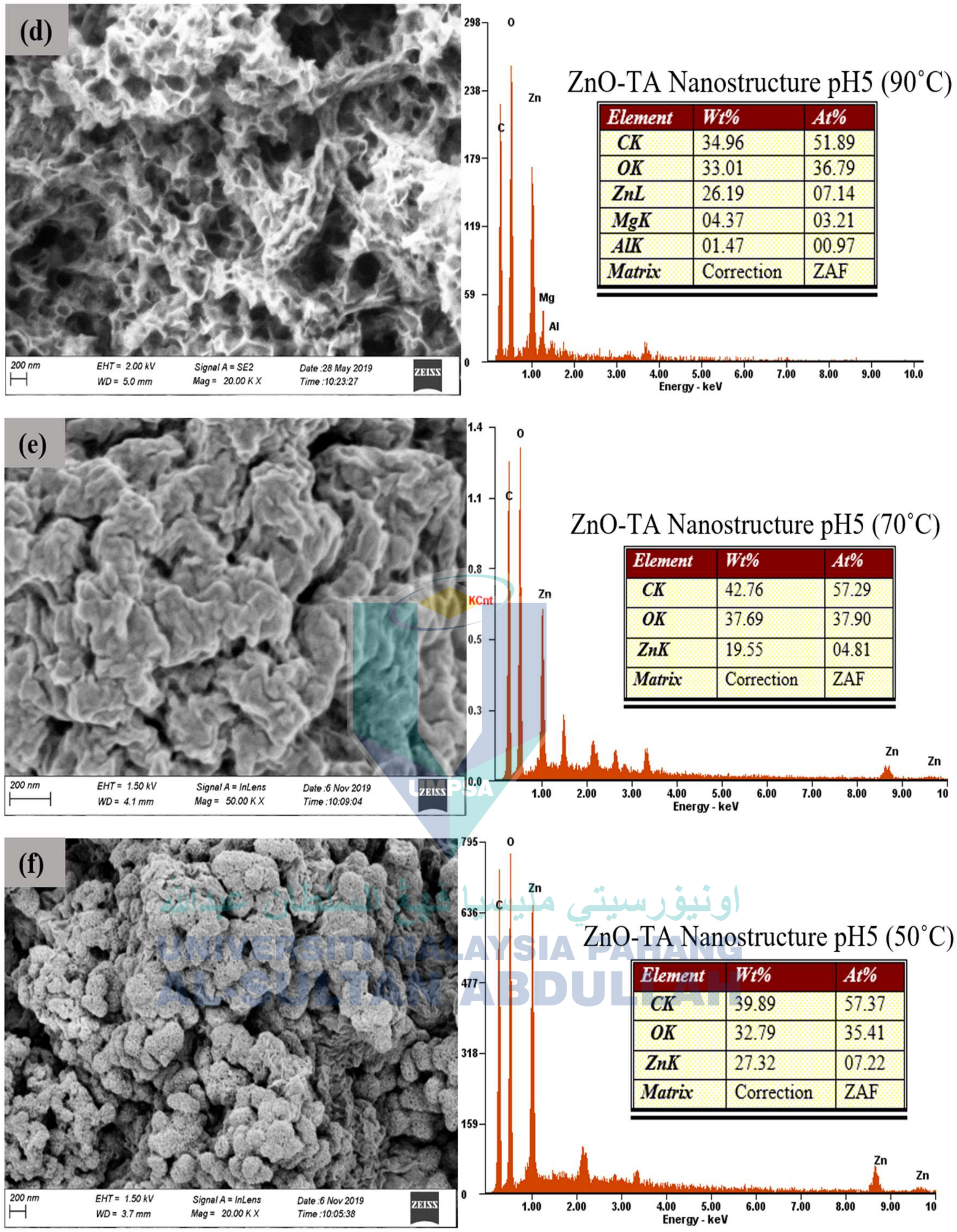

Figure 4.2 continued

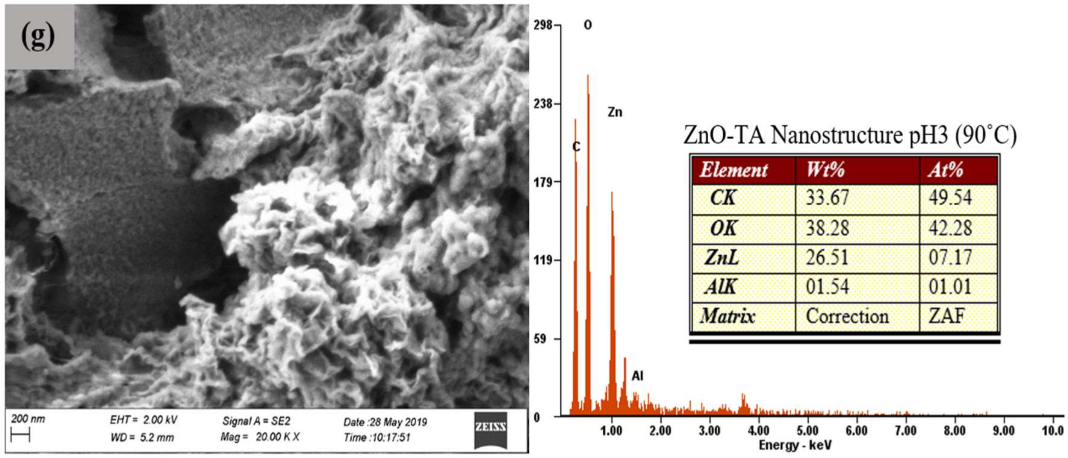

Figure 4.2 continued.

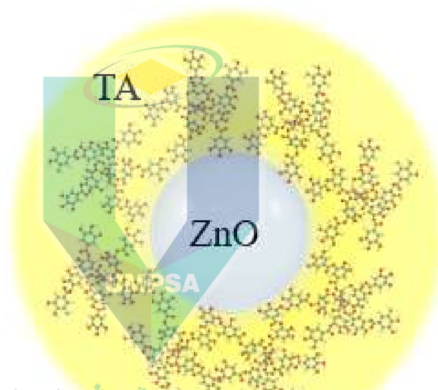

Scheme 4.1: Illustration on the TA binding on the surface of ZnO nanostructure.

Also, the conditions of ZnO-TA nanostructures can be explain based on the Brønsted-Lowry acid/base theory (Wiśniewska, Chibowski, & Urban, 2017). The Lewis hard and soft acids based on Brønsted-Lowry acid/base theory is broadly employed in metal/ligand inorganic chemistry for describing the stability of nanostructures and their compounds as well as any related reaction mechanisms which aid in explaining the morphological transition phenomenon (Šutka, Järvekülg, & Gross, 2019; Yuan et al., 2018). As the TA is introduced (for instance, with the amount of TA created the sample to be in ~ pH 3) to the ZnO nanostructure sample, the hydroxyl groups of TA adsorbed on the surface of ZnO surface which yield a Brønsted bases surrounding in the highly acidic medium that further accept the protons created from the reaction. Further details on acid/base theory and the relation with the energy level in terms of chemical bonding of ZnO and ZnO-TA nanostructures are explained in **Subchapter 4.2.1**.

Further on this, it is also noted that the reason for the increased in d_m as the morphological structure changed upon the introduction of TA to the ZnO nanostructure sample is due to the changes of the pH medium (from neutral to acidic medium). An acidic solution has a high concentration of hydrogen ions and this proved the decrease of OH- ion density in the sample (Shin et al., 2010) which also effect the morphological changes due to the dynamic growth explained by the Ostwald ripening (OR) phenomenon (Munjal, Kumar, Kumar, & Banati, 2019). In this case, the classical crystal model of OR take place when larger ZnO nanostructure reacted with acidic solution which induced the aggregation small crystalline nuclei. The OR process is the fundamental theory for OA as mentioned previously. OA is a process that took OR as part of the reaction in which the dissolution, precipitation, and ripening during the particle motion, collision, and aggregation processes formed those unique crystallographic orientations. Hence, the different is that the formation of complex nanostructure crystals with wide varieties morphologies including rods, chains, platelet, multipods and branched nanowires are mainly explained by OA which cannot be justified by classical OR (Cao, Gong, Shu, Zhu, & Liang, 2019; Greer, 2013). The mechanism for an oriented attachment (OA) during formation of suspension of ZnO nanostructures can be described as shown in **Scheme 4.2.**

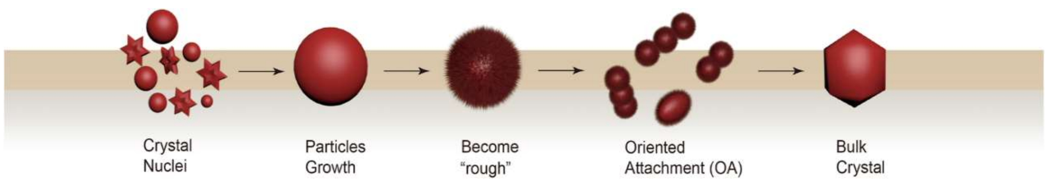

Scheme 4. 2: Illustration on the mechanism of OA adopted from (Cao et al., 2019)

4.1.2 Crystalline Structure Determination

The structural nature of the synthesised ZnO and ZnO-TA nanostructures are confirmed using XRD diffractogram as shown in **Figure 4.3.** It is revealed that the polycrystalline wurtzite structure of ZnO with the observed peak positions in agreement with reported data in Joint Committee on Powder Diffraction Standards (JCPDS, card no: 043-0002 obtained from library) are indexed for hexagonal ZnO as indicated in **Figure 4.3 (a)**. Noted that, for diffractogram test, the amount of sample is expanded for pure ZnO nanostructures with the total of five pure samples synthesised at temperatures of 90, 80, 70, 60 and 50 ℃. Three prominent peaks corresponding to reflections from [100], [002] and [101] atomic planes of ZnO phase. It shows the stability, probable directions for grain growth and are appointed as minimum energy growth phases of ZnO crystal. The presence of other low intensity reflections corresponding to [102], [110], [103], [200], [112] and [201] atomic planes of hexagonal ZnO lattice. In all the test samples for pure ZnO nanostructures, no peak corresponding to other phases or element emerged in the XRD analysis.

Surprisingly, further added TA concentration in as-synthesised ZnO-TA nanostructures samples inhibits the dominancy of crystalline phase by vanishing the peak intensities. It is observed that the addition of TA does dispel the diffraction peaks positions of the ZnO nanostructures as demonstrated in **Figures 4.3(b)** and **(c)** for samples made at pH 5 and pH 3, respectively, implied the absence of any significant lattice on the ZnO wurtzite structure. Only one sample from pH 5 shows the presence of complete ZnO atomic planes. It is believed that during the deposition of the samples on the glass substrate, the amount of ZnO dropped is higher than the TA molecule. Thus, only TA molecules with amorphous spectrum structure in nature are exhibited as they imprinted over ZnO nanostructures in accordance with FESEM analysis.

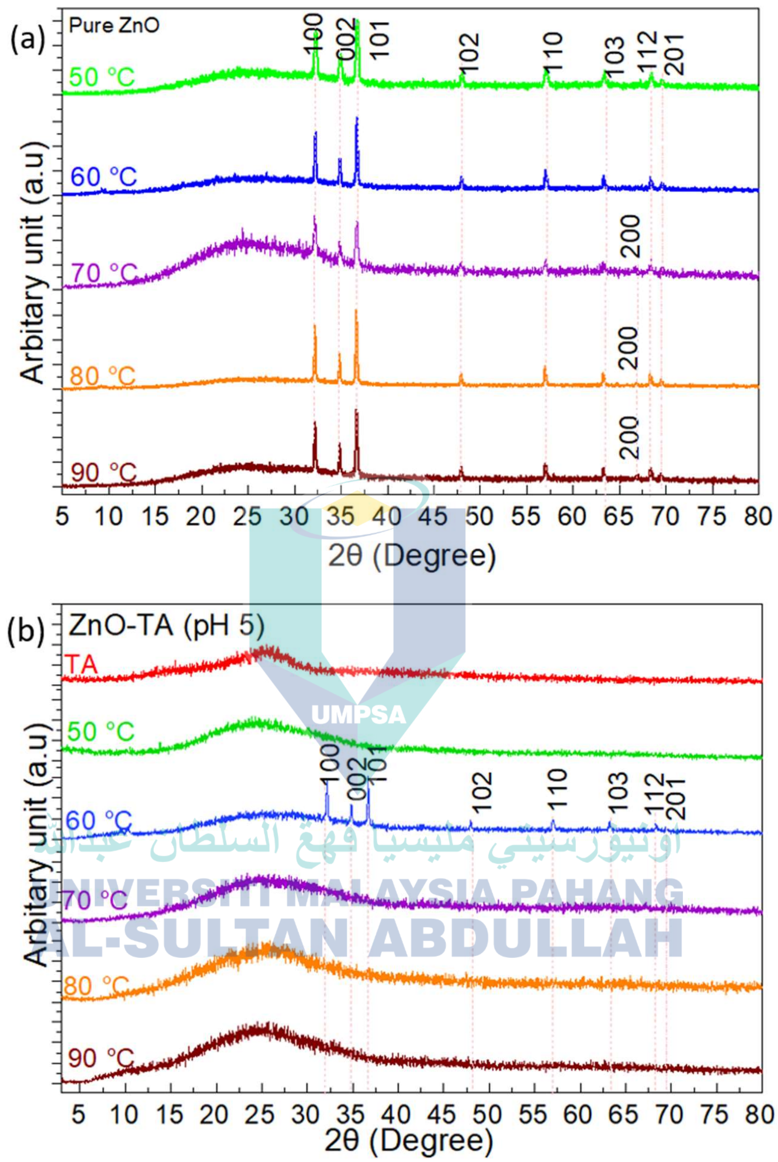

Figure 4. 3**:** XRD diffractograms for (a) pure ZnO nanostructures synthesised at 50, 60, 70, 80 and 90 °C with (b) the XRD peaks of ZnO-TA prepared at pH 5 and (c) pH 3 using pure ZnO nanostructures synthesised at 50, 60, 70, 80 and 90 °C. No responses relating to Zn or ZnO have been observed in some of the samples prepared at pH 5 and pH 3, suggesting the domination of TA in all samples.

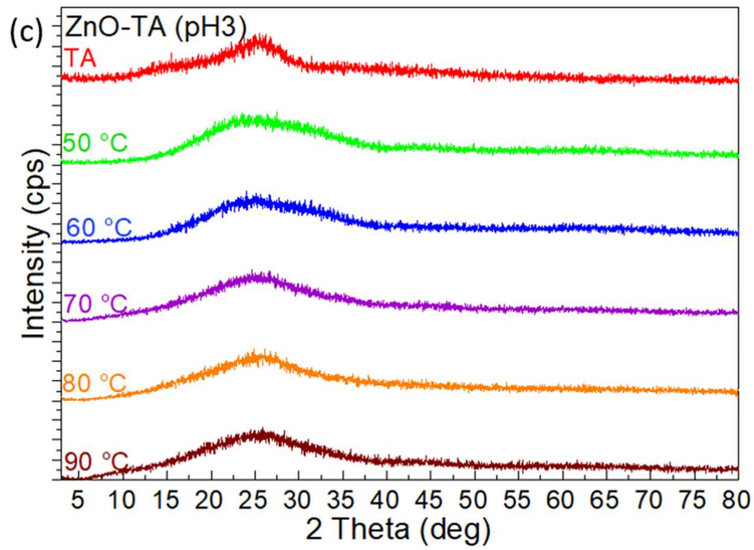

Figure 4.3 continued

The structural informations on the crystallite size (*D*), lattice parameters (*a*, *c* and *V*) with position parameter (*u*) and ZnO bond length (*L*) for both pure ZnO and ZnO-TA nanostructures data obtained from the XRD results are tabulated in **Table 4.2.** The *D* is obtained based on the calculation of known Debye-Scherrer's equation (**Equation 3.7**). The calculated *D* is 8.52, 8.03, 5.79, 7.91 and 9.93 nm corresponding to pure ZnO nanostructures synthesised at 50, 60, 70, 80 and 90 °C, respectively. The crystalline size (*D*) of the pristine pure ZnO nanostructures is parallel to the particle size obtained from TEM which shows a significant decreased from 8.52 nm to 8.07 nm and 5.7909 nm as the pure ZnO are synthesised in temperature increase from 50, 60 and 70 ˚C. The mean *D* of the pristine are later increased to 7.91 nm and 9.9313 nm after increased in reaction temperature of 80 and 90˚C respectively. While as ZnO are capped with TA, dominancy of TA is obvious as the XRD graph showing amorphous structure with only one sample have crystalline peak with crystalline size of 14.99 nm. The obtained crystalline size show a minor variation with the synthetic conditions. The biggest deviation in crystalline size is observed for the ZnO synthesized with addition of TA (pH 5). It shall be noted that, the percentage of Zn^{2+} released from the ZnO-TA nanostructures was contribution from the increase of TA concentration (decrease in pH). These results indicated that the TA caused the dissolution of ZnO nanostructures due to the modification effects of combined pH solution and complexation reaction.

Table 4.2**:** The lattice parameters and the density of each pristine ZnO, and ZnO-TA evaluated from the XRD patterns. D are the crystalline diameter while as monitored, the lattice parameter include the lattice constant α and c represent basal and height parameter respectively, length L, volume V, and u representing internal atomic position.

Pristine Nanostructure	**pH**	**Temperature (℃)**	***D* (nm)**	**Lattice Parameters** *α*(Å)	*c*(Å)	*V*(Å^3)	*u*	*L*(Å)
ZnO	7	90	9.93	3.39	5.39	56.08	0.13	2.81
		80	7.91	3.80	5.36	55.84	0.16	2.68
		70	5.79	4.45	5.36	55.85	0.22	2.47
		60	8.03	3.59	5.48	57.01	0.14	2.79
		50	8.52	3.48	5.51	57.33	0.13	2.84
ZnO-TA	5	60	14.99	2.63	5.49	57.12	0.07	3.06

The parameters of lattice in ZnO-TA nanostructures given by *a* and *c* are calculated. Lattice parameters *a* and *c* represent the edge length of the basal plane hexagon and the axial height of the unit cell perpendicular to the basal plane respectively. The base lattice constant (*α)* Pure ZnO nanostructure increasing from ~ 3.48 to ~4.45 as the synthesised temperature are increase from 50 to 70 ˚C. The base lattice constant are then decrease to ~3.39 Å as the synthesised temperature increase to 90 ˚C. While the height of lattice constant (*c*) for pure ZnO nanostructure increasing from ~3.36 to 3.48 Å as the synthesised temperature increase from 50 to 90 ˚C. Besides base and height of lattice constant, the length (*L*) of are also calculated. The length of the crystalline structure of pure ZnO nanostructure decreasing from 2.84 to 2.47 Å upon the rising of reaction temperature form 50 to 70 ˚C. the length of crystalline structure later increase to 2.81 Å as the synthesised temperature reach 90 ˚C. While as for ZnO-TA of pH5, the base and height lattice constant decrease to 2.63 and 5.49 Å respectively while the length of the lattice increase to 3.06 Å.

The wurtzite structure of ZnO is composed of two inter-penetrating 8 hexagonal close packed (hcp) sub-lattices containing four atoms per unit cell of one type. Every atom of one kind is surrounded by four atoms of the other kind placed at the corner of a tetrahedron or vice versa. These sub-lattices are displaced with respect to each other along the *c*-axis by the amount u, known as internal parameter. The fractional atomic coordinates of oxygen is expressed in terms of u which is also linked with anion-cation bond length parallel to the c-axis. The pure ZnO nanostructure results into increase of internal parameter (u) from 0.13~ to 0.22 correspond with the increase of synthesised temperature from 50 to 70˚C. The internal parameter are then decrease back to ~ 0.13 as the synthesised temperature continue increase to 90˚C. From the lattice constant, it results into the volume of the crystalline structure (V). The V shows a decreased from 57.3364 to 55.8547 Å^3 as the synthesised temperature increase from 50 to 70 ˚C, the V are later increase to 56.08 Å^3 upon the increased in reaction temperatures to 90 ˚C. Thus, the increase in volume shows a lattice contraction that yield the increased in grain size formation (Wei et al., 2007). While ZnO-TA nanostructure showing the smallest internal lattice parameter, u of ~0.07. From the lattice constant calculated, the ZnO-TA crystalline structure showing volume of 57.12 $\mathring{A}^3$.

Zn^{2+} known for its 0.06 nm ionic radii and thus, the decrease in particle size results in increase the value of lattice constant. Thus, to be compared with the results obtain, it shows that ZnO-TA nanostructure have larger value of lattice constant that may be occur due to surface dissolve of ZnO by TA. From the results, pure ZnO nanostructure showing smaller crystalline diameter compared to ZnO-TA nanostructure. The increase of crystalline nanostructure of ZnO-TA nanostructure are due to aggregation that occurred as discuss in subchapter 4.1.1. The XRD data of ZnO-TA with addition of further TA indicate there is only one sample with peaks corresponding to ZnO was found, which disclose the dominancy of TA that affect their wurtzite structure at low pH level and high concentration. Increase in TA concentration beyond 2% caused the distortion of as synthesised ZnO-TA lattice and at some points in which the reflections of ZnO disappeared and TA single amorphous peak dominated. It needs to be noted that the decrease of the particle size is accompanied with a significant increase in the yield. It may be, therefore, assumed that the increase of the yield is caused by an increased supersaturation which primarily affects nucleation of smaller crystallites and the growth of which is hindered. By capping ZnO with TA, cause to crystals to growth with higher aspect ratio of 3:1. Letting the pH to reach acidity medium also leads to a truncation of the capping pyramids clearly exposing well developed faces. With respect to the wurtzite structure of the prepared ZnO one can assume there are three preferential growth directions: along the *z*-axis.

4.2 Chemical Structure

4.2.1 Chemical Bonding

FTIR is one of the confirmatory technique for nanostructures formation and highlights the behaviour such as the vibrational and rotational modes of the existing molecules. The technique helps to identify the functional and possible phytochemical molecules involved in the stabilisation of pure ZnO and ZnO-TA nanostructures as shown in **Figure 4.4**. For pure ZnO nanostructures shown in **Figure 4.4 (a)** synthesised at 50, 70 and 90℃ which are measured to have pH 7, shows the available broad peak at region around 3400 cm^{-1} indicated the presence of O-H stretching and deformation in the external band of pure ZnO nanostructures due to water adsorption on surface of ZnO. This is confirmed by other literatures that suggested that at average of 3400 cm^{-1} is due to the O-H stretching caused by the loss of water molecule (B. Kumar, Smita, Cumbal, & Debut, 2014; Markova-Deneva, 2010; Shahwan et al., 2011; V. Parthasarathi, 2011; Vaezi & Sadrnezhaad, 2007; Xiong, Pal, Serrano, Ucer, & Williams, 2006; Zak, Abrishami, Majid, Yousefi, & Hosseini, 2011). A small hump at 2047, 2064 and 2079 cm^{-1} for synthesised samples at 50, 70 and 90 ˚C, respectively, indicated the presence O-C-O band (Husain, Rahman, Ali, & Alvi, 2013). While the other small peak in between region 1300 to 1600 cm^{-1} indicated the C=O stretching. Both type of stretching of O-C-O and C=O are due to the atmospheric absorption at the preparation time of sample in non-vacuum system (Husain et al., 2013; P. R. Kumar et al., 2014; Zak et al., 2011) with less significant in sample at 90℃ which might be due to the high- temperature exposure which eliminate the trace of atmospheric absorption. Moreover, several small humps have been formed in the area around 700 to 1100 cm^{-1}, which proved the presence of C-H and =C-H functional groups. The very small amount of carbon-hydrogen functional group is because of the effect of trisodium citrate. The presence of the peaks in the area of 500 to 540 cm^{-1} are due to the stretching mode of ZnO (Hedayati, 2015; Kumar, Jung, Bharathi, Lim, & Kim, 2014; Vaezi & Sadrnezhaad, 2007; Xiong, Pal, Serrano, Ucer, & Williams, 2006).

Meanwhile, the presence of adsorbed TA molecules as functional groups on the surface of ZnO nanostructures are indicated in **Figures 4.4** (**b)** and **(c**). TA has yield some chemical alterations on the surface of pure ZnO nanostructures during the formation process. A broad band of pure TA at 3400 cm^{-1} which is also almost similar to the strong peak exhibits by pure ZnO nanostructures may have originated from the polyphenols that are present in the system. This band is assigned to the hydroxyl groups (O-H) H-bonded broad and strong and C-H (aromatic medium) (Wahyono, Astuti, Wiryawan, Sugoro, & Jayanegara, 2019). TA also showing small hump at peak of 2043 cm^{-1} in which are due to C-H stretching vibration of alkane groups. Besides, Tannic acid contains some aromatic esters due to the signal characteristics of carbonyl groups C=O stretching (1501 cm^{-1}) and C-O (1384 cm-1). Stated that C=O stretching and C-O vibration observed near 1500-1600 cm^{-1} and 1300-1100 cm^{-1} range respectively (Husain, Rahman, Ali, & Alvi, 2013; Wahyono et al., 2019).

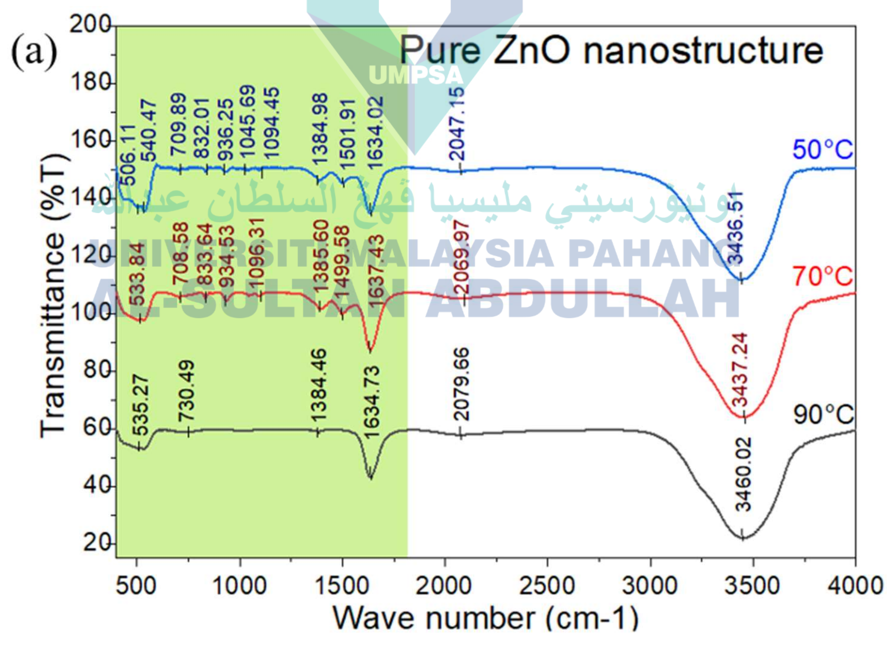

Figure 4.4: Chemical bonding studied by using FTIR which recorded for (a) selected pure ZnO nanostructures synthesised at 50, 70 and 90℃ as well as for the prepared ZnO-TA nanostructure samples of (b) pH5 and (c) pH3.

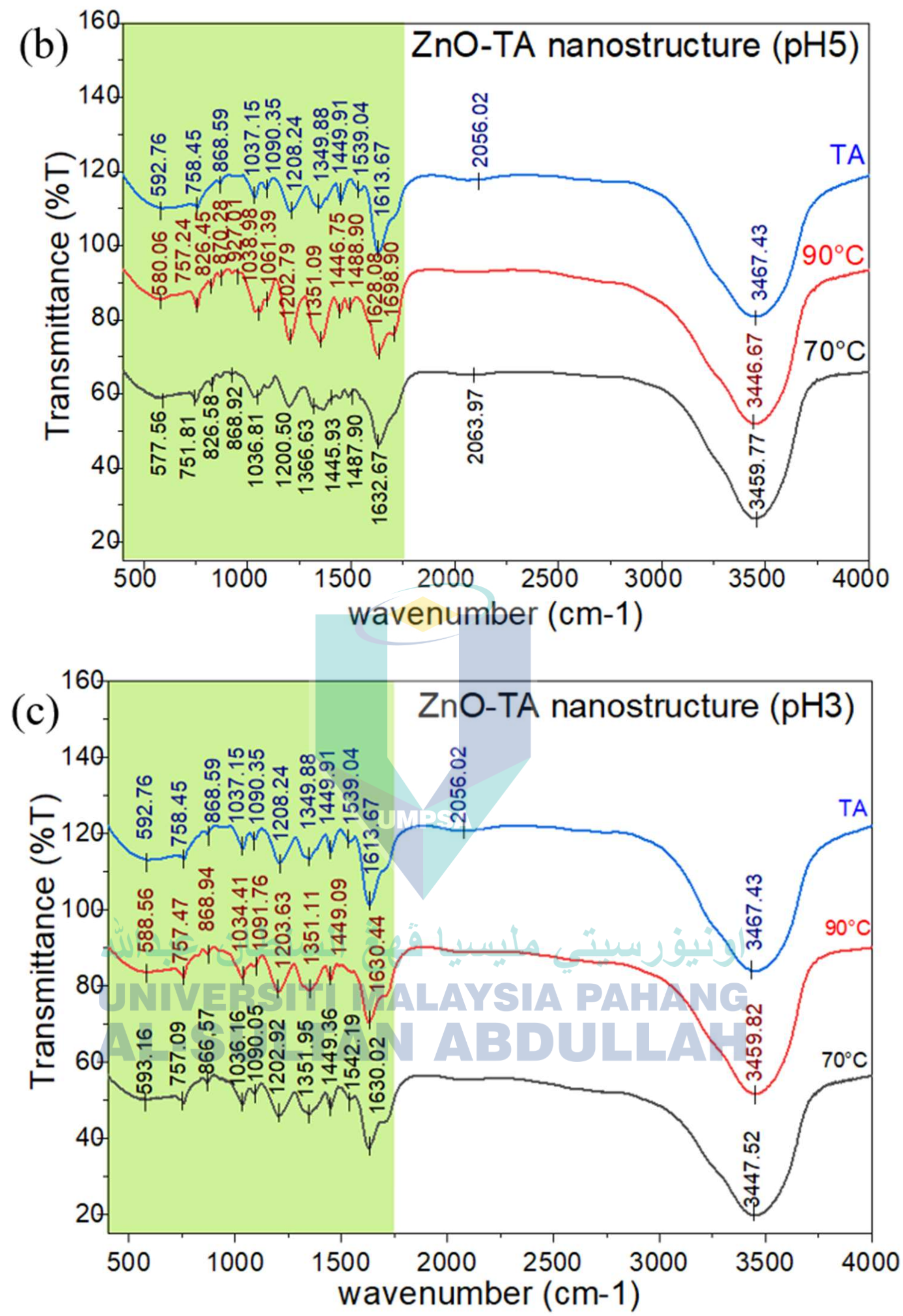

Figure 4.4 contnued

As for ZnO-TA nanostructure, the sample showing combine region peaks as pure ZnO nanostructure and TA. As shown in **Figure 4.4** (**b** and **c**), it can be clearly seen that the number of peak are increasing compared to pure ZnO nanostructure. For pH5 samples, the strong peaks at 2446 and 3459 cm^{-1} are dominantly influence by O-H stretching for synthesised samples of 90 and 70˚C, respectively. Also, at pH3, strong and wide peaks are shown at 3446 and 3447 cm^{-1} for 90 and 70˚C samples, respectively. Besides, the peak at region of at 580 and 577 cm^{-1} shows the bonding of Zn-O, for both 90 and 70˚C, respectively. While, the ZnO-TA nanostructure at pH3 shows the peaks at 588 and 593 cm^{-1}. The peak are slightly shifted compared to pure ZnO nanostructure samples as discussed beforehand (**Figure 4.4** (**a**)).The shifted may be associated with oxygen deficiency and/or oxygen vacancy defect complex in ZnO nanostructure. The intensity of the oxygen-deficiency related defect-complex band does not appear to change much on the particle size but it were indicating the probability of bulk defects (Xiong et al., 2006). Meanwhile, the O-H stretching are dominant in both TA and ZnO-TA nanostructure samples. This is due to loss of water molecule as it is dried into powder. Besides, the significant different between pure and TA capped ZnO nanostructures is the increasing number of peak presence in region between 700 to 1500 cm^{-1}. This region indicates the stretching of C=O and C-O bond. The peak around this region are not really significant as the carbon element are only presence CO^2 due to non-vacuum condition during synthesising process. While for ZnO-TA, the stretching are dominant due to presence of element C=O in TA. As we know, TA molecular are $C_{76}H_{53}O_{46}$, thus the increase of carboxylate element dominate in the sample (Estrada-Urbina, Cruz-Alonso, Santander-González, Méndez-Albores, & Vázquez-Durán, 2018; Zak, Abrishami, Majid, Yousefi, & Hosseini, 2011). The spectral signatures of carboxylate impurities essentially increasing, indicating the possible association of phenolic group form TA with zinc carboxylate and conversion to ZnO during synthesising. The intensity of the hydroxyl peak follows an increasing trend as compared with the synthesised pure ZnO nanostructure.

The structural analysis from FTIR also determined by surface chemistry of solids related to the acid/base theories, determination on surface acidity or basicity theories is difficult to tackle. The main focus here is on the concept of Lewis hard and soft acid bases, which is commonly used in metal / ligand inorganic chemistry to define the stability of nanostructures and their compounds as well as any associated reaction mechanisms, help in the morphological transition phenomenon based on the theory of Brønsted-Lowry acid / base and also the prediction of reactivity of frontier molecular orbital (FMO) theory (Laminack, Baker, & Gole, 2015; Šutka et al., 2019; Yuan et al., 2018). Basically, most of metal oxide surfaces including ZnO nanostructures are hydroxylated to certain level when aqueous (water) vapour is exist under normal condition. In this case, these hydroxyl surfaces are considered to act as Brønsted acid or base spots as the system provide ability to donate or accept a proton (Zn2+ ions), respectively. The consideration on cationic Zn centres (Zn2+) according to hard/soft acid/base theory which acts as Lewis acid sites is also known for its LUMO (Lowest Unoccupied Molecular Orbital) energy with the anionic lattice oxygen (O2−) centres serve as Lewis bases and known for its HOMO (Highest Occupied Molecular Orbital) energy as illustrate in scheme 1(B). The combined activity involves the interaction between Zn cations (LUMO) with the ligand (significant filled-empty interaction) (HUMO) which induce a bonding atomic orbital that aaccounts for the produced properties as illustrated in **Scheme 4.3.**

Theoretically, the intimate orbital interactions produced energy that is greater than the stabilising energy which helps in occupying the Lewis pair of electron to the newly formed atomic orbitals. The orbital frontier interaction (HOMOLUMO interaction) resulted in the development of molecular orbit requiring high stability, in which resulting in an immediate decrease in energy. It is therefore presumed that the related acid species energy difference (LUMO) with base species (HOMO) accounted for the ZnO propensity to have a morphological change as the system contracts with TAs under specific conditions. The catalytic activity efficiency of ZnO nanostructures or other metal oxides does depend on the ability of acid/base sites. Here, as the Zn nanostructures are mixed to TA solution (mild acidic 3>pH<7), The phenolic hydroxyl bonds adhered to the surface of the ZnO nanostructure formed as Brønsted bases in a mild acid solution and were capable of receiving ionic protons as shown in the molecular orbital diagram (**Scheme 4.3**). Exciton dissociation typically stimulated by charge transfer occurs from the reaction between acceptor and donor particles. The exciton dissociation is constructive at the interface area (LUMO) between the material particles with different electron affinity (EA) and ionisation potential (IP) as in HOMO (Breazu et al., 2018).

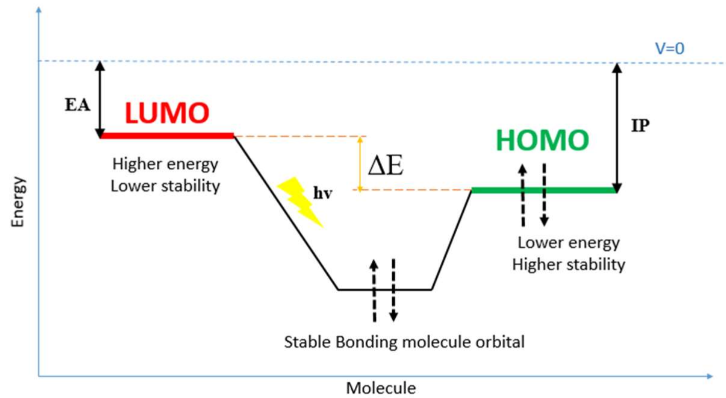

Scheme 4. 3: Schematic illustration on HOMO-LUMO interaction in FMO perspective adopted from (Che Lah & Kamaruzaman, 2019).

4.3 Optical Properties

4.3.1 Absorbance Characteristic

The optical characteristic for both ZnO and ZnO-TA nanostructures were carried out using UV-Vis spectrophotometer with the focused on the surface plasmon resonance (SPR) characteristic absorbance behaviour based on the several samples prepared. To analyse the characteristics of UV light for both ZnO and ZnO-TA nanostructures, water, which acts as the solvent is used as a baseline in monitoring the absorbance of the prepared samples. The absorbance wavelength range is fixed between 200 to 800 nm. The pure ZnO samples synthesised at different reaction temperatures (50, 60, 70, 80 and 90°C) with five samples treated with different pH based on different added TA concentration were critically observed (as discussed in **subsection 3.2.3** from **Chapter 3**). The effect of added solution of TA on pure ZnO nanostructure samples is monitored based on the range of peak absorbance obtained for each group of measured pH. Based on the test, the results of the absorbance peak obtained are summarised in **Table 4.3**. The pure ZnO nanostructure samples indicated the absorbance peaks at shorter wavelength as compared to ZnO-TA nanostructures. Hence, the initial significant effect can be deduced from the location of the wavelength number between pure ZnO and the treated ZnO samples with TA in which proved that the presence of TA control the larger formation (due to the aggregation process) of ZnO nanostructures.

Table 4.3 : Summary on the absorbance peak for the as-synthesised ZnO nanostructures at different reaction temperatures and ZnO-TA nanostructures obtained from different pH values upon the addition of the TA solution. Noted that the samples with mild acidic pH (pH 6 to pH 3) showed blue-shift peak absorbance characteristic due to influence of acidic nature of TA.

Nanostructure	**pH**	**Temperature (℃)**	d_m **(nm)**	**Absorbance Peak (~ nm)**
ZnO	7 (neutral)	90	13	381
		80	-	379.5
		70	8	380
		60	-	382
		50	8	379
ZnO-TA	6	90	-	300
		80		317.5
		70		320.5
		60		320.5
		50		300.5
	5	90	-	300
		80		308
		70		310.5
		60	-	312
		50		300
	4	90	-	308
		80		312
		70		321.5
		60		303
		50		309
	3	90	-	317
		80		318
		70	23	317.5
		60	-	318
		50		313
TA	3	-	-	310

The observation on blue-shifting pattern of the wavelength number of TA treated ZnO nanostructures is based on the pure ZnO nanostructure absorbance peaks shown in **Figure 4.5**. For pure ZnO nanostructure (pH7) the absorbance peaks were shown at the range of 380 till 386 nm and proved to be in accordance with the existing literatures reported on the ZnO nanostructures (Jayaseelan et al., 2012; Matinise et al., 2017; Ogunyemi et al., 2019; Suresh et al., 2015; Velmurugan et al., 2016) . Also, some of the works showed that the SPR characteristic of ZnO nanostructures can be found at the wavelength in between 350 to 400 nm in which the peak position for similar size distribution range (as discussed in **Section 4.1**) is mainly influenced by the interparticle distance and also the types of encompassing media. Thus, the SPR absorbance is very delicate and super sensitive to the presence of surrounding nature, size and morphology of the nanostructure (Agrawal et al., 2018; Gupta & Kant, 2018; Jung, Yeo, Kim, Ki, & Gu, 2018; Velmurugan et al., 2016). For pure ZnO nanostructures without any influence of other molecules, electrons are able to move freely as the conduction and valence band located near to each other (narrow bandgap). Theoretically, the free electrons would enhanced the increase of the SPR absorption band intensity which directly indicates the collective oscillation resonance of ZnO nanostructure based on the excitation of surface electromagnetic waves at the air-ZnO interface due to the variation of chemical oxidation and photochemical control (Agrawal et al., 2018; Noginov et al., 2006).

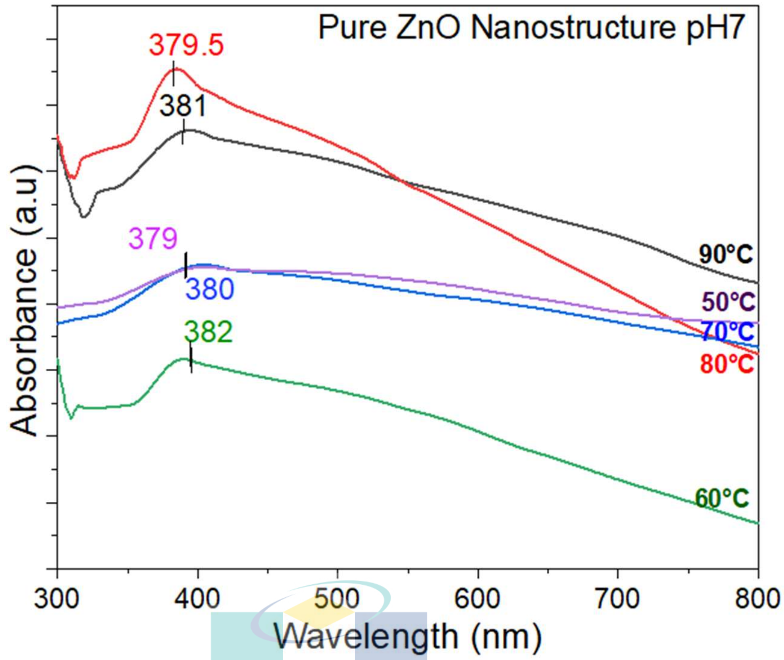

Figure 4. 5: The UV-Vis absorbance spectra for ZnO nanostructures synthesised at 50, 60, 70, 80 and 90°C. Noted that all samples showed narrow range of absorbance peak with varying of intensity that indicate the varying size distribution of nanostructures.

It is observed that for pure ZnO nanostructures synthesised at different reaction temperatures demonstrated different varying intensities and bandwidth range resulting from the variation of d_m size and size distribution of the nanostructures but with narrow range frequency resonance absorption at specified ZnO range. These are due to the polarisation of electrons contributed by a stronger ionic core which is the result from the enhanced electric field wave (Hitanshu Kumar, 2014). Thus, the polarisation force is re-establish in creating dipolar wavering among the presence electrons. Meanwhile, the SPR absorption band expanded as the smaller nanostructure size presence which proved the emergence of quantum size phenomenon. Moreover, the increasing integrated peak area of the band indicates the decrease in the inter-particle gap, which is evidence of larger nanostructures with the probabilities of aggregation (Addison & Brolo, 2006; Dmitruk, Alexeenko, Kotko, Vedral, & Pinchuk, 2012; Mayer et al., 2019; Noginov et al., 2006; Scholl, Koh, & Dionne, 2012; Zhang et al., 2019) .

In the present study, the ZnO nanostructures are originally stable due to the presence of negative surface charges which prevent two particles from aggregating in the presence of strong columbic repulsion (energy). However, as the van der walls forces become dominant, the nanostructures are triggered to aggregations and forming large cluster of structure. The nature of the prepared ZnO nanostructures seems to quickly sediment at the bottom of the glass vial, this is due to the water solvent which shows the highly hydrophobic behaviour which may be changed to hydrophilic via irradiation with a light of energy more than the ZnO band gap (with a wavelength less then 375 nm) without any influence of other molecules in surrounding medium (Das, Choi, Kar, & Myoung, 2009; Feng et al., 2004; Kar, Das, Choi, Lee, & Myoung, 2010; Kekkonen et al., 2010; Lü et al., 2010; Papadopoulou et al., 2009; Tarwal & Patil, 2010).

The characteristics of having shorter wavelength spectra in the range of ~ 379 to ~382 nm for all peak absorbance of ZnO nanostructures indicated that that the as-synthesised ZnO nanostructures shown an excellent characteristics of UV absorbent particles for UVA wavelength (at the range of 320 to 400 nm) with UVB wavelengths contributed particularly from ZnO-TA nanostructures (280 to 320 nm) and were consistent with the other reported studies on ZnO nanostructures (Es'haghi, 2018) which have summarised in **Table 4.3**. From the peak wavelength number, the as-synthesised ZnO nanostructures proved to be able to absorbed UV-A which majorly known to cause a skin damage to human being if they continuously directly exposed (Craig, Earnshaw, & Virós, 2018; D'Orazio, Jarrett, Amaro-Ortiz, & Scott, 2013; Dale Wilson, Moon, & Armstrong, 2012).

Figure 4.6 (a) shows the absorbance spectrum of pure TA**.** The TA absorbance of UV showed peak at wavelength of ~ 310 nm at concentration of 1M. The TA shows the absorbance characteristic at shorter wavelength compared to pure ZnO nanostructure discussed beforehand. Whilst, **Figure 4.6 (b** to **e)** represented the UV-Vis absorbance spectra for ZnO-TA nanostructures prepared at different added TA drop wise solution which yield different pH values. Noted that the ZnO-TA nanostructures exhibited SPR peak in the range of ~ 300 to ~321.5 nm which is shorter than the one exhibited by pure

ZnO nanostructures. The ZnO-TA nanostructures showed the average peak absorbance position at ~ 316.7 , ~ 310.7 , ~ 306.1 and ~ 311.8 nm for pH 3 (**Figure 4.6(b)**), pH 4 (**Figure 4.6(c)**), pH 5 (**Figure 4.6(d)**) and pH 6 (**Figure 4.6(e)**), respectively. Particularly, for ZnO-TA nanostructures in the presence of TA, two absorption bands are clearly noticed. This proposes that two major phases coincide in the ZnO-TA nanostructures. One is assuredly the oxygen-rich ZnO phase whose absorption band is in the vicinity of that of the original pure ZnO phase. The second factor is the chemical inhomogeneity due to the presence of a higher amount of oxygen with the existing of phenolic group of TA.

The peak absorbance showed a significant blue-shifted behaviour which tend to accommodates at shorter wavelength as compared to the pure ZnO nanostructures samples. The blue-shift occurred due to the decrease in size of the nanostructures and was believed is due to the increased in the concentration of TA (decreases the pH value). Theoretically, the TA tends to slowly dominates the ZnO nanostructure and caused the increased in the number of free electrons (Desai, Mankad, Gupta, & Jha, 2012). This caused the increased in the acidity of the ZnO samples which then effected the structure (tend to disaggregation the structures) and increased the reactivity of the nanoparticle (Buazar et al., 2015; Mohammadi & Ghasemi, 2018). The reactivity of phenolic hydroxyl groups contributed from the TA structure increased the amount of oxygen anions which then imparted in the reaction with ZnO ions to established a stable five-numbered ring complex. The condition encouraged the relocation of the lone pairs associated with the other two hydroxyl groups and stabilise the complex (Fu & Chen, 2019).

In addition to the band shift, the absorption band becomes distinctly broader with increasing oxygen element. The broad band in ZnO-TA is assigned to the overlap of multiple spectral phases with distinctive chemical bonding states and stoichiometry system (inhomogeneous broadening) as verified by the FTIR results (**Section 4.1.3**). The inhomogeneity appears naturally from the dissimilarity in the number of valence electrons between oxygen and extension of H-bonding atoms. That is to say that, while pure ZnO and ZnO-TA are promoted by their own microscopic crystal structures, with the absence of crystal structure for ZnO-TA, thereby yielding ZnO-TA complexes.

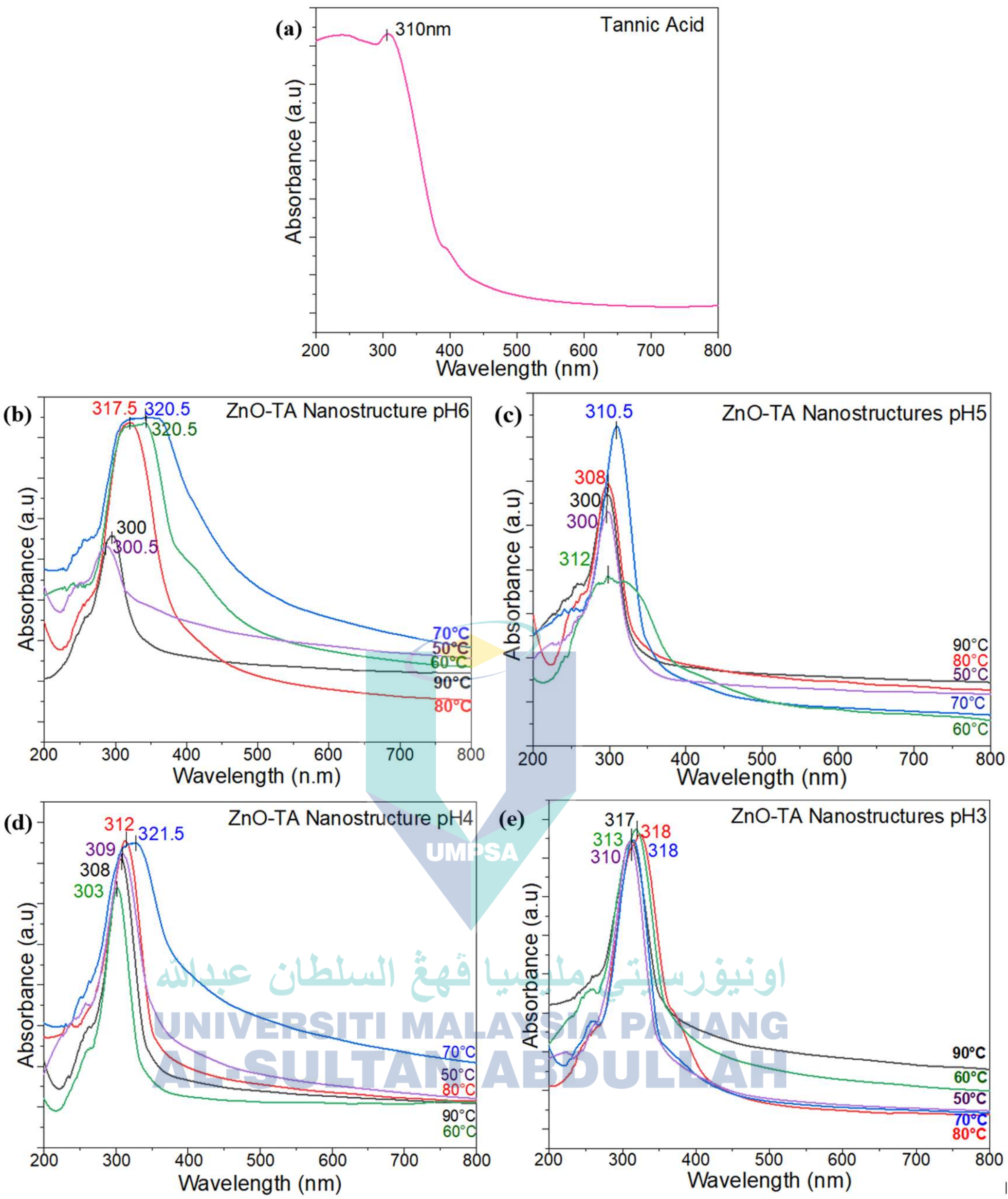

Figure 4. 6: UV-Vis absorbance spectra for (a) pure TA and ZnO-TA nanostructures prepared at (b) pH 6, (c) pH 5, (d) pH 4 and (e) pH3 based upon the addition of TA solution. As ZnO are capped with TA, the absorbance peak encountered blue-shifting due to the domination of TA and the higher releasement of more free electrons.

Energy Band Gap, *Eg*

The changes in the bandgap structure with d_m variation of the ZnO nanostructure was studied using conventional optical absorption technique. Principally, the conventional technique, which involves measuring optical absorption coefficient with the Tauc method, has been employed for examining a variety of semiconducting materials. Hence, this typical method does conclusively distinguish between the different bandgaps whose results can be seen in **Figures 4.7** and **4.8** for both pure and TA capped ZnO nanostructures, respectively. The details of the experiment are presented in **Section 3.3.1 (Chapter 3).**

In physics, the band gap, *Eg* of a semiconductor can be of two basic types, a direct band gap or an indirect band gap between conduction band and valance band. The direct band gap is due to the crystal momentum of the electrons and holes are in both the conduction band and the valence band is the same in which an electron will directly emit a photon. While, the indirect band are due to photon unable to be release in directly, because the electron has to pass through an intermediate state and transfer momentum to the crystal lattice (Abdi et al., 2012).

Figure 4.7 shows the Tauc plot of direct band gap of pure ZnO nanostructure samples synthesised at 50, 60, 70, 80 and 90°C with the obtained *Eg* values of 3.30, 3.53, 3.45, 3.55 and 3.48 eV, respectively. This indicated that the synthesised ZnO has bandgap energy that are relevant to the values range reported by other reported works on pristine ZnO nanostructures (Bhuyan, Mishra, Khanuja, Prasad, & Varma, 2015). In fact, pure ZnO nanostructures are known for having direct *Eg* and classify as semiconductors (Suvith, Devu, & Philip, 2019). The conventional semiconductors have a bandgap in between 1 to 1.5 eV, whereas, wide-bandgap materials such as ZnO nanostructures have bandgaps in between 2 to 4 eV (Yoshikawa, Matsunami, & Nanishi, 2007). As the d_m size of ZnO nanostructures is reduced, more donor atom of Zn available which provides additional carriers that yields the shifting of Fermi level towards the conduction band which caused the widening of *Eg*. Hence, a narrow band gap produced by the synthesised ZnO nanostructures should have a high photo-catalytic activity for any target reactions.

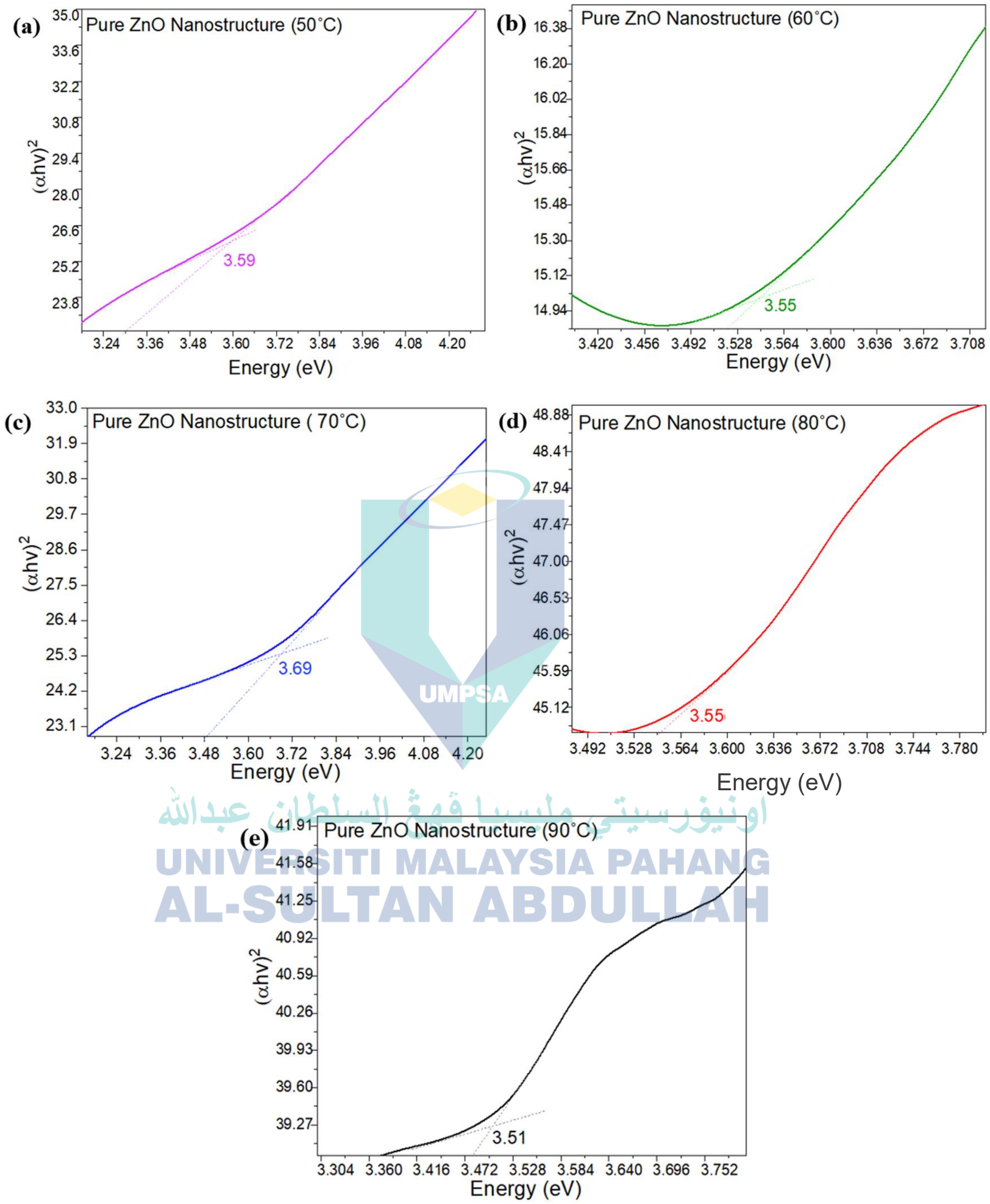

Figure 4. 7: The Tauc plot of direct *Eg* on pure ZnO nanostructures synthesised at temperatures of (a) 50˚C, (b) 60˚C ,(c) 70˚C ,(d) 80˚C and (e) 90˚C. The absorption peaks possess longer wavelengths with increasing the d_m indicating that the band gap becomes smaller at larger $d_m$particle size.

Figure 4.8 shows the Tauc plot of direct *Eg* for ZnO-TA nanostructures prepared at different pH 6 (**Figure 4.8(a)**), pH 5 (**Figure 4.8(b))**, pH 4 (**Figure 4.8(c))** and pH 3 (**Figure 4.8(d))**. As TA content is increased within ZnO nanostructure system (decrease in pH), the shifting position of the UV absorption band to a shorter wavelength infers increasing *Eg* values. The summary of the recorded *Eg* for both ZnO and ZnO-TA nanostructures is tabulated in **Table 4.4**. There is no significant trend on the values of obtained *Eg* when compared between the pH value between the prepared ZnO-TA nanostructures. However, when compared to the pure ZnO nanostructure *Eg*, most of the prepared ZnO –TA nanostructures possess wider *Eg*. **Table 4.4** compares the $(\alpha h\nu)^2$ and $(\alpha h\nu)^{1/2}$ *Eg* of pure and TA added ZnO nanostructures. As can be seen, the band gap of ZnO-TA shows slightly higher *Eg* compared to pure ZnO nanostructure which indicated that the TA could extend the spectral band and prove to possess influence on the optical absorbance of the other semiconductor and in this case, the ZnO nanostructures. The sensitivity is due to the increase in the repulsion of free electron in TA structure (Jordan Hanania, 2015). Noted that there is absence of linear changes pattern that could be desire in the current work. The addition of TA shows a point where the aggregationd structures of ZnO could be reduced in d_m and later at some point the d_m is increased due to the changes in pH value. In this case, pH 5 is consider as the point of transition from smaller d_m to larger d_m structure formation upon decreasing the pH. The condition is related to the releasement of free electron in form of oxygen ring which react with the phenolic groups of TA (Zhao, Gnanaseelan, Jehnichen, Simon, & Pionteck, 2019) and as more phenols are introduced at some point, the lesser the *Eg* is created which yields more aggregationd nanostructure of the system.

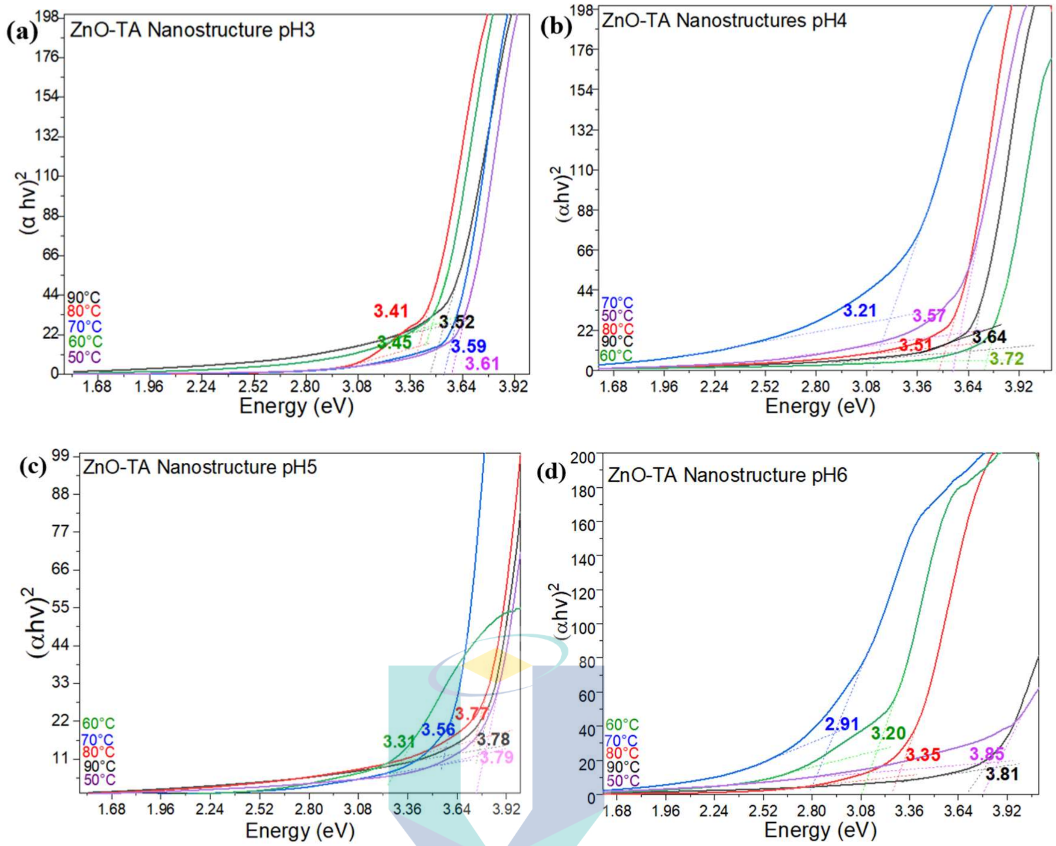

Figure 4. 8: Tauc plot on direct *Eg*, $(\alpha hv)2$ for ZnO-TA nanostructures prepared at (a) pH 3, (b) pH 4, (c) pH 5 and (d) pH6 based upon the addition of TA solution. As ZnO are capped with TA, the band gap is widen due to the domination of TA in which more free electron are release that preventing aggregation to occurred.

Table 4. 4: The summary on $(\alpha hv)^2$ *Eg* for pure and TA added ZnO nanostructures at different reaction temperatures. Noted that only TA is calculated for the $(\alpha hv)^{1/2}$. The absorbtion value (α) used are (2.303 x A) which A are obtain from the absorbance plot.

Nanostructure	**pH**	**Temperature (℃)**	**d_m from TEM(nm)**	***Eg* ($(\alpha h\nu)^2$, eV)**	***Eg* ($(\alpha h\nu)^{1/2}$, eV)**
ZnO	7	90	13	3.51	-
		80	-	3.55	
		70	8	3.69	

Table 4.4 continued

Nanostructure	**pH**	**Temperature (℃)**	**d_m from TEM(nm)**	***Eg* ((αhv) ^{2}, eV)**	***Eg* ((αhv) $^{1/2}$, eV)**
		60˚C	-	3.55	
		50˚C	8	3.59	
		90 ˚C		3.81	
		80˚C		3.35	
	6	70˚C	-	2.91	
		60˚C		3.20	
		50˚C		3.85	
		90 ˚C	-	3.78	
		80˚C		3.77	
	5	70˚C	18	3.56	
		60˚C	-	3.31	-
ZnO-TA		50˚C		3.79	
		90 ˚C		3.64	
		80˚C		3.51	
	4	70˚C	-	3.21	
		60˚C		3.72	
		50˚C		3.52	
		90 ˚C	-	3.52	
		80˚C		3.41	
	3	70˚C	23	3.59	
		60˚C	-	3.45	
		50˚C		3.61	
TA	3		-	3.5	3.501

Theoretically, the *Eg* widening is explained by the interaction of the unshared electrons of oxygen in isolated phenyl group of TA with the π −electron sextet of the aromatic ring. The *p* band of phenols located entirely overlapping with the oxygen 2*p* band becomes non-occupied and therefore masked by much more absorbing conjugated system and accordingly give rise to an overlapping complex band system which cause the valence band maximum to increase (Görög, 2018). Besides, the Zn 4 *s* conduction band which determine the minimum is not affected by the addition of phenolic of TA (Gowrishankar, Balakrishnan, & Gopalakrishnan, 2014; Hu & Zhao, 2018; Kumagai, Harada, Akamatsu, Matsuzaki, & Oba, 2017; T. Wang, Ni, & Janotti, 2017) . Nonetheless, due to the fusion effect of valence band maximum shifting and the minimum conduction band, the *Eg* becomes wider as compared to pure ZnO nanostructure samples.

In fact, it is known that by integrating a wide-bandgap semiconductor nanostructure on application (*i.e.*, photodetector), the UV range can be broadened. Basically, wider bandgap offers better merit for high-performance UV photodetector. This is also one of the core for the TA implication on ZnO nanostructures in terms of UV protection agent (Liao, Koide, & Alvarez, 2007; Liao, Wang, Teraji, Koizumi, & Koide, 2010). It is noted that the calculated for both direct $(\alpha h\nu)^2$ and indirect $(\alpha h\nu)^{1/2}$ *Eg* of TA are comparable and shown in **Figure 4.9.** TA is an amorphous semiconductor as the values (3.50 eV for $(\alpha h\nu)^2$ and 3. 48 for $(\alpha h\nu)^{1/2}$ are similar to those of each semiconductor alone. Specifically, the typical amorphous semiconductor behaviour would able to dominate the optical transition to a first approximation which cause a significant charge localisation that leads to a significant difference between the size of *Eg* (Sánchez-Vergara, Alonso-Huitron, Rodriguez-Gómez, & Reider-Burstin, 2012).

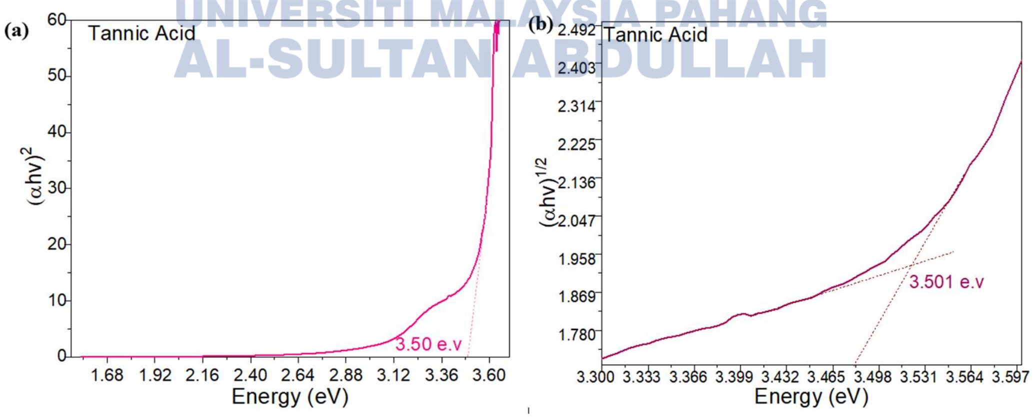

Figure 4. 9: The Tauc plot of (a) $(\alpha h\nu)^2$ and (b) $(\alpha h\nu)^{1/2}$ Eg of TA. Noticed that both showing slightly similar value of Eg which indicate TA as an amorphous semiconductor material.

4.3.2 Emission Characteristic

The emission spectrum of PL was carried out at room temperature under a 900 nm excitation wavelength of Xe lamp to further investigate the condition systems of pure ZnO nanostructures and the interact condition between TA and ZnO nanostructures, and the results are shown in **Figure 4.10**. The emitted emission intensity obtained at ~ 388 nm as shown in **Figure 4.10(a)** indicates the near band-edge emission (NBE) characteristic for pure ZnO nanostructures (M. H. Huang et al., 2001) . Whilst, the prominent, broad emission peak at ~ 580 nm arises from the recombination effect of photo-excited holes with singly-ionized (Zn+O) oxygen vacancies which cause deep-level (DL) trap emission (Lin, Fu, & Jia, 2001; Q.-l. Ma et al., 2019). It shall be noted that the emission intensity in the visible spectrum region (phosphorescence band range) for pure ZnO nanostructures is relatively discernible because of the significant structural defects.

Figure 4.10 (b and **c)** displays the emission spectrum of the Zn-TA nanostructures with the pH of 3 and 5, respectively, which retained a high-intensity emission band centred at around ~580 to ~590 nm (DL emission) which also shifted down to around ~ 472 to ~ 427 nm with the presence of a low-intensity broad emission band from ~ 315 to ~380 nm (corresponds to the NBE). At this stage, the influence of TA polymer on the surface of pure ZnO nanostructures can be deduced based on the emission of the pure TA as indicated in **Figure 4.10 (d)** which shows a strong band at ~ 577 nm with a low intensity band at ~ 335 nm. It is assumed that the NBE intensity of the core ZnO nanostructures displays substantial dependence on the TA molecule layer thickness. The NBE (zoom image) to DL emission that shows the highest intensity is from the pure ZnO nanostructures prepared at pH7 (**Figure 4.10 (a)**). The NBE emission intensity for all samples prepared at pH3 exhibit similar width of hump with intensity is ~3.2 times lower than that of the pure ZnO nanostructures (**Figure 4.10 (a)**). Additionally, the emission of DL range was significantly suppressed. A high ratio of the NBE to DL emission is crucial for perceiving outstanding quality of UV-based optoelectronic devices such as solar cells and LEDs.

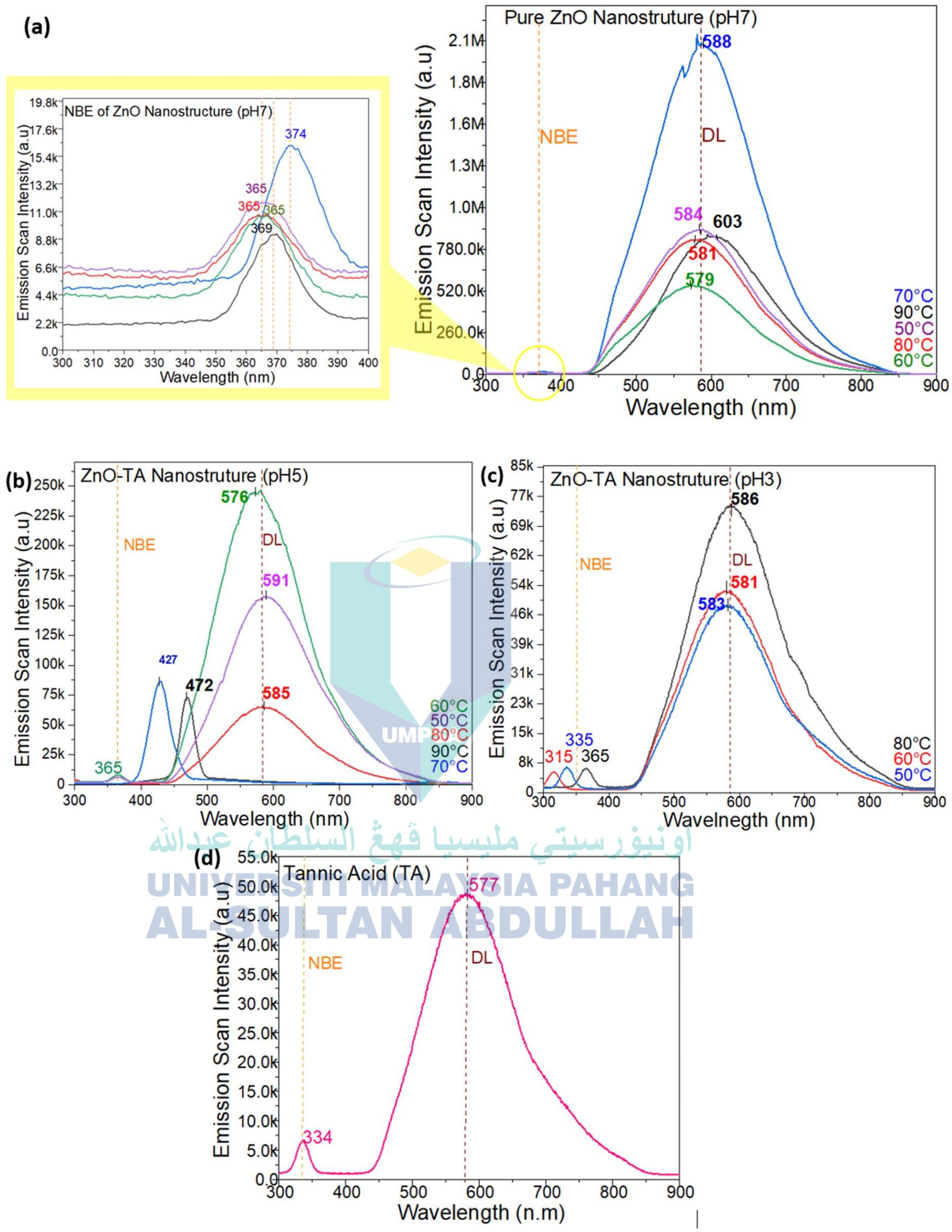

Figure 4. 10: Normalised room temperature PL emission spectra of (a) pure and (b to c) TA coated ZnO nanostructure. The pure TA emission spectrum is also noted in (d).

The emission spectra for both pure ZnO and ZnO-TA nanostructures at synthesised temperature of 60˚C are normalised to confirm that the intensity of the NBE emission (zoom image) for the pure ZnO nanostructure sample is similar to that for the ZnO-TA nanostructures, as shown in **Figure 4.11**. The relative ratio intensity of the NBE and DL emission for both pure ZnO and ZnO-TA nanostructures is calculated. It is noted that the DL intensity ratio for the pure ZnO and ZnO-TA of pH5 and pH3 sample is 11:5:1, and that for the NBE intensity ratio is 4:3:2, demonstrating a decrease in the DL and NBE emission intensity as concentration of TA are increasing. Besides, the intensity ration of DL to NBE of each sample are calculated where pure ZnO nanostructure show ratio of 52:1 which higher compared to the ratio of ZnO-TA nanostructure with 29:1 and 10:1 for sample of pH5 and pH3. The DL intensity for the ZnO-TA nanostructures was suppressed due to the increase in the excited electrons transferred from the ZnO to the TA, which reacts as an electron acceptor (na, Sun, Jiang, Feng, & Li, 2009; Vietmeyer, Seger, & Kamat, 2007). Noted that the overall changes pattern of the emission peak position of all samples are summarised in **Table 4.5.**

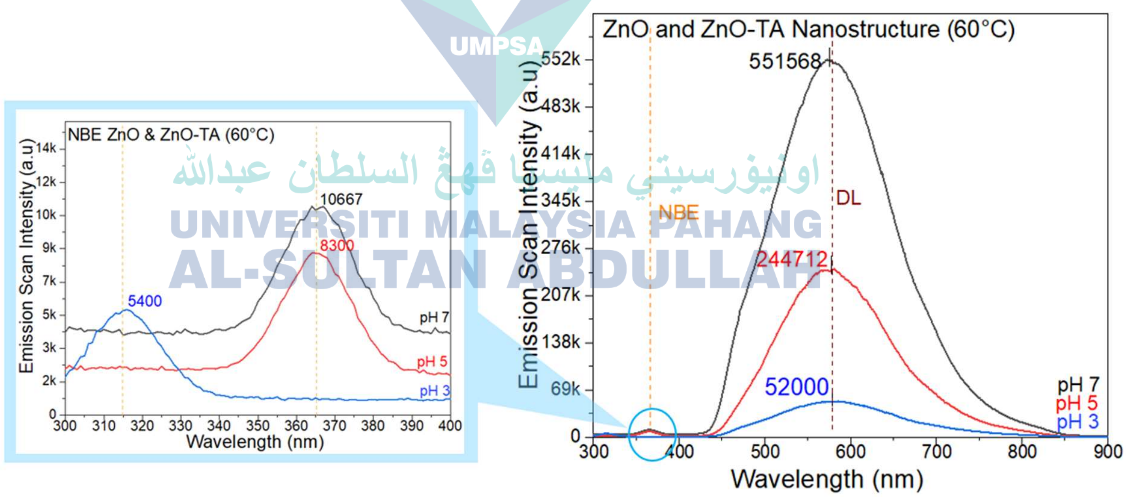

Figure 4. 11: Normalised room temperature PL emission spectra of pure and TA coated ZnO nanostructure synthesised in temperature 60˚C

Theoretically, the NBE emission from pure ZnO nanostructures is correlated with the excitons bound (as noted in **Figure 4.10**) to shallow donors, whilst, the DL emission is caused by the oxygen vacancy-related defects in ZnO nanostructures, for instance, the singly-ionised (Zn + O) oxygen vacancies, which creates the recombination centres (Ahn, Kim, Kim, Mohanta, & Cho, 2009; Tam et al., 2006). The significant enhancement of the NBE emission from the ZnO-TA nanostructures formed due to the ZnO sheathing vindicated from the combined of the three identified effects which discussed further below.

First, the emission of PL is augmented by the overlapping NBE emissions created by the ZnO core and TA layer as the emission wavelength range from ZnO overlaps that from TA. Based on the several reported published studies, the NBE emission peak of ZnO and TA exist at a wavelength range of 361 to 393 nm and 310 to 400 nm, respectively, based upon the changes of the morphology, synthesis procedure, and reaction temperature of the complex nanostructures (Haj-Hmeidi, Röder, Cammi, & Ronning, 2019; Joseph & Anappara, 2016; C.-H. Li & Zuo, 2019; J. H. Lim et al., 2006; López-Vidrier et al., 2017; Lou, Bezusov, Li, & Dubova, 2019; Mo et al., 2019; Wu et al., 2019; Zou, Wang, & Li, 2019). On that account, it is not straightforward to de-convolute both the emission (i.e., the PL emission caused by ZnO and TA) as they overlap with each other except if the NBE of TA occurrence takes place below 361 nm.

Second, the emission created by the TA outer layer is augmented by the carrier transfer from the ZnO core to the TA outer layer. Theoretically, as the ZnO core nanostructures are excited due to the electron-hole pairs interaction, the photoelectrons and photoholes through the interface between ZnO core and TA outer layer are generated. Consequently, the carrier density in the TA outer layer is significantly increase as compared to the ones in the ZnO nanocore structures. Upon the electron-hole recombination occurrence in both the ZnO core nanostructure and the TA outer layer, the photons are generated. The total amount of recombination probability is remarkably higher and thus, the production of more photons are expected in the TA outer layer than in the ZnO core nanostructure. Hence, the emission from the ZnO core nanostructure is not intense as compared to that the TA layer.

Third, the visible emission and non-radiative recombination (the cause in lowering the light generation efficiency and increasing heat losses) is squash down which cause a formation of depletion region at the outer surface of the ZnO core nanostructure. This condition yield a condition where the E_F level (as discussed in **Section 4.2.1.1**) is reduced than the E_g levels at the defects related visible emission (Zn interstitials and their complexes with O vacancies) as well as the non-radiative transition-related defects (Kabir et al., 2019; Y. Ma et al., 2019; Tu et al., 2019).

Table 4. 5: The summary on the emission peak position of the as-synthesised pure ZnO and ZnO-TA nanostructures. Noted that the samples with acidic pH (pH 5 and pH 3) showed blue-shift peak emission characteristic due to influence of TA as a capping agent.

Nanostructure	**pH**	**Temperature**	d_m **(nm)**	**PL Emission Peak (nm)**
ZnO	7	90 ˚C	13	663
		80˚C	-	581
		70˚C	8	588
		60˚C	-	579
		50˚C	8	584
	5	90 ˚C	-	472
		80˚C	-	585
		70˚C	18	427
		60˚C	-	576
		50˚C	-	591
	3	80˚C	-	586
		60˚C	-	581
		50˚C	-	583
TA	3	-	-	577

4.4 Antibacterial Efficiency

4.4.1 Inhibitory of *S. aureus* Microbe

Apart from physical and optical analyses, the present work also observed the behaviour of antimicrobial property of pure ZnO and ZnO-TA nanostructures. The observation is mainly focused on the influenced of the nanostructures towards the inhibitory effect on bacteria which always found in sweat. The bacterial inhibition test for both pure ZnO and ZnO-TA nanostructure suspensions were tested against an organism known as *staphylococcus aureus* (*S. aureus*). The main reason for choosing *S. aureus* as the colonising bacteria in the test is because it is the most abundant skin colonising-bacteria and the most important cause for any skin infection on human being (Kluytmans & Wertheim, 2005; Otto, 2010; Wertheim, Melles, et al., 2005; Wertheim, Verveer, et al., 2005). *S. Aureus* colonise approximately 30% of healthy individuals through a mechanism that illustrates competition between colonization-resistant host factors and *S. aureus* virulence factors promoting colonisation and further subsequent infection (Alonzo & Torres, 2013; Gorwitz et al., 2008; Miller & Diep, 2008).

The pure ZnO and ZnO-TA nanostructure samples are tested on *S. Aureus* organism at ambient temperature (35˚C). The antibacterial activities of pure ZnO and ZnO-TA nanostructures are assayed based on the concentration of the bacteria recovered from the inoculated treated test. The results demonstrated that the suspended bacteria remained mostly viable over 5 minutes, whereas the survival rates of *S. aureus* exposed to pure ZnO and ZnO-TA nanostructures declined to 99.39% and 99.69% within 24 hours. The observation is mainly attempted to quantify according to the bacterial survival rate, which is based on the loss in microbial viability with time. The details on the test carried out for both samples are summarised in **Table 4.6**. Both samples showed positive performance in inhibiting the growth of *S.aureus* bacteria.

Table 4.6: AATCC 100 assessment result of microbes inhibitory between ZnO and ZnO-TA nanostructure against *S. aureus* species. Notice that the performance of ZnO-TA nanostructure agaisn microbes *S. auerues* are slightly better compared too pure ZnO

nanostructure due to presence of phenolic compound and acidic condition. Bacterial concentration are count by bacterial colony counter machine.

Sample	Bacteria type	Bacteria concentration 5 minutes after inoculation (CPU/sample)	Bacteria concentration 24 hour after inoculation (CPU/sample)	Percent of bacterial reduction after 24 hour (%)
ZnO Nanostructure	Stapylococcus aureus	1.02×10^5	6.22×10^2	99.39
ZnO-TA Nanostructure		1.02×10^5	3.08×10^2	99.69
Controlled sample		1.02×10^5	$>1.02 \times 10^5$	Null

Figure 4.12 shows the pictures of *S. aureus* exposed to pure ZnO and ZnO-TA nanostructures for 24 hours in **Figure 4.12(a)** and **4.12 (b),** respectively. The muddy colour shows the spot of *S. aureus* growth. These results indicated that the antibacterial efficacy of ZnO-TA nanostructures was remarkably higher than that of pure ZnO nanostructures. This can be ascribed to the benefits of TA capped ligand and the slight limitation of ZnO nanostructures. ZnO-TA nanostructure sample had a d_m of 18 ± 2 nm that ease the attachment to the surface of the organism and the positive surface charge on ZnO-TA nanostructures enables a straight forward inter-particle interaction and the negativelycharged organism membranes (Wingett, Louka, Anders, Zhang, & Punnoose, 2016). Additionally, *S. aureus*, which is a type of strain organism representing Gram-positive bacteria, displayed a delicate survival rate in comparison to the other famous organism strain such as *E. coli* (found in the lower intestine of warm-blooded organisms) (Saadatian-Elahi, Teyssou, & Vanhems, 2008). Hence, reduce the resistant efficiency towards the antibacterial effect of the ZnO-TA nanostructures. These results support the previous assumption that *S. aureus* could not tolerate ZnO-TA nanostructure medium.

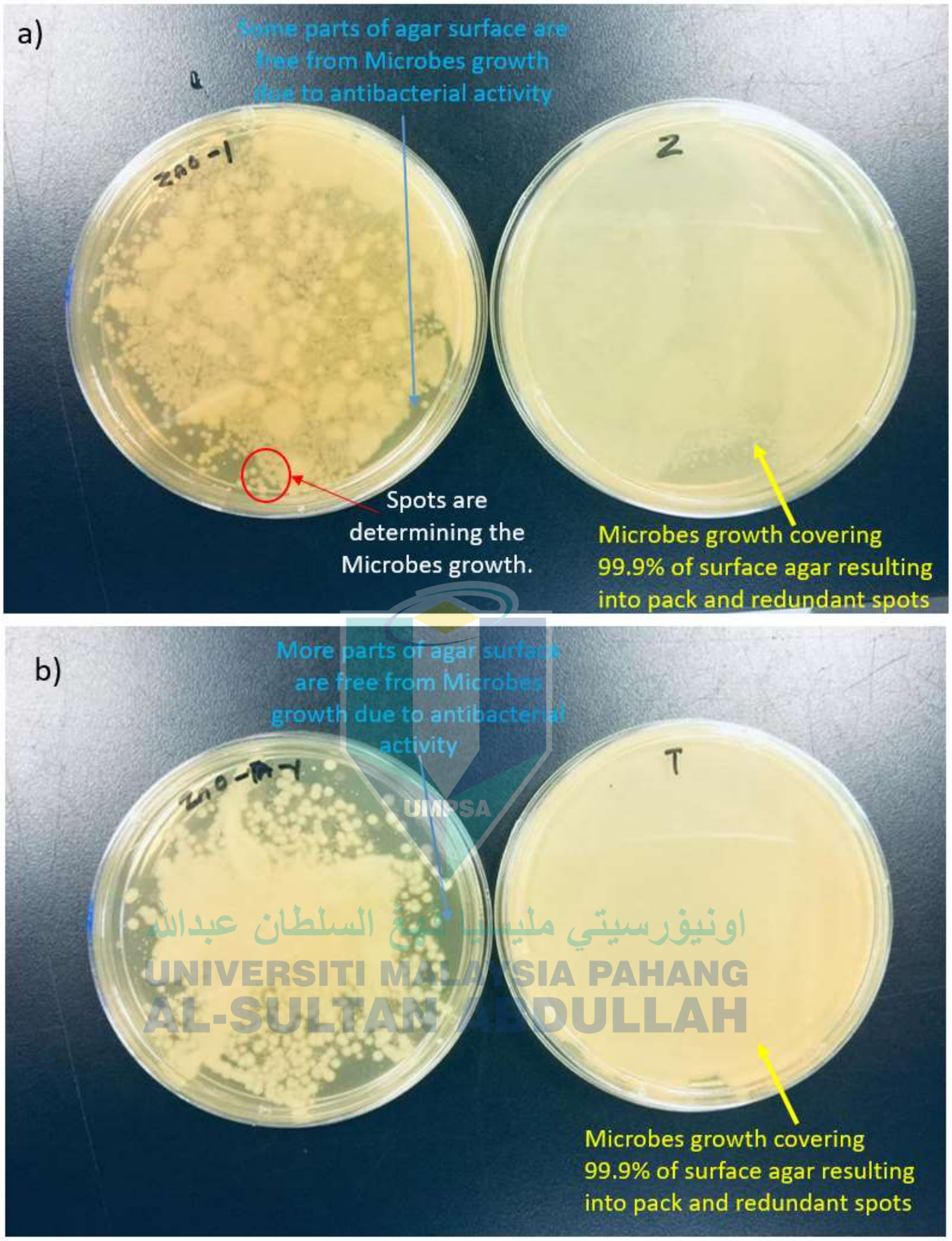

Figure 4. 12: Total viable microbes count for (a) pure ZnO nanostructure and (b) ZnO-TA nanostructure 24 hours after inoculation. Z and T represent the control (Staphylococcus aureus without treatment).

It is also found that the pH of the nanostructure medium influence the amount of survival bacteria strain. It is shown that by lowering the pH value enabled quick and effective killing of up to 99.69% of *S. aureus* strain within 24 hours. The explainations are based on these three reasons. First, the non-existence of the outer membrane layer and the existence of teichoic acid molecules of negatively charge bacteria within a thick peptidoglycan cell wall (20 to 80 nm) on the surface of *S. aureus* induced higher attraction towards the positively charged and yield more specific site to be disrupted by positively charged molecules (Malanovic & Lohner, 2016; Silhavy, Kahne, & Walker, 2010). Second, the *S. aureus* owns a very small number of tiny channels of porins within the outer membrane that used to assist in blocking the access of the particles into the strain cell, making them defenceless (Garni, Thamboo, Schoenenberger, & Palivan, 2017; L. Wang, Hu, & Shao, 2017). Last one, *S. aureus* has a small dimension (sphere, internal diameter, ~0.5 to 1 μm) that may accounted for more detail interaction with the ZnO-TA nanoparticles, resulting in better antibacterial activity compared to the larger size bacteria strain (Monteiro et al., 2015; Schwibbert, Menzel, Epperlein, Bonse, & Krüger, 2019).

4.5 Summary

The experimental result are presented and discussed in this chapter. The morphological structure of the pure ZnO and ZnO-TA nanostructures are first to be discussed based on the obtained d_m. ZnO-TA nanostructures exhibited slight larger d_m as compared to pure ZnO nanostructures. Besides, the surface morphology showed that the morphology of the pure ZnO nanostructures possess nanoplate-kind of structure while for ZnO-TA nanostructures have significant interlink in between the nanostructures caused by the connected ZnO nanoplates in the presence of TA. TA controls the breakable level off carbon and oxygen molecule which increase the mass percent of carbon in EDX results. Apart from these, ZnO nanostructures also showed clear crystallite structure based on the Joint Committee on Powder Diffraction standards with three prominent peaks correspond to reflections at [100], [002] and [101] atomic planes of ZnO phases. While for ZnO-TA nanostructures, TA vanishes the peak intensities belongs to ZnO which implies the absence of significance lattice on the ZnO wurtzite structures. Only one sample showed crystalline peaks of ZnO which is believed caused by the deposition process of the samples on the glass substrate, the concentration amount of ZnO nanostructures dropped is higher than the TA ligand.

FTIR test that revealed the chemical structure showed that the pure ZnO nanostructures have stretching bond not only at ZnO element but also the O-H stretching that usually occurred due to the loss of H_2O molecule. Additionally, the stretchings on C=O and O-C-O are observed due to the atmospheric absorption in non-vacuum system. As for ZnO-TA nanostructures, the FTIR results showed similar peak strecthcing as pure ZnO nanostructures with additional stretching at hydroxyl group (O-H) H-bonded broad and string and C-H (aromatic medium) as TA are known to have aromatic esters. Shifiting in ZnO strectching which is associated to the oxygen vacancy defect complex is observed. The FTIR results also determined the surface chemistry of solids which relates to the acid base theories.

The localised surface plasmon resonance (LSPR) characteristic indicated the absorbance behaviour for both pure ZnO and ZnO-TA nanostructures. For pure ZnO nanostructures (pH7) the absorbance peaks were shown at the range of ~380 till ~386 nm and proved to be in accordance with the existing literatures reported on the ZnO nanostructures. The pure TA sample showed ab absorbance of LSPR peak at the wavelength of ~ 310 nm. The ZnO-TA nanostructures at pH 3, 4, 5 and 6 showed the average peak absorbance position at ~ 316.7, ~ 310.7 , ~ 306.1 and ~ 311.8 nm respectively. Particularly, for ZnO-TA nanostructures, two LSPR bands are clearly noticed. This proposes that two major phases coincide in the ZnO-TA nanostructures. One is assuredly the oxygen-rich ZnO phase whose absorption band is in the vicinity of that of the original pure ZnO phase. The second phase is the chemical inhomogeneity due to the presence of a higher amount of oxygen with the existing of phenolic group of TA.

From the LSPR peak, the Tauc plots are constructed which demonstrated the E_g of the sample. The direct Eg of pure ZnO nanostructures synthesised at 50, 60, 70, 80 and 90°C are 3.30, 3.53, 3.45, 3.55 and 3.48 Ev, respectively. Meanwhile, as TA is introduced and the concentration amount is gradually increased (decrease in pH), the shifting to a shorter wavelength of the LSPR infers by the increasing of *Eg* for ZnO-TA nanostructures. Noted that, there is no significant trend on the values of obtained for *Eg* when compared between the pH value between the prepared ZnO-TA nanostructures. However, when compared to the *Eg* for pure ZnO nanostructure, most of the prepared ZnO –TA nanostructures possess wider *Eg* which indicated that the TA could extend the spectral band and prove to possess influence on the optical absorbance of the other semiconductor and in this case, the ZnO nanostructures.

The emission characteristic is one of the optical properties of the nanostructures. The emitted emission intensity obtained for pure ZnO sample are at ~ 388 nm. Whilst, the prominent, broad emission peak arises from the recombination effect of photo-excited holes with singly-ionized (Zn+O) oxygen vacancies which cause deep-level (DL) trap emission. At this stage, the influence of TA polymer on the surface of pure ZnO nanostructures can be deduced based on the emission of the pure TA which shows a strong band at ~ 577 nm with a low intensity band at ~ 335 nm. It is assumed that the NBE intensity of the core ZnO nanostructures displays substantial dependence on the TA molecule layer thickness. The DL intensity for the ZnO-TA nanostructures was suppressed due to the increase in the excited electrons transferred from the ZnO to the TA, which reacts as an electron acceptor.

The properties of antimicrobial is determined from the AATCC 100 method with pure ZnO and ZnO-TA nanostructures are surpressed for the inhibitory of *S. aureus* bacteria. The ZnO-TA nanostructures showed to have better performance with efficiency of 99.67% compared to 99.38% efficiency of pure ZnO nanostructures. The pH medium influenced the amount of survival bacteria strain. It is shown that by lowering the pH value enabled quick and effective killing of up to 99.69% of *S. aureus* strain within 24 hours. Finally, a summary of findings where the objectives and conclusions are included is presented in the next chapter. Some recommendations for further studies were also suggested.

CHAPTER 5

CONCLUSION

5.1 Introduction

The as-synthesised pure ZnO and ZnO-TA nanostructures and their respective properties have successfully carried out. The results of the nanostructures performance were studied both the analytically and experimentally. The output performance of different measured properties for both pure ZnO and ZnO-TA nanostructures were determined based on the four main properties ,that are, physical properties, chemical structure, optical property and antimicrobial efficiency. The surface morphological analysis are determined from TEM and FESEM characterisation while for crystalline structure properties are determine from XRD analysis, the chemical bonding properties are discovered from FTIR analysis and optical properties of the nanostructure are determined from UV-Vis and photoluminescence testing in shich determining the band gap energy. Meanwhile, for antibacterial property, the efficiency is determined from the AATCC100 experiment. Some of the results of the experiment were validated with analytical results such as the energy band gap. Overall, the results showed that the ZnO-TA nanostructures have slightly larger size with better performances in absorbing the UV, outstanding band gap and maximum productivity of antibacterial efficiency. Also, few recommendations for future studies were discussed in the last section of this chapter.

5.2 Summary of the Findings

The main purpose of the current study is to monitor the properties effects of TA in the as-synthesised ZnO nanostructures which falls under the second objective. To achieve the second objective, it is a must to fulfil the first objective of the proposed work.

Hence, it is proved that the proposed work has successfully synthesised the pure ZnO nanostructures via a low cost and environmentally friendly hydrothermal method at 70˚C. Later, the work proposed the drop-wise method to produced the ZnO-TA nanostructures by introduced the amount of TA solution based upon their final pH for each samples. The final pHs obtained are pH3 until pH6. Later, to confirm the achievement of the successful synthesis and preparation methods for pure ZnO and ZnO-TA nanostructures,properties characterisations were done. The d_m of pure ZnO synthesised at 90℃ is 10 ± 5 nm . As the temperature is decreases to 70 and 50℃ the particle size is reduced to similar d_m at 8 ± 2 nm as well as the particle size distribution is confined in the range of 4 to 30 nm. As the ZnO is introduced to TA. The size distributions of the nanostructures are drastically changed in which the histograms show the d_m of 18 ± 3 nm and 22 ± 4 nm, for pH 5 and 3. The chacracterisation analysis were divided into four main categories that are, physical property, chemical structure, optical property and antimicrobial efficiency. Based on the overall results and discussion that have been made, it is true that ZnO-TA nanostructures possesses better overall properties performance compared to pure ZnO nanostructures.

The first key parameter properties is the observation on the aggregation of the nanostructures. As discussed in **Section 4.1.1** under the surface morphology (physical property), TA is found to caused the aggregation between individual ZnO nanostructures. The results showed that the ZnO-TA nanostructures have a slight larger d_m ompared to pure ZnO nanostructures. The caused is due to the increased in the TA concentration (decreases the pH value) that yield an increased in the aggregation ability which observed from the coalescence of small nanostructures based on the attachment growth process that depends fully on the amount of the projected available nanostructures (Ahmad, 2014). The attachment of the nanostructures is caused by the acidic surrounding which led to a jump to contact. In acidic condition, the presence of proton which attack the surface of ZnO is high. At lower pH (<pH 6), the tendency to produce a soluble ion of Zn^{2+} and $Zn(OH)^+$ are higher. Therefore, the aggregation occurred as the protonation of the phenolic group take place in which reduced the accessibility of the functional group to squeeze between the ZnO nanocrystals (jump contact) and created larger attached particle as determined from the mean diameter of nanostructure as discussed.

The second key parameter is the chemical structure from FTIR results. The FTIR test that revealed the chemical structure showed that the pure ZnO nanostructures have stretching bond not only at ZnO element but also the O-H stretching that usually occurred due to the loss of H_2O molecule. Additionally, the stretchings on C=O and O-C-O are observed due to the atmospheric absorption in non-vacuum system. As for ZnO-TA nanostructures, the FTIR results showed similar peak strecthcing as pure ZnO nanostructures with additional stretching at hydroxyl group (O-H) H-bonded broad and string and C-H (aromatic medium) as TA are known to have aromatic esters. Shifiting in ZnO strectching which is associated to the oxygen vacancy defect complex is observed. The FTIR results also determined the surface chemistry of solids which relates to the acid base theories.

The third key parameter properties is the influenced of TA in the optical characteristic. ZnO-TA nanostructures possesses shorter LSPR wavelengths as compared to the pure ZnO nanostructures. The blue-shifted behaviours which accommodated at shorter wavelength proved the small d_m of the system and caused by the increased in the concentration of TA (decreases the pH values). TA tends to slowly dominated the ZnO nanostructures by the increased in the number of free electrons released when in contact with ZnO structures (Desai et al., 2012). Thus, increased the acidity of the ZnO nanostructures surrounding medium which then increased the reactivity of the nanostructures and affected the surface structures (tend to disaggregationd the structures).

Based on the output obtained from LSPR absorbance results, *Eg* is calculated for both pure ZnO and ZnO-TA nanostructures. Results showed that the *Eg* of most of the prepared ZnO –TA nanostructures are wider (3.41 –3.81) compared to the pure ZnO nanostructures (3.55-3.64). As discussed in **Section 4.3.1.1**, the *Eg* of ZnO-TA nanostructures showed slight higher values as compared to pure ZnO nanostructures which caused the extension of the spectral bandwidth. The caused is due to the increase in the repulsion of free electron in TA structure (Jordan Hanania, 2015). The condition is related to the releasement of free electron in form of oxygen ring which react with the phenolic groups of TA (Zhao et al., 2019) and as more phenols are introduced at some point, the lesser the energy gap is created which yields more aggregationd nanostructure of the system.

The fourth which is the last key parameter studied by the current work is related to the antimicrobial efficiency. The antimicrobial efficiency of ZnO-TA nanostructures shown to have remarkable performance with the killing percentage of up to 99.69% of *S. aureus* strain within 24 hours than that of pure ZnO nanostructures (99.39%). This can be ascribed to the increased benefits of ZnO nanostrcutures due to the presence of TA ligand. *S. aureus*, which is a type of strain organism representing Gram-positive bacteria, displayed a delicate survival rate. Thus, these underpinned the assumption that the ZnO-TA nanostructure medium could not be tolerated by *S. aureus*.

5.3 Contribution to the knowledge

The aims of the project are to determined the influenced of TA in ZnO nanostructures system and the effect on the properties of the structures. The overall results indicated that TA does influenced the properties of ZnO nanostruture. TA caused the aggregation of the ZnO nanostructures which yields better LSPR and results in wider *Eg* compared to pure ZnO nanostructure. For antibacterial efficiency, TA improved the antibacterial efficiency of the ZnO nanostructures. Thus, the rsilts could apply as a based of argument in applying ZnO-TA nanostructure into fabrics especially for sports attire as it improved the ability for UV absorber and inhibitor for the growth of *S.aureus* bacteria which presence at human skin due to sweat.

5.4 Future Works

There are several matters that should be taken into consideration for further research. It includes the constraint that occurs during experiments. Further works might need to explore different methods of synthesis to produce purest sample without the possibilities of the presence of impurities in the sample which could affect the overall propertiesof ZnO nanostructures. Methods such as sol gel and wet chemical are some of the recommended method.

On another notes, further works could also used other tyoes of characterisation equipments in order to have precise properties determination. XPS testing should also be done as it can lead to the plotting of Fermi Level which can help researcher to have better understanding on the energy level diagram of the nanostructure. Besides, as for antimicrobial test, detail test should be done by undergo the bacterial colony under TEM to determine the details on inhibitory of the bacteria count. A number of possible future studies using the same experimental set up are apparent and it would be of interest to assess the effects of experiment validation.

REFERENCES

Abdelmohsen, A. H., Rouby, W. M. A. E., Ismail, N., & Farghali, A. A. (2017). Morphology Transition Engineering of ZnO Nanorods to Nanoplatelets Grafted Mo8O23-MoO2 by Polyoxometalates: Mechanism and Possible Applicability to other Oxides. Scientific Reports, 7(1), 5946. doi:10.1038/s41598-017-05750-x

Abdi, M. M., Ekramul Mahmud, H. N. M., Abdullah, L. C., Kassim, A., Zaki Ab. Rahman, M., & Chyi, J. L. Y. (2012). Optical band gap and conductivity measurements of polypyrrole-chitosan composite thin films. Chinese Journal of Polymer Science, 30(1), 93-100. doi:10.1007/s10118-012-1093-7

Addison, C. J., & Brolo, A. G. (2006). Nanoparticle-Containing Structures as a Substrate for Surface-Enhanced Raman Scattering. Langmuir, 22(21), 8696-8702. doi:10.1021/la061598c

Agrawal, A., Cho, S. H., Zandi, O., Ghosh, S., Johns, R. W., & Milliron, D. J. (2018). Localized Surface Plasmon Resonance in Semiconductor Nanocrystals. Chemical Reviews, 118(6), 3121-3207. doi:10.1021/acs.chemrev.7b00613

Ahmad, T. (2014). Reviewing the Tannic Acid Mediated Synthesis of Metal Nanoparticles. Journal of Nanotechnology, 2014, 1-11. doi:10.1155/2014/954206

Ahn, C. H., Kim, Y. Y., Kim, D. C., Mohanta, S. K., & Cho, H. K. (2009). A comparative analysis of deep level emission in ZnO layers deposited by various methods. Journal of Applied Physics, 105(1), 013502. doi:10.1063/1.3054175

Akiyama, H., Fujii, K., Yamasaki, O., Oono, T., & Iwatsuki, K. (2001). Antibacterial action of several tannins against Staphylococcus aureus. Journal of Antimicrobial Chemotherapy, 48(4), 487-491. doi:10.1093/jac/48.4.487

Albrecht, M. A., Evans, C. W., & Raston, C. L. (2006). Green chemistry and the health implications of nanoparticles. Green Chemistry, 8(5), 417-432. doi:10.1039/B517131H

Alonzo, F., & Torres, Victor J. (2013). A Lesson in Survival: S. aureus versus the Skin. Cell Host & Microbe, 13(1), 3-5. doi:https://doi.org/10.1016/j.chom.2013.01.001

Anbuvannan, M., Ramesh, M., Viruthagiri, G., Shanmugam, N., & Kannadasan, N. (2015). Synthesis, characterization and photocatalytic activity of ZnO nanoparticles prepared by biological method. Spectrochim Acta A Mol Biomol Spectrosc, 143, 304-308. doi:10.1016/j.saa.2015.01.124

Andrade, R. G., Ginani, J. S., Lopes, G. K. B., Dutra, F., Alonso, A., & Hermes-Lima, M. (2006). Tannic acid inhibits in vitro iron-dependent free radical formation. Biochimie, 88(9), 1287-1296. doi:https://doi.org/10.1016/j.biochi.2006.02.006

Arakha, M., Saleem, M., Mallick, B. C., & Jha, S. (2015). The effects of interfacial potential on antimicrobial propensity of ZnO nanoparticle. Sci Rep, 5, 9578. doi:10.1038/srep09578

Ashraf, R., Riaz, S., Hussain, S. S., & Naseem, S. (2015). Effect of pH on Properties of ZnO Nanoparticles. Materials Today: Proceedings, 2(10), 5754-5759. doi:10.1016/j.matpr.2015.11.123

Asres, K., Mazumder A Fau - Bucar, F., & Bucar, F. (2006). Antibacterial and antifungal activities of extracts of combretum molle. (0014-1755 (Print)).

Baek, Y.-W., & An, Y.-J. (2011). Microbial toxicity of metal oxide nanoparticles (CuO, NiO, ZnO, and Sb2O3) to Escherichia coli, Bacillus subtilis, and Streptococcus aureus. Science of The Total Environment, 409(8), 1603-1608. doi:https://doi.org/10.1016/j.scitotenv.2011.01.014

Baldwin, S., Odio, M. R., Haines, S. L., O'Connor, R. J., Englehart, J. S., & Lane, A. T. (2001). Skin benefits from continuous topical administration of a zinc oxide/petrolatum formulation by a novel disposable diaper. Journal of the European Academy of Dermatology and Venereology, 15(s1), 5-11. doi:10.1046/j.0926-9959.2001.00002.x

Banoee, M., Seif, S., Nazari, Z. E., Jafari-Fesharaki, P., Shahverdi, H. R., Moballegh, A., . . . Shahverdi, A. R. (2010). ZnO nanoparticles enhanced antibacterial activity of ciprofloxacin against Staphylococcus aureus and Escherichia coli. Journal of Biomedical Materials Research Part B: Applied Biomaterials, 93B(2), 557-561. doi:10.1002/jbm.b.31615

Bhuyan, T., Mishra, K., Khanuja, M., Prasad, R., & Varma, A. (2015). Biosynthesis of zinc oxide nanoparticles from Azadirachta indica for antibacterial and photocatalytic applications. Materials Science in Semiconductor Processing, 32, 55-61. doi:10.1016/j.mssp.2014.12.053

Bian, S.-W., Mudunkotuwa, I. A., Rupasinghe, T., & Grassian, V. H. (2011). Aggregation and Dissolution of 4 nm ZnO Nanoparticles in Aqueous Environments: Influence of pH, Ionic Strength, Size, and Adsorption of Humic Acid. Langmuir, 27(10), 6059-6068. doi:10.1021/la200570n

Blum, J. L., Edwards, J. R., Prozialeck, W. C., Xiong, J. Q., & Zelikoff, J. T. (2015). Effects of Maternal Exposure to Cadmium Oxide Nanoparticles During Pregnancy on Maternal and Offspring Kidney Injury Markers Using a Murine Model. Journal of toxicology and environmental health. Part A, 78(12), 711-724. doi:10.1080/15287394.2015.1026622

Books, C. (2017). Tannic Acid properties

Brayner, R., Ferrari-Iliou, R., Brivois, N., Djediat, S., Benedetti, M. F., & Fiévet, F. (2006). Toxicological Impact Studies Based on Escherichia coli Bacteria in

Ultrafine ZnO Nanoparticles Colloidal Medium. Nano Letters, 6(4), 866-870. doi:10.1021/nl052326h

Breazu, C., Socol, M., Preda, N., Matei, E., Rasoga, O., Girtan, M., . . . Stanculescu, A. (2018). On the properties of organic heterostructures prepared with nano-patterned metallic electrode. Applied Surface Science, 443, 592-602. doi:https://doi.org/10.1016/j.apsusc.2018.02.103

Buazar, F., Bavi, M., Kroushawi, F., Halvani, M., Khaledi-Nasab, A., & Hossieni, S. A. (2015). Potato extract as reducing agent and stabiliser in a facile green one-step synthesis of ZnO nanoparticles. Journal of Experimental Nanoscience, 11(3), 175-184. doi:10.1080/17458080.2015.1039610

Buzzini, P., Arapitsas, P., Goretti, M., Turchetti, B., Pinelli, P., Ieri, F., & Romani, A. (2008). Antimicrobial and antiviral activity of hydrolysable tannins. Mini-Reviews in Medicinal Chemistry, 8(12), 1179-1187. doi:10.2174/138955708786140990

Cao, D., Gong, S., Shu, X., Zhu, D., & Liang, S. (2019). Preparation of ZnO Nanoparticles with High Dispersibility Based on Oriented Attachment (OA) Process. Nanoscale research letters, 14(1), 210. doi:10.1186/s11671-019-3038-3

Chakrabarti, S., & Banerjee, P. (2014). Preparation and characterization of multifunctional cotton fabric by coating with sonochemically synthesized zinc oxide nanoparticle-flakes and a novel approach to monitor its self-cleaning property. The Journal of The Textile Institute, 106(9), 963-969. doi:10.1080/00405000.2014.955962

Che Lah, N. A., & Kamaruzaman, A. (2019). The optical quantification measurement on aggregated aqueous ZnO nanostructures upon exposure to tannic acid. Materials Research Express, 6(12), 125046. doi:10.1088/2053-1591/ab5754

Chey, C. O. (2015). Synthesis of ZnO and transition metals doped ZnO nanostructures.

Chiang, H.-M., Xia, Q., Zou, X., Wang, C., Wang, S., Miller, B., . . . Fu, P. (2012). Nanoscale ZnO Induces Cytotoxicity and DNA Damage in Human Cell Lines and Rat Primary Neuronal Cells. Journal of nanoscience and nanotechnology, 12, 2126-2135. doi:10.1166/jnn.2012.5758

Cho, W.-S., Duffin, R., Howie, S. E. M., Scotton, C. J., Wallace, W. A. H., Macnee, W., . . . Donaldson, K. (2011). Progressive severe lung injury by zinc oxide nanoparticles; the role of Zn2+ dissolution inside lysosomes. Particle and fibre toxicology, 8, 27-27. doi:10.1186/1743-8977-8-27

Cipriano-Salazar, M., Rojas-Hernández, S., Olivares-Pérez, J., Jiménez-Guillén, R., Cruz-Lagunas, B., Camacho-Díaz, L. M., & Ugbogu, A. E. (2018). Antibacterial activities of tannic acid against isolated ruminal bacteria from sheep. Microbial Pathogenesis, 117, 255-258. doi:https://doi.org/10.1016/j.micpath.2018.01.045

Cole, C., Shyr, T., & Ou-Yang, H. (2016). Metal oxide sunscreens protect skin by absorption, not by reflection or scattering. Photodermatol Photoimmunol Photomed, 32(1), 5-10. doi:10.1111/phpp.12214

Coppo, E., & Marchese, A. (2014). Antibacterial activity of polyphenols. Current Pharmaceutical Biotechnology, 15(4), 380-390. doi:10.2174/138920101504140825121142

Craig, S., Earnshaw, C. H., & Virós, A. (2018). Ultraviolet light and melanoma. The Journal of Pathology, 244(5), 578-585. doi:10.1002/path.5039

D'Orazio, J., Jarrett, S., Amaro-Ortiz, A., & Scott, T. (2013). UV radiation and the skin. International journal of molecular sciences, 14(6), 12222-12248. doi:10.3390/ijms140612222

Dale Wilson, B., Moon, S., & Armstrong, F. (2012). Comprehensive review of ultraviolet radiation and the current status on sunscreens. The Journal of clinical and aesthetic dermatology, 5(9), 18-23.

Das, S. N., Choi, J. H., Kar, J. P., & Myoung, J. M. (2009). Tunable and reversible surface wettability transition of vertically aligned ZnO nanorod arrays. Applied Surface Science, 255(16), 7319-7322. doi:https://doi.org/10.1016/j.apsusc.2009.03.090

Desai, R., Mankad, V., Gupta, S., & Jha, P. (2012). Size Distribution of Silver Nanoparticles: UV-Visible Spectroscopic Assessment. Nanoscience and Nanotechnology Letters, 4(1), 30-34. doi:10.1166/nnl.2012.1278

Dmitruk, I., Alexeenko, A., Kotko, A., Vedral, J., & Pinchuk, A. (2012). Size and Temperature Effects on the Surface Plasmon Resonance in Silver Nanoparticles. Plasmonics, 7. doi:10.1007/s11468-012-9359-z

Dong, G., Liu, H., Yu, X., Zhang, X., Lu, H., Zhou, T., & Cao, J. (2018). Antimicrobial and anti-biofilm activity of tannic acid against Staphylococcus aureus. Natural Product Research, 32(18), 2225-2228. doi:10.1080/14786419.2017.1366485

Dutta, R. K., Sharma, P. K., Bhargava, R., Kumar, N., & Pandey, A. C. (2010). Differential Susceptibility of Escherichia coli Cells toward Transition Metal-Doped and Matrix-Embedded ZnO Nanoparticles. The Journal of Physical Chemistry B, 114(16), 5594-5599. doi:10.1021/jp1004488

Elumalai, K., & Velmurugan, S. (2015). Green synthesis, characterization and antimicrobial activities of zinc oxide nanoparticles from the leaf extract of Azadirachta indica (L.). Applied Surface Science, 345, 329-336. doi:10.1016/j.apsusc.2015.03.176

Es'haghi, Z. (2018). Green and Chemical Synthesis of Zinc Oxide Nanoparticles and Size Evaluation by UV–Vis Spectroscopy.

Espitia, P. J. P., Soares, N. d. F. F., Coimbra, J. S. d. R., de Andrade, N. J., Cruz, R. S., & Medeiros, E. A. A. (2012). Zinc Oxide Nanoparticles: Synthesis, Antimicrobial Activity and Food Packaging Applications. Food and Bioprocess Technology, 5(5), 1447-1464. doi:10.1007/s11947-012-0797-6

Estrada-Urbina, J., Cruz-Alonso, A., Santander-González, M., Méndez-Albores, A., & Vázquez-Durán, A. (2018). Nanoscale Zinc Oxide Particles for Improving the Physiological and Sanitary Quality of a Mexican Landrace of Red Maize. Nanomaterials, 8(4). doi:10.3390/nano8040247

Fakhari, S., Jamzad, M., & Kabiri Fard, H. (2019). Green synthesis of zinc oxide nanoparticles: a comparison. Green Chemistry Letters and Reviews, 12(1), 19-24. doi:10.1080/17518253.2018.1547925

Feng, X., Feng, L., Jin, M., Zhai, J., Jiang, L., & Zhu, D. (2004). Reversible Super-hydrophobicity to Super-hydrophilicity Transition of Aligned ZnO Nanorod Films. Journal of the American Chemical Society, 126(1), 62-63. doi:10.1021/ja038636o

Fiedot-Tobola, M., Ciesielska, M., Maliszewska, I., Rac-Rumijowska, O., Suchorska-Wozniak, P., Teterycz, H., & Bryjak, M. (2018). Deposition of Zinc Oxide on Different Polymer Textiles and Their Antibacterial Properties. Materials (Basel), 11(5). doi:10.3390/ma11050707

Fu, Z., & Chen, R. (2019). Study of Complexes of Tannic Acid with Fe(III) and Fe(II). Journal of Analytical Methods in Chemistry, 2019, 6. doi:10.1155/2019/3894571

Gan, Y. X., Jayatissa, A. H., Yu, Z., Chen, X., & Li, M. (2020). Hydrothermal Synthesis of Nanomaterials. Journal of Nanomaterials, 2020, 8917013. doi:10.1155/2020/8917013

Garni, M., Thamboo, S., Schoenenberger, C.-A., & Palivan, C. G. (2017). Biopores/membrane proteins in synthetic polymer membranes. Biochimica et Biophysica Acta (BBA) - Biomembranes, 1859(4), 619-638. doi:https://doi.org/10.1016/j.bbamem.2016.10.015

Gholizadeh, A., Reyhani, A., Parvin, P., Mortazavi, S. Z., & Mehrabi, M. (2018). Enhancement of Si solar cell efficiency using ZnO nanowires with various diameters. Materials Research Express, 5(1), 015040. doi:10.1088/2053-1591/aaa534

Godfrey, H. R., Godfrey Nj Fau - Godfrey, J. C., Godfrey Jc Fau - Riley, D., & Riley, D. (2001). A randomized clinical trial on the treatment of oral herpes with topical zinc oxide/glycine. (1078-6791 (Print)).

Görög, S. (2018). Ultraviolet-visible spectrophotometry in pharmaceutical analysis.

Gorwitz, R. J., Kruszon-Moran, D., McAllister, S. K., McQuillan, G., McDougal, L. K., Fosheim, G. E., . . . Kuehnert, M. J. (2008). Changes in the Prevalence of Nasal Colonization with Staphylococcus aureus in the United States, 2001–2004. The Journal of Infectious Diseases, 197(9), 1226-1234. doi:10.1086/533494

Gowrishankar, S., Balakrishnan, L., & Gopalakrishnan, N. (2014). Band gap engineering in Zn(1−x)CdxO and Zn(1−x)MgxO thin films by RF sputtering. Ceramics International, 40(1, Part B), 2135-2142. doi:https://doi.org/10.1016/j.ceramint.2013.07.130

Greer, H. (2013). Non-classical crystal growth of inorganic and organic materials. Materials Science and Technology, 30, 611. doi:10.1179/1743284713Y.0000000433

Grice, E. A., Kong, H. H., Conlan, S., Deming, C. B., Davis, J., Young, A. C., . . . Segre, J. A. (2009). Topographical and temporal diversity of the human skin microbiome. Science (New York, N.Y.), 324(5931), 1190-1192. doi:10.1126/science.1171700

Grice, E. A., & Segre, J. A. (2011). The skin microbiome. Nature reviews. Microbiology, 9(4), 244-253. doi:10.1038/nrmicro2537

Gupta, B. D., & Kant, R. (2018). Recent advances in surface plasmon resonance based fiber optic chemical and biosensors utilizing bulk and nanostructures. Optics & Laser Technology, 101, 144-161. doi:https://doi.org/10.1016/j.optlastec.2017.11.015

Haj-Hmeidi, Y., Röder, R., Cammi, D., & Ronning, C. (2019). Electroluminescence of intrashell transitions in Eu doped single ZnO nanowires. Nanotechnology, 30(9), 095201. doi:10.1088/1361-6528/aaf82c

He, L., Liu, Y., Mustapha, A., & Lin, M. (2011). Antifungal activity of zinc oxide nanoparticles against Botrytis cinerea and Penicillium expansum. Microbiol Res, 166(3), 207-215. doi:10.1016/j.micres.2010.03.003

Hedayati, K. (2015). Fabrication and Optical Characterization of Zinc Oxide Nanoparticles Prepared via a Simple Sol-gel Method. Journal of Nanostructures, 5(4), 395-401. doi:10.7508/jns.2015.04.010

Hitanshu Kumar, P. B. B. a. R. R. S. (2014). Development of CdS ZnS Quantum Dots and their Core. International Journal of Scientific & Engineering Research, 5(5).

Hu, H.-C., & Zhao, B. (2018). Metal-Organic Frameworks Based on Multicenter-Bonded [MI]8 (M=Mn, Zn) Clusters with Cubic Aromaticity. Chemistry – A European Journal, 24(63), 16702-16707. doi:10.1002/chem.201801227

Huang, J., Yin, Z., & Zheng, Q. (2011). Applications of ZnO in organic and hybrid solar cells. Energy & Environmental Science, 4(10), 3861-3877. doi:10.1039/C1EE01873F

Huang, M. H., Wu, Y., Feick, H., Tran, N., Weber, E., & Yang, P. (2001). Catalytic Growth of Zinc Oxide Nanowires by Vapor Transport. Advanced Materials, 13(2), 113-116. doi:10.1002/1521-4095(200101)13:2<113::AID-ADMA113>3.0.CO;2-H

Husain, S., Rahman, F., Ali, N., & Alvi, P. A. (2013). Nickel Sub-lattice Effects on the Optical Properties of ZnO Nanocrystals. Journal of Optoelectronics Engineering, 1(1), 28-32. doi:10.12691/joe-1-1-5

Iravani, S., & Zolfaghari, B. (2013). Green synthesis of silver nanoparticles using Pinus eldarica bark extract. Biomed Res Int, 2013, 639725. doi:10.1155/2013/639725

Jayaseelan, C., Rahuman, A. A., Kirthi, A. V., Marimuthu, S., Santhoshkumar, T., Bagavan, A., . . . Rao, K. V. (2012). Novel microbial route to synthesize ZnO nanoparticles using Aeromonas hydrophila and their activity against pathogenic bacteria and fungi. Spectrochim Acta A Mol Biomol Spectrosc, 90, 78-84. doi:10.1016/j.saa.2012.01.006

Jones, N., Ray, B., Ranjit, K. T., & Manna, A. C. (2008). Antibacterial activity of ZnO nanoparticle suspensions on a broad spectrum of microorganisms. FEMS Microbiol Lett, 279(1), 71-76. doi:10.1111/j.1574-6968.2007.01012.x

Jordan Hanania, K. S., Jason Donev. (2015). Band gap - Energy Education.

Joseph, J., & Anappara, A. A. (2016). Microwave-assisted hydrothermal synthesis of UV-emitting carbon dots from tannic acid. New Journal of Chemistry, 40(9), 8110-8117. doi:10.1039/C6NJ02107G

Jung, H.-Y., Yeo, I.-S., Kim, T.-U., Ki, H.-C., & Gu, H.-B. (2018). Surface plasmon resonance effect of silver nanoparticles on a TiO2 electrode for dye-sensitized solar cells. Applied Surface Science, 432, 266-271. doi:https://doi.org/10.1016/j.apsusc.2017.04.237

Kabir, A., Bouanane, I., Boulainine, D., Zerkout, S., Schmerber, G., & Boudjema, B. (2019). Photoluminescence Study of Deep Level Defects in ZnO Thin Films. Silicon, 11(2), 837-842. doi:10.1007/s12633-018-9876-2

Kar, J. P., Das, S. N., Choi, J. H., Lee, T. I., & Myoung, J. M. (2010). Study of the morphological evolution of ZnO nanostructures on various sapphire substrates. Applied Surface Science, 256(16), 4995-4999. doi:https://doi.org/10.1016/j.apsusc.2010.03.040

Kekkonen, V., Hakola, A., Kajava, T., Sahramo, E., Malm, J., Karppinen, M., & Ras, R. H. A. (2010). Self-erasing and rewritable wettability patterns on ZnO thin films. Applied Physics Letters, 97(4), 044102. doi:10.1063/1.3460915

Khan, M. F., Ansari, A. H., Hameedullah, M., Ahmad, E., Husain, F. M., Zia, Q., . . . Aliev, G. (2016). Sol-gel synthesis of thorn-like ZnO nanoparticles endorsing mechanical stirring effect and their antimicrobial activities: Potential role as nano-antibiotics. Sci Rep, 6, 27689. doi:10.1038/srep27689

Kharissova, O. V., Dias, H. V., Kharisov, B. I., Perez, B. O., & Perez, V. M. (2013). The greener synthesis of nanoparticles. Trends Biotechnol, 31(4), 240-248. doi:10.1016/j.tibtech.2013.01.003

Khatami, M., Alijani, H. Q., Heli, H., & Sharifi, I. (2018). Rectangular shaped zinc oxide nanoparticles: Green synthesis by Stevia and its biomedical efficiency. Ceramics International, 44(13), 15596-15602. doi:10.1016/j.ceramint.2018.05.224

Khatami, M., Varma, R. S., Zafarnia, N., Yaghoobi, H., Sarani, M., & Kumar, V. G. (2018). Applications of green synthesized Ag, ZnO and Ag/ZnO nanoparticles for making clinical antimicrobial wound-healing bandages. Sustainable Chemistry and Pharmacy, 10, 9-15. doi:10.1016/j.scp.2018.08.001

Khorsand Zak, A., Abd. Majid, W. H., Mahmoudian, M. R., Darroudi, M., & Yousefi, R. (2013). Starch-stabilized synthesis of ZnO nanopowders at low temperature and optical properties study. Advanced Powder Technology, 24(3), 618-624. doi:10.1016/j.apt.2012.11.008

Kluytmans, J. A. J. W., & Wertheim, H. F. L. (2005). Nasal Carriage of Staphylococcus aureus and Prevention of Nosocomial Infections. Infection, 33(1), 3-8. doi:10.1007/s15010-005-4012-9

Kondawar, S. B., Acharya, S. A., & Dhakate, S. R. (2011). Microwave assisted hydrothermally synthesized nanostructure zinc oxide reinforced polyaniline nanocomposites. Advanced Materials Letters, 2(5), 362-367. doi:10.5185/amlett.2011.9107am2011

Krol, A., Pomastowski, P., Rafinska, K., Railean-Plugaru, V., & Buszewski, B. (2017). Zinc oxide nanoparticles: Synthesis, antiseptic activity and toxicity mechanism. Adv Colloid Interface Sci, 249, 37-52. doi:10.1016/j.cis.2017.07.033

Kumagai, Y., Harada, K., Akamatsu, H., Matsuzaki, K., & Oba, F. (2017). Carrier-Induced Band-Gap Variation and Point Defects in Zn3N2 from First Principles. Physical Review Applied, 8(1), 014015. doi:10.1103/PhysRevApplied.8.014015

Kumar, P. R., Jung, Y. H., Bharathi, K. K., Lim, C. H., & Kim, D. K. (2014). High capacity and low cost spinel Fe3O4 for the Na-ion battery negative electrode materials. Electrochimica Acta, 146, 503-510. doi:https://doi.org/10.1016/j.electacta.2014.09.081

Kuppusamy, S. N. a. K. A. (2013). Extracellular Synthesis of Zinc Oxide Nanoparticle using Seaweeds of Gulf.

Kuppusamy, S. N. a. K. A. (2013). Extracellular synthesis of zinc oxide nanoparticle using seaweeds of gulf of Mannar, India.

Lah, N. A. B. C. (2016). Conductivity studies of the size-induced metal-insulator transition (SIMIT) in silver nanoparticles. University of Oxford.

Laminack, W., Baker, C., & Gole, J. (2015). Sulfur-Hz(CHx)y(z = 0,1) functionalized metal oxide nanostructure decorated interfaces: Evidence of Lewis base and Brönsted acid sites – Influence on chemical sensing. Materials Chemistry and Physics, 160, 20-31. doi:https://doi.org/10.1016/j.matchemphys.2015.03.070

Laura Soriano, M., Zougagh, M., Valcarcel, M., & Rios, A. (2018). Analytical Nanoscience and Nanotechnology: Where we are and where we are heading. Talanta, 177, 104-121. doi:10.1016/j.talanta.2017.09.012

Lee, C.-T. (2010). Fabrication Methods and Luminescent Properties of ZnO Materials for Light-Emitting Diodes. Materials, 3(4), 2218-2259. doi:10.3390/ma3042218

Lee, J.-H., Park, J.-H., Cho, H. S., Joo, S. W., Cho, M. H., & Lee, J. (2013). Anti-biofilm activities of quercetin and tannic acid against Staphylococcus aureus. Biofouling, 29(5), 491-499. doi:10.1080/08927014.2013.788692

Li, C.-H., & Zuo, J.-L. (2019). Self-Healing Polymers Based on Coordination Bonds. Advanced Materials, n/a(n/a), 1903762. doi:10.1002/adma.201903762

Li, J.-M., Zeng, X.-L., Huang, Q., & Xu, Z.-A. (2012). Morphological diversity and alternate evolution in tin-assisted vapor-transport-grown ZnO micro-nanocrystal tetrapods. CrystEngComm, 14(22), 7800-7806. doi:10.1039/C2CE25963J

Li, M., Li, G., Jiang, J., Zhang, Z., Dai, X., & Mai, K. (2015). Ultraviolet Resistance and Antimicrobial Properties of ZnO in the Polypropylene Materials: A Review. Journal of Materials Science & Technology, 31(4), 331-339. doi:10.1016/j.jmst.2014.11.022

Liao, M., Koide, Y., & Alvarez, J. (2007). Single Schottky-barrier photodiode with interdigitated-finger geometry: Application to diamond. Applied Physics Letters, 90(12), 123507. doi:10.1063/1.2715440

Liao, M., Wang, X., Teraji, T., Koizumi, S., & Koide, Y. (2010). Light intensity dependence of photocurrent gain in single-crystal diamond detectors. Physical Review B, 81(3), 033304. doi:10.1103/PhysRevB.81.033304

Lim, J. H., Kang, C. K., Kim, K. K., Park, I. K., Hwang, D. K., & Park, S. J. (2006). UV Electroluminescence Emission from ZnO Light-Emitting Diodes Grown by High-Temperature Radiofrequency Sputtering. Advanced Materials, 18(20), 2720-2724. doi:10.1002/adma.200502633

Lim, S. H., Darah, I., & Jain, K. (2006). Antimicrobial activities of tannins extracted from rhizophora apiculata barks. Journal of Tropical Forest Science, 18(1), 59-65.

Lin, B., Fu, Z., & Jia, Y. (2001). Green luminescent center in undoped zinc oxide films deposited on silicon substrates. Applied Physics Letters, 79(7), 943-945. doi:10.1063/1.1394173

Lopes, L. C. S., Brito, L. M., Bezerra, T. T., Gomes, K. N., Carvalho, F. A. A., Chaves, M. H., & Cantanhede, W. (2018). Silver and gold nanoparticles from tannic acid: synthesis, characterization and evaluation of antileishmanial and cytotoxic activities. An Acad Bras Cienc, 90(3), 2679-2689. doi:10.1590/0001-3765201820170598

Lopes, L. C. S., Brito, L. M., Bezerra, T. T., Gomes, K. N., Carvalho, F. A. D. A., Chaves, M. H., & CantanhÊDe, W. (2018). Silver and gold nanoparticles from tannic acid: synthesis, characterization and evaluation of antileishmanial and cytotoxic activities. Anais da Academia Brasileira de Ciências, 90, 2679-2689.

López-Vidrier, J., Gutsch, S., Blázquez, O., Hiller, D., Laube, J., Kaur, R., . . . Zacharias, M. (2017). Modulation of the electroluminescence emission from ZnO/Si NCs/p-Si light-emitting devices via pulsed excitation. Applied Physics Letters, 110(20), 203104. doi:10.1063/1.4983722

Lou, W., Bezusov, A., Li, B., & Dubova, H. (2019). Recent advances in studying tannic acid and its interaction with proteins and polysaccharides. Food Science and Technology, 13. doi:10.15673/fst.v13i3.1452

Lü, J., Huang, K., Chen, X., Zhu, J., Meng, F., Song, X., & Sun, Z. (2010). Reversible wettability of nanostructured ZnO thin films by sol–gel method. Applied Surface Science, 256(14), 4720-4723. doi:https://doi.org/10.1016/j.apsusc.2010.02.080

Ma, Q.-l., Ma, S., Huang, Y. M., Shao, H., Deng, H., & Zhang, Z. (2019). Tunable emission colours of ZnO nanocrystals by forming nanocomposites with a nematic liquid crystal N-(4-methoxybenzylidene)-4-ethoxybenzenamine. Materials Research Innovations, 23(5), 294-298. doi:10.1080/14328917.2018.1464777

Ma, Y., Choi, T.-W., Cheung, S. H., Cheng, Y., Xu, X., Xie, Y.-M., . . . Tsang, S.-W. (2019). Charge transfer-induced photoluminescence in ZnO nanoparticles. Nanoscale, 11(18), 8736-8743. doi:10.1039/C9NR02020A

Machado, T. B., Pinto, A. V., Pinto, M. C. F. R., Leal, I. C. R., Silva, M. G., Amaral, A. C. F., . . . Netto-dosSantos, K. R. (2003). In vitro activity of Brazilian medicinal plants, naturally occurring naphthoquinones and their analogues, against methicillin-resistant Staphylococcus aureus. International Journal of Antimicrobial Agents, 21(3), 279-284. doi:https://doi.org/10.1016/S0924-8579(02)00349-7

Malanovic, N., & Lohner, K. (2016). Gram-positive bacterial cell envelopes: The impact on the activity of antimicrobial peptides. Biochimica et Biophysica Acta

(BBA) - Biomembranes, 1858(5), 936-946. doi:https://doi.org/10.1016/j.bbamem.2015.11.004

Maremanda, K. P., Khan, S., & Jena, G. (2014). Zinc protects cyclophosphamide-induced testicular damage in rat: involvement of metallothionein, tesmin and Nrf2. Biochem Biophys Res Commun, 445(3), 591-596. doi:10.1016/j.bbrc.2014.02.055

Matinise, N., Fuku, X. G., Kaviyarasu, K., Mayedwa, N., & Maaza, M. (2017). ZnO nanoparticles via Moringa oleifera green synthesis: Physical properties & mechanism of formation. Applied Surface Science, 406, 339-347. doi:10.1016/j.apsusc.2017.01.219

Mayer, M., Potapov, P. L., Pohl, D., Steiner, A. M., Schultz, J., Rellinghaus, B., . . . Fery, A. (2019). Direct Observation of Plasmon Band Formation and Delocalization in Quasi-Infinite Nanoparticle Chains. Nano Letters, 19(6), 3854-3862. doi:10.1021/acs.nanolett.9b01031

Mentes Colak, S., Yapici, B., & Yapici, A. (2010). Determination of antimicrobial activity of tannic acid in pickling process. Romanian Biotechnological Letters, 15.

Miajlovic, H., Fallon, P. G., Irvine, A. D., & Foster, T. J. (2010). Effect of filaggrin breakdown products on growth of and protein expression by Staphylococcus aureus. The Journal of allergy and clinical immunology, 126(6), 1184-1190.e1183. doi:10.1016/j.jaci.2010.09.015

Michen, B., Geers, C., Vanhecke, D., Endes, C., Rothen-Rutishauser, B., Balog, S., & Petri-Fink, A. (2015). Avoiding drying-artifacts in transmission electron microscopy: Characterizing the size and colloidal state of nanoparticles. Scientific Reports, 5, 9793-9793. doi:10.1038/srep09793

Miller, L. G., & Diep, B. A. (2008). Colonization, Fomites, and Virulence: Rethinking the Pathogenesis of Community-Associated Methicillin-Resistant Staphylococcus aureus Infection. Clinical Infectious Diseases, 46(5), 752-760. doi:10.1086/526773

Mo, X., Li, Z., Liu, C., Tao, X., Zhou, Y., Long, H., . . . Ouyang, Y. (2019). Improving and manipulating green-light electroluminescence in solution-processed ZnO nanocrystals via erbium doping. Journal of Luminescence, 213, 127-132. doi:https://doi.org/10.1016/j.jlumin.2019.05.021

Mohammadi, F. M., & Ghasemi, N. (2018). Influence of temperature and concentration on biosynthesis and characterization of zinc oxide nanoparticles using cherry extract. Journal of Nanostructure in Chemistry, 8(1), 93-102. doi:10.1007/s40097-018-0257-6

Monteiro, J. M., Fernandes, P. B., Vaz, F., Pereira, A. R., Tavares, A. C., Ferreira, M. T., . . . Pinho, M. G. (2015). Cell shape dynamics during the staphylococcal cell cycle. Nature communications, 6, 8055-8055. doi:10.1038/ncomms9055

Munjal, P., Kumar, L., Kumar, S., & Banati, H. (2019). Evidence of Ostwald Ripening in opinion driven dynamics of mutually competitive social networks. Physica A: Statistical Mechanics and its Applications, 522, 182-194. doi:https://doi.org/10.1016/j.physa.2019.01.109

Murphy, M. A. (2018). Early Industrial Roots of Green Chemistry and the history of the BHC Ibuprofen process invention and its Quality connection. Foundations of Chemistry, 20(2), 121-165. doi:10.1007/s10698-017-9300-9

na, Z., Sun, J., Jiang, D., Feng, T., & Li, Q. (2009). Anchoring Zinc Oxide Quantum Dots on Functionalized Multi-Walled Carbon Nanotubes by Covalent Coupling. Carbon, 47, 1214-1219. doi:10.1016/j.carbon.2008.12.044

No, I. J., Lee, S., Kim, S. H., Cho, J. W., & Shin, P.-K. (2013). Morphology Control of ZnO Nanowires Grown by Hydrothermal Methods Using Au Nanodots on Al doped ZnO Seed Layer. Japanese Journal of Applied Physics, 52(2R), 025003. doi:10.7567/jjap.52.025003

Noginov, M. A., Zhu, G., Bahoura, M., Adegoke, J., Small, C. E., Ritzo, B. A., . . . Shalaev, V. M. (2006). Enhancement of surface plasmons in an Ag aggregate by optical gain in a dielectric medium. Optics Letters, 31(20), 3022-3024. doi:10.1364/OL.31.003022

Nohynek, G. J., & Dufour, E. K. (2012). Nano-sized cosmetic formulations or solid nanoparticles in sunscreens: a risk to human health? Arch Toxicol, 86(7), 1063-1075. doi:10.1007/s00204-012-0831-5

Ogunyemi, S. O., Abdallah, Y., Zhang, M., Fouad, H., Hong, X., Ibrahim, E., . . . Li, B. (2019). Green synthesis of zinc oxide nanoparticles using different plant extracts and their antibacterial activity against Xanthomonas oryzae pv. oryzae. Artif Cells Nanomed Biotechnol, 47(1), 341-352. doi:10.1080/21691401.2018.1557671

Orlowski, P., Zmigrodzka, M., Tomaszewska, E., Ranoszek-Soliwoda, K., Czupryn, M., Antos-Bielska, M., . . . Krzyzowska, M. (2018). Tannic acid-modified silver nanoparticles for wound healing: the importance of size. Int J Nanomedicine, 13, 991-1007. doi:10.2147/IJN.S154797

Otto, M. (2010). Staphylococcus colonization of the skin and antimicrobial peptides. Expert review of dermatology, 5(2), 183-195. doi:10.1586/edm.10.6

P. Singh, R., K. Shukla, V., S. Yadav, R., K. Sharma, P., K. Singh, P., & C. Pandey, A. (2011). Biological Approach Of Zinc Oxide Nanoparticles Formation And Its

Characterization. Advanced Materials Letters, 2(4), 313-317. doi:10.5185/amlett.indias.204

Padmavathy, N., & Vijayaraghavan, R. (2008). Enhanced bioactivity of ZnO nanoparticles-an antimicrobial study. Sci Technol Adv Mater, 9(3), 035004. doi:10.1088/1468-6996/9/3/035004

Papadopoulou, E. L., Zorba, V., Pagkozidis, A., Barberoglou, M., Stratakis, E., & Fotakis, C. (2009). Reversible wettability of ZnO nanostructured thin films prepared by pulsed laser deposition. Thin Solid Films, 518(4), 1267-1270. doi:https://doi.org/10.1016/j.tsf.2009.02.077

Payne, D. E., Martin, N. R., Parzych, K. R., Rickard, A. H., Underwood, A., & Boles, B. R. (2013). Tannic acid inhibits Staphylococcus aureus surface colonization in an IsaA-dependent manner. Infection and immunity, 81(2), 496-504. doi:10.1128/IAI.00877-12

Prasanta Sutradgar, M. S. (2015). Synthesis of zinc oxide nanoparticles using tea leaf extract-and it application for solar cell

Raghupathi, K. R., Koodali, R. T., & Manna, A. C. (2011). Size-Dependent Bacterial Growth Inhibition and Mechanism of Antibacterial Activity of Zinc Oxide Nanoparticles. Langmuir, 27(7), 4020-4028. doi:10.1021/la104825u

Rai, M., Yadav, A., & Gade, A. (2009). Silver nanoparticles as a new generation of antimicrobials. Biotechnol Adv, 27(1), 76-83. doi:10.1016/j.biotechadv.2008.09.002

Ramesh, M., Anbuvannan, M., & Viruthagiri, G. (2015). Green synthesis of ZnO nanoparticles using Solanum nigrum leaf extract and their antibacterial activity. Spectrochim Acta A Mol Biomol Spectrosc, 136 Pt B, 864-870. doi:10.1016/j.saa.2014.09.105

Reed, P., Atilano, M. L., Alves, R., Hoiczyk, E., Sher, X., Reichmann, N. T., . . . Pinho, M. G. (2015). Staphylococcus aureus Survives with a Minimal Peptidoglycan Synthesis Machine but Sacrifices Virulence and Antibiotic Resistance. PLoS pathogens, 11(5), e1004891-e1004891. doi:10.1371/journal.ppat.1004891

Ryu, S., Song, P. I., Seo, C. H., Cheong, H., & Park, Y. (2014). Colonization and infection of the skin by S. aureus: immune system evasion and the response to cationic antimicrobial peptides. International journal of molecular sciences, 15(5), 8753-8772. doi:10.3390/ijms15058753

Saadatian-Elahi, M., Teyssou, R., & Vanhems, P. (2008). Staphylococcus aureus, the major pathogen in orthopaedic and cardiac surgical site infections: A literature review. International Journal of Surgery, 6(3), 238-245. doi:https://doi.org/10.1016/j.ijsu.2007.05.001

Sadeghi, B., Garmaroudi, F. S., Hashemi, M., Nezhad, H. R., Nasrollahi, A., Ardalan, S., & Ardalan, S. (2012). Comparison of the anti-bacterial activity on the nanosilver shapes: Nanoparticles, nanorods and nanoplates. Advanced Powder Technology, 23(1), 22-26. doi:10.1016/j.apt.2010.11.011

Sánchez-Vergara, M. E., Alonso-Huitron, J. C., Rodriguez-Gómez, A., & Reider-Burstin, J. N. (2012). Determination of the Optical GAP in Thin Films of Amorphous Dilithium Phthalocyanine Using the Tauc and Cody Models. Molecules, 17(9), 10000-10013. doi:10.3390/molecules170910000

Sawai, J. (2003). Quantitative evaluation of antibacterial activities of metallic oxide powders (ZnO, MgO and CaO) by conductimetric assay. Journal of Microbiological Methods, 54(2), 177-182. doi:10.1016/s0167-7012(03)00037-x

Schechter, J. F., Wilkinson, R. D., & Carpio, J. D. (1984). Anaphylaxis Following the Use of Bacitracin Ointment: Report of a Case and Review of the Literature. JAMA Dermatology, 120(7), 909-911. doi:10.1001/archderm.1984.01650430095017

Scholl, J. A., Koh, A. L., & Dionne, J. A. (2012). Quantum plasmon resonances of individual metallic nanoparticles. Nature, 483, 421. doi:10.1038/nature10904

https://www.nature.com/articles/nature10904#supplementary-information

Schwibbert, K., Menzel, F., Epperlein, N., Bonse, J., & Krüger, J. (2019). Bacterial Adhesion on Femtosecond Laser-Modified Polyethylene. Materials (Basel, Switzerland), 12(19), 3107. doi:10.3390/ma12193107

Selvarajan, E., & Mohanasrinivasan, V. (2013). Biosynthesis and characterization of ZnO nanoparticles using Lactobacillus plantarum VITES07. Materials Letters, 112, 180-182. doi:10.1016/j.matlet.2013.09.020

Sharma, V., Anderson, D., & Dhawan, A. (2012). Zinc oxide nanoparticles induce oxidative DNA damage and ROS-triggered mitochondria mediated apoptosis in human liver cells (HepG2). Apoptosis, 17(8), 852-870. doi:10.1007/s10495-012-0705-6

Shi, L.-E., Li, Z.-H., Zheng, W., Zhao, Y.-F., Jin, Y.-F., & Tang, Z.-X. (2014). Synthesis, antibacterial activity, antibacterial mechanism and food applications of ZnO nanoparticles: a review. Food Additives & Contaminants: Part A, 31(2), 173-186. doi:10.1080/19440049.2013.865147

Shin, C. M., Heo, J. H., Park, J. H., Lee, T. M., Ryu, H., Shin, B. C., . . . Kim, H. K. (2010). The effect of pH on ZnO hydrothermal growth on PES flexible substrates. Physica E: Low-dimensional Systems and Nanostructures, 43(1), 54-57. doi:https://doi.org/10.1016/j.physe.2010.06.013

Siddiqi, K. S., & Husen, A. (2017). Plant Response to Engineered Metal Oxide Nanoparticles. Nanoscale research letters, 12(1), 92-92. doi:10.1186/s11671-017-1861-y

Siddiqi, K. S., Ur Rahman, A., Tajuddin, & Husen, A. (2018). Properties of Zinc Oxide Nanoparticles and Their Activity Against Microbes. Nanoscale Res Lett, 13(1), 141. doi:10.1186/s11671-018-2532-3

Siddiqi, K. S., Ur Rahman, A., Tajuddin, & Husen, A. (2018). Properties of Zinc Oxide Nanoparticles and Their Activity Against Microbes. Nanoscale research letters, 13(1), 141-141. doi:10.1186/s11671-018-2532-3

Silhavy, T. J., Kahne, D., & Walker, S. (2010). The bacterial cell envelope. Cold Spring Harbor perspectives in biology, 2(5), a000414-a000414. doi:10.1101/cshperspect.a000414

Sirelkhatim, A., Mahmud, S., Seeni, A., Kaus, N. H. M., Ann, L. C., Bakhori, S. K. M., . . . Mohamad, D. (2015). Review on Zinc Oxide Nanoparticles: Antibacterial Activity and Toxicity Mechanism. Nanomicro Lett, 7(3), 219-242. doi:10.1007/s40820-015-0040-x

Smijs, T. G., & Pavel, S. (2011). Titanium dioxide and zinc oxide nanoparticles in sunscreens: focus on their safety and effectiveness. Nanotechnol Sci Appl, 4, 95-112. doi:10.2147/NSA.S19419

Stassi, S., Cauda, V., Ottone, C., Chiodoni, A., Pirri, C. F., & Canavese, G. (2015). Flexible piezoelectric energy nanogenerator based on ZnO nanotubes hosted in a polycarbonate membrane. Nano Energy, 13, 474-481. doi:10.1016/j.nanoen.2015.03.024

Surabhi Siva Kumar, P. V., Vanka Ranga Rao and Gollapalli Nageswara Rao. (2013). <Synthesis, characterization and optical properties of ZnO NPs.pdf>.

Suresh, D., Nethravathi, P. C., Udayabhanu, Rajanaika, H., Nagabhushana, H., & Sharma, S. C. (2015). Green synthesis of multifunctional zinc oxide (ZnO) nanoparticles using Cassia fistula plant extract and their photodegradative, antioxidant and antibacterial activities. Materials Science in Semiconductor Processing, 31, 446-454. doi:10.1016/j.mssp.2014.12.023

Šutka, A., Järvekülg, M., & Gross, K. A. (2019). Photocatalytic Nanoheterostructures and Chemically Bonded Junctions Made by Solution-Based Approaches. Critical Reviews in Solid State and Materials Sciences, 44(3), 239-263. doi:10.1080/10408436.2018.1485549

Suvith, V. S., Devu, V. S., & Philip, D. (2019). Tannic acid mediated synthesis of nanostructured NiO and SnO2 for catalytic degradation of methylene blue. Optical and Quantum Electronics, 52(1), 12. doi:10.1007/s11082-019-2131-2

Tam, K. H., Cheung, C. K., Leung, Y. H., Djurišić, A. B., Ling, C. C., Beling, C. D., . . . Ge, W. K. (2006). Defects in ZnO Nanorods Prepared by a Hydrothermal Method. The Journal of Physical Chemistry B, 110(42), 20865-20871. doi:10.1021/jp063239w

Tao, P., Feng, Q., Jiang, J., Zhao, H., Xu, R., Liu, S., . . . Song, Z. (2012). Electroluminescence from ZnO nanowires homojunction LED grown on Si substrate by simple chemical vapor deposition. Chemical Physics Letters, 522, 92-95. doi:10.1016/j.cplett.2011.12.009

Tarwal, N. L., & Patil, P. S. (2010). Superhydrophobic and transparent ZnO thin films synthesized by spray pyrolysis technique. Applied Surface Science, 256(24), 7451-7456. doi:https://doi.org/10.1016/j.apsusc.2010.05.089

Thema, F. T., Manikandan, E., Dhlamini, M. S., & Maaza, M. (2015). Green synthesis of ZnO nanoparticles via Agathosma betulina natural extract. Materials Letters, 161, 124-127. doi:https://doi.org/10.1016/j.matlet.2015.08.052

Tintino, S. R., Oliveira-Tintino, C. D. M., Campina, F. F., Silva, R. L. P., Costa, M. d. S., Menezes, I. R. A., . . . Balbino, V. Q. (2016). Evaluation of the tannic acid inhibitory effect against the NorA efflux pump of Staphylococcus aureus. Microbial Pathogenesis, 97, 9-13. doi:https://doi.org/10.1016/j.micpath.2016.04.003

Tu, N., Van Bui, H., Trung, D. Q., Duong, A.-T., Thuy, D. M., Nguyen, D. H., . . . Huy, P. T. (2019). Surface oxygen vacancies of ZnO: A facile fabrication method and their contribution to the photoluminescence. Journal of Alloys and Compounds, 791, 722-729. doi:https://doi.org/10.1016/j.jallcom.2019.03.395

Tuomela, S., Autio, R., Buerki-Thurnherr, T., Arslan, O., Kunzmann, A., Andersson-Willman, B., . . . Lahesmaa, R. (2013). Gene expression profiling of immune-competent human cells exposed to engineered zinc oxide or titanium dioxide nanoparticles. PloS one, 8(7), e68415-e68415. doi:10.1371/journal.pone.0068415

Vaezi, M. R., & Sadrnezhaad, S. K. (2007). Nanopowder synthesis of zinc oxide via solochemical processing. Materials & Design, 28(2), 515-519. doi:https://doi.org/10.1016/j.matdes.2005.08.016

Velmurugan, P., Park, J. H., Lee, S. M., Yi, Y. J., Cho, M., Jang, J. S., . . . Oh, B. T. (2016). Eco-friendly approach towards green synthesis of zinc oxide nanocrystals and its potential applications. Artif Cells Nanomed Biotechnol, 44(6), 1537-1543. doi:10.3109/21691401.2015.1059840

Vietmeyer, F., Seger, B., & Kamat, P. V. (2007). Anchoring ZnO Particles on Functionalized Single Wall Carbon Nanotubes. Excited State Interactions and Charge Collection. Advanced Materials, 19(19), 2935-2940. doi:10.1002/adma.200602773

Wahab, R., Ansari, S. G., Kim, Y. S., Seo, H. K., Kim, G. S., Khang, G., & Shin, H.-S. (2007). Low temperature solution synthesis and characterization of ZnO nano-flowers. Materials Research Bulletin, 42(9), 1640-1648. doi:10.1016/j.materresbull.2006.11.035

Wahyono, T., Astuti, D., Wiryawan, K., Sugoro, I., & Jayanegara, A. (2019). Fourier Transform Mid-Infrared (FTIR) Spectroscopy to Identify Tannin Compounds in The Panicle of Sorghum Mutant Lines. IOP Conference Series: Materials Science and Engineering, 546, 042045. doi:10.1088/1757-899X/546/4/042045

Wang, L., Hu, C., & Shao, L. (2017). The antimicrobial activity of nanoparticles: present situation and prospects for the future. International journal of nanomedicine, 12, 1227-1249. doi:10.2147/IJN.S121956

Wang, P., Lombi, E., Zhao, F. J., & Kopittke, P. M. (2016). Nanotechnology: A New Opportunity in Plant Sciences. Trends Plant Sci, 21(8), 699-712. doi:10.1016/j.tplants.2016.04.005

Wang, T., Ni, C., & Janotti, A. (2017). Band alignment and p-type doping of ZnSnN2. Physical Review B, 95(20), 205205. doi:10.1103/PhysRevB.95.205205

Wang, Z. L. (2004). ZnO Nanostructure

Wei, Z., Xia, T., Ma, J., Feng, W., Dai, J., Wang, Q., & Yan, P. (2007). Investigation of the lattice expansion for Ni nanoparticles. Materials Characterization, 58(10), 1019-1024. doi:https://doi.org/10.1016/j.matchar.2006.08.004

Weinrick, B., Dunman, P. M., McAleese, F., Murphy, E., Projan, S. J., Fang, Y., & Novick, R. P. (2004). Effect of mild acid on gene expression in Staphylococcus aureus. Journal of bacteriology, 186(24), 8407-8423. doi:10.1128/JB.186.24.8407-8423.2004

Welsh, F. S. (2008). Identification of 1850s Brown Zinc Paint Made with Franklinite and Zincite at the U.S. Capitol. APT Bulletin: The Journal of Preservation Technology, 39(1), 17-30. doi:10.2307/25433934

Wertheim, H. F. L., Melles, D. C., Vos, M. C., van Leeuwen, W., van Belkum, A., Verbrugh, H. A., & Nouwen, J. L. (2005). The role of nasal carriage in Staphylococcus aureus infections. The Lancet Infectious Diseases, 5(12), 751-762. doi:https://doi.org/10.1016/S1473-3099(05)70295-4

Wertheim, H. F. L., Verveer, J., Boelens, H. A. M., van Belkum, A., Verbrugh, H. A., & Vos, M. C. (2005). Effect of Mupirocin Treatment on Nasal, Pharyngeal, and Perineal Carriage of Staphylococcus aureus in Healthy Adults. Antimicrobial Agents and Chemotherapy, 49(4), 1465. doi:10.1128/AAC.49.4.1465-1467.2005

Wijesekara, N., Dai, F. F., Hardy, A. B., Giglou, P. R., Bhattacharjee, A., Koshkin, V., . . . Wheeler, M. B. (2010). Beta cell-specific Znt8 deletion in mice causes marked defects in insulin processing, crystallisation and secretion. Diabetologia, 53(8), 1656-1668. doi:10.1007/s00125-010-1733-9

Wilson, H. F., Tang, C., & Barnard, A. S. (2016). Morphology of Zinc Oxide Nanoparticles and Nanowires: Role of Surface and Edge Energies. The Journal of Physical Chemistry C, 120(17), 9498-9505. doi:10.1021/acs.jpcc.6b01479

Wingett, D., Louka, P., Anders, C. B., Zhang, J., & Punnoose, A. (2016). A role of ZnO nanoparticle electrostatic properties in cancer cell cytotoxicity. Nanotechnology, science and applications, 9, 29-45. doi:10.2147/NSA.S99747

Wiśniewska, M., Chibowski, S., & Urban, T. (2017). Comparison of adsorption affinity of ionic polyacrylamide for the surfaces of selected metal oxides. Adsorption Science & Technology, 35(5-6), 582-591. doi:10.1177/0263617417702385

Wu, Y., Li, X., Wei, S., Liu, Y., Ma, M., Huang, L., & Pan, D. (2019). Ligand-assisted synthesis of monodispersed and small-sized ZnO nanoparticles and their application in electroluminescence device. Materials Research Express, 6(8), 085060. doi:10.1088/2053-1591/ab2027

Xiong, G., Pal, U., Serrano, J. G., Ucer, K. B., & Williams, R. T. (2006). Photoluminesence and FTIR study of ZnO nanoparticles: the impurity and defect perspective. physica status solidi c, 3(10), 3577-3581. doi:10.1002/pssc.200672164

Yamamoto, O. (2001). Influence of particle size on the antibacterial activity of zinc oxide. International Journal of Inorganic Materials, 3(7), 643-646. doi:https://doi.org/10.1016/S1466-6049(01)00197-0

Yi, G.-C., Wang, C., & Park, W. I. (2005). ZnO nanorods: synthesis, characterization and applications. Semiconductor Science and Technology, 20(4), S22-S34. doi:10.1088/0268-1242/20/4/003

Yoshikawa, A., Matsunami, H., & Nanishi, Y. (2007). Development and Applications of Wide Bandgap Semiconductors. In K. Takahashi, A. Yoshikawa, & A. Sandhu (Eds.), Wide Bandgap Semiconductors: Fundamental Properties and Modern Photonic and Electronic Devices (pp. 1-24). Berlin, Heidelberg: Springer Berlin Heidelberg.

Yuan, S., Feng, L., Wang, K., Pang, J., Bosch, M., Lollar, C., . . . Zhou, H.-C. (2018). Stable Metal–Organic Frameworks: Design, Synthesis, and Applications. Advanced Materials, 30(37), 1704303. doi:10.1002/adma.201704303

Zak, A. K., Abrishami, M. E., Majid, W. H. A., Yousefi, R., & Hosseini, S. M. (2011). Effects of annealing temperature on some structural and optical properties of ZnO nanoparticles prepared by a modified sol–gel combustion method. Ceramics International, 37(1), 393-398. doi:https://doi.org/10.1016/j.ceramint.2010.08.017

Zamboni, P., Cisno, C., Marchetti, F., Mazza, P., Fogato, L., Carandina, S., . . . Liboni, A. (2003). Minimally invasive surgical management of primary venous ulcers vs. compression treatment: a randomized clinical trial. European Journal of Vascular and Endovascular Surgery, 25(4), 313-318. doi:https://doi.org/10.1053/ejvs.2002.1871

Zhang, J., Sun, Y., Feng, R., Liang, W., Liang, Z., Guo, W., . . . Jiang, L. (2019). Plasmonic nanoparticle-film-assisted photoelectrochemical catalysis across the entire visible-NIR region. Nanoscale, 11(47), 23058-23064. doi:10.1039/C9NR07191A

Zhao, X., Gnanaseelan, M., Jehnichen, D., Simon, F., & Pionteck, J. (2019). Green and facile synthesis of polyaniline/tannic acid/rGO composites for supercapacitor purpose. Journal of Materials Science, 54(15), 10809-10824. doi:10.1007/s10853-019-03654-x

Zou, Q., Wang, R., & Li, Y. (2019). Minireview on the eletrochemical biosensors for the detection of heavy metal ions in water.

Appendices

Gant Chart on Master Research Planning

	TASK	MILESTONE	DURATION	MONTH																			
				2019				2020												2021			
				9	10	11	12	1	2	3	4	5	6	7	8	9	10	11	12	1	2	3	4
1	**Chapter 1: Introduction**	comeout with problem statement, objective, and research scope	4 months																				
	Sample Preparation	Produced high yield, pure and stable ZnO and ZnO-TA nanostructure																					
2	Chapter 2: Literature review	literates on others study related to research	9 months																				
	Characterisation testing on physical and optical structure	Performed test on UV absorbance, transmittance and light emission by using UV-Vis and PL.																					
3	Chapter 3: methodology	Plan on method of synthesising and characterisation techniques details.	9 months																				

Gant Chart continued

	TASK	MILESTONE	DURATION	MONTH																			
				2019				2020												2021			
				9	10	11	12	1	2	3	4	5	6	7	8	9	10	11	12	1	2	3	4
	Characterisation Testing on morphologycal structure	Performed TEM and FESEM with clear morphologycal structure of ZnO and ZnO-TA nanostructure																					
4	Chapter 4: Result and Discussion	Plot results on each characterisation and discuss results which relate to finding and theory																					
	Characterisation testing on bacterial growth	Performed bacterial growth testing from the fabric infused with ZnO by using Agar method.	7 months																				
5	Chapter 5: Conclusion and Recommendation	discuss on limitation of research and implementation for further finding	14 months																				
	Finalize project with data publication in conference, journal and final report , Pre-Viva, Viva	Published paper and submitted report thesis regarding the research																					

APPENDIX 2

ISI (Q4)

Mater. Res. Express 6 (2019) 125046 https://doi.org/10.1088/2053-1591/ab5754

Materials Research Express

PAPER

The optical quantification measurement on aggregated aqueous ZnO nanostructures upon exposure to tannic acid

RECEIVED
15 September 2019

REVISED
17 October 2019

ACCEPTED FOR PUBLICATION
13 November 2019

PUBLISHED
22 November 2019

Nurul Akmal Che Lah and Aqilah Kamaruzaman

Innovative Manufacturing Mechatronics and Sports (IMAMS) Lab, Faculty of Manufacturing Engineering, Universiti Malaysia Pahang, 26600, Pekan, Pahang, Malaysia

E-mail: akmalcl@ump.edu.my

Keywords: ZnO nanostructures, tannic acid, quantification, optical properties

Abstract

Herein, a facile eco-friendly green hydrothermal approach was developed in the preparation of pristine, stable and safer aqueous zinc oxide (ZnO) nanostructures at high yield in the presence of tannic acid (TA) conducted both at low and high reaction temperatures (50, 70 and 90 °C). The TA acted as a reducing agent and also a stabiliser which later capped around the ZnO nanostructures. The absorption spectrum confirmed the formation of ZnO nanostructures with the intense peak range at ~365 to 405 nm. The acid-driven solvent based on the Brønsted-Lowry acid/base theory described the acid solvent interaction in pristine ZnO-TA samples which caused the proton mechanism transfer between the Zn and oxygen components. Based on TEM and SEM analyses, pristine ZnO-TA nanostructures are well distributed and formed nanoplatelet hexagonal aggregate morphology upon the addition of TA with the smallest mean diameter size of 7 ± 1.2 nm. A surprising role of TA was also found out where the presence of TA could influence the formation of smaller ZnO-TA nanostructures upon the addition of TA (increased the H^+ concentration) at lower pH value (pH = 5) in pristine ZnO-TA samples which further influence the morphological formation of smaller nanostructures according to the pH of the aqueous solution. The complexation of reaction + +

+

aggregates of ZnO-TA nanostructures. These results indicated that the TA caused the dissolution of ZnO nanostructures due to the effects of combined pH solution modification and alteration of complexation reaction.

1. Introduction

For the past few decades, Zinc Oxide (ZnO) nanostructures have received an abundance of immense attention particularly in commercial biomedical- and nanobiotechnology-enabled consumer products [1–4]. The dominant features exhibit by these nanoparticles includes the efficacy as excellent anti-fungal, anti-microbial, ultra-violet-filtering capability agents and the credits of their nature that are majorly non-toxic and ecofriendly [5–7]. They possess very strong non-neurotoxicological effects even at a very high concentration of gram-positive and gram-negatice bacteria which also proved as one of the current important element apart from silver nanostructures used in cosmetics, medical devices, sunscreen and bio-sensors applications [8–12]. In our case, the expectation to produce a good performance of ZnO nanostructures due to the contribution of safe capping ligand that able to improve the catalytic activity of the semiconductor system. Thus, the capping agents or ligands are needed in stabilising the encapsulated ZnO nanostructures [13–16].

APPENDIX 3

SCOPUS INDEX (MUCET 2019)

Available online at www.sciencedirect.com

ScienceDirect

materialstoday: PROCEEDINGS

ELSEVIER

Materials Today: Proceedings 00 (2019) 0000–0000 www.materialstoday.com/proceedings

11th Malaysian Technical Universities Conference on Engineering & Technology: Materials Science

Formation of ZnO Nanoparticles in the Presence of Tannic Acid.

Aqilah Kamaruzaman*, Nurul Akmal Che Lah

Innovative Manufacturing, Mechatronics, Sports (Imams) Lab, Faculty of Manufacturing Mechatronics Engineering Technology, Universiti Malaysia Pahang, 26600, Pekan, Pahang, Malaysia

Abstract

Zinc Oxide nanoparticles (ZnO NPs) have received abundance attention due to their ability to provide as a good semiconductor and UV absorbance materials. In this research, ZnO NPs are synthesised by hydrothermal method which employed a green synthesis method of which fully assisted by the Tannic Acid (TA). The controllable morphologies and mean sizes of ZnO NPs are observed to increased due to aggregation that occurred due to the influence of acidic medium (TA molecule). The morphological properties are discussed based on the TEM and FESEM images which indicated the average size of 14nm and 32.7nm for ZnO NPs and ZnO-TA NPs obtained, respectively. Meanwhile, the optical properties are discussed based on the UV-Vis absorbance spectroscopy results. The UV absorbance performance showed the behavior of absorbance peak at shorter wavelength as the ZnO NPs are capped with TA. The absorbance peak is shifted from UV-A region to UV-C region which indicated the transition from ZnO NPs to ZnO-TA respectively.

Keywords: Zinc Oxide Nanoparticles; Tannic acid; green synthesis; hydrothermal method; TEM; FESEM; UV-Visible

1. Introduction

Zinc Oxide nanoparticle had gained huge attention of interest in contemporary research due to its unique structure and properties. Particularly, the superior performance of ZnO NPs in detecting Ultraviolet (UV) ray had gained a huge potential in development of semiconductor-and LEDs- based materials [1, 2]. The ability of ZnO NPs in photonic and electronic material (semiconductor) is due to its large excitonic energy (~60 meV) and wide direct band gap (3.37 eV) which makes it able to be involved in various applications in optoelectronic research and technologies [3-6]. The wide bandgap of ZnO NPs raised up by tiny size group of ZnO NPs (average diameter 100 nm) is important to be considered as functional material for effective UV absorber which exhibits optical transparency in the range of 400 to 700 nm wavelengths.

Besides, few previously reported research erect the biocompatible ability of ZnO NPs which can be applied without coating together to inhibit microbial growth and is indexed as a generally recognized as safe (GRAS) material by the U.S. Food and Drug Administration [6-10].

The most common method in synthesizing nanoparticles are wet chemical, hydrothermal, sol-gel and green synthesis method [11, 12]. Herein, for the synthesis of ZnO NPs, the hydrothermal method in the presence of stabilizing agent of Sodium Tri-citrate which resembles a green synthesis method with the usage of green reductant chemical, Tannic Acid (TA) were employed. The combination of both hydrothermal and green synthesis method is well accepted through many research due to its beneficial as cost-effective and ecologically method in synthesizing ZnO NPs [12-15]. Basically, the green synthesis method approach is by manipulating reagents from natural resources such as glucose, plant extracts and biodegradable polymers as capping agents [16] and in the present work, TA is used as both the capping agent and second size influencer. TA has been proved to influence the synthesis of metal size [13, 17]. The previous study has been shown to produce ZnO NPs excellent properties with sizes in the range of 23 to 48nm [18-21].